

KINETICS OF THE REACTION OF GROUND STATE OXYGEN ATOMS WITH TRICHLORO-ETHYLENE FROM 295 TO 1127 K; COMPARISON TO OTHER O + CHLORO-ETHYLENE REACTIONS

Jasmina Hranisavljevic and Arthur Fontijn
High-Temperature Reaction Kinetics Laboratory, The Isermann Department of Chemical Engineering, Rensselaer Polytechnic Institute, Troy, NY 12180-3590

key words: chloro-ethylenes, high-temperature kinetics, oxidation

INTRODUCTION

Chlorinated hydrocarbons frequently occur in wastes and present a major pollution hazard from waste incinerators. Compounds such as chlorinated olefins are toxic and carcinogenic by themselves and their oxidation and pyrolysis products may be involved in the formation of highly toxic chloro-furans and -dioxins.¹⁻³ In order to influence the incineration process, such that hazardous emissions are reduced, kinetic models based on realistic kinetic data are needed.¹ Few measurements on individual oxidation reactions of chloro-ethylenes are available for the 700-1500 K regime of prime incineration interest. We have recently reported on the reactions of ground state oxygen atoms with monochloro-ethylene (1), 1,1-dichloro-ethylene (2) and *trans* 1,2-dichloro-ethylene (3) in the 290-1200 K range,⁴ and compared these to ethylene⁵. The series is now expanded to trichloro-ethylene (4), one of the compounds most commonly encountered in municipal wastes.

It is known that below about 500 K, in O-atom olefin reactions, addition to the double bond dominates.⁶ In the earlier study we found that, below about 700 K, the temperature dependences of the rate coefficients of the four reactions mentioned differ only slightly from each other. However, the magnitude of the rate coefficients was found to decrease substantially in the sequence $k_{C_2H_4}(T) > k_1(T) \approx k_2(T) > k_3(T)$, in agreement with the preferential attack of O-atoms at the site of the unsubstituted olefinic C-atom. While these trends were shown to continue at higher temperatures for the first three members of this sequence, a sharp increase was observed in $k_3(T)$ above about 700 K. It was thought that this increase may be attributed to H-atom abstraction from the weakened C-H bond. A method was developed for estimating rate coefficients, for H-abstraction from organic molecules by O-atoms, over wide temperature ranges.^{4,7} The sum of the $k_{ABS}(T)$ thus obtained, and the $k_{ADD}(T)$ based on the extrapolation of a transition state theory (TST) expression for addition,⁶ was shown to be in good agreement with the experimental data for reaction (3). The same type of calculations also suggested a negligible influence of abstraction on the other discussed reactions in the investigated temperature range, in agreement with the experiments.

These results, and those of a study of O-atom reactions with the four C₄H₈ butenes,⁷ suggested that it is possible to predict the high temperature rate coefficients for O-atom reactions with olefins, with good accuracy, by:

- i) taking a few experimental points below 500 K
- ii) using those points with the Singleton and Cvetanovic TST expression⁶ to obtain $k_{ADD}(T)$ over the temperature range of interest, and
- iii) adding the estimated $k_{ABS}(T)$ to the $k_{ADD}(T)$ to obtain the overall $k(T)$.

In the present work we check the validity of this approach for the trichloro-ethylene reaction.

EXPERIMENTAL TECHNIQUE

The measurements were performed in two different HTP (high-temperature photochemistry) reactors. The older design reactor,⁸ here referred to as reactor A, is shown in Fig. 1, while reactor B⁹ is shown in Fig. 2. The reactant gases were introduced into the heated bath gas through cooled inlets. Ground state oxygen atoms were produced by photolysis of O₂ through a MgF₂ window, or SO₂ through a Suprasil quartz window. Flash photolysis FP was used in reactor A, while both flash photolysis and laser photolysis LP were employed in reactor B. The relative concentrations of oxygen atoms were monitored by fluorescence of the 130.2-130.6 nm resonance triplet. The source of resonance radiation was a microwave discharge flow lamp through which He flowed at 2.0 mbar. The O-atom fluorescence was monitored with a photomultiplier tube through a CaF₂ window ($\lambda > 125$ nm).

The operational procedures have been previously described.^{8,10,11} The experiments were carried out under pseudo-first-order conditions $[O] \ll [C_2HCl_3]$, for which the fluorescence intensity I , proportional to $[O]$, can be written as

$$I = I_0 \exp(-k_{ps1}t) + B \quad (5)$$

Here, $I_0 + B$ is the intensity at time $t=0$, k_{ps1} is the pseudo-first-order rate coefficient, and B is the background due to scattered light. The values of k_{ps1} were obtained by fitting¹² the observed $\ln I$ vs. t profiles to eq. 5. In all cases exponential $\ln I$ vs. t plots were obtained, as verified by a two stage residual analysis.¹³ Plots of typically five or six k_{ps1} obtained over a range of C₂HCl₃ concentrations were used to obtain rate coefficients k_4 for the temperature of the experiment; uncertainty analysis was used as previously described.¹¹

RESULTS

The experimental conditions were varied over wide ranges of the flash or laser energy, total gas concentration (pressure), average gas velocity, cooled inlet to observed reaction zone distance, and residence time. Residual analyses showed the independence of the results of these implicit parameters. The rate coefficients obtained are shown in Figs. 3 and 4. There is a good agreement between the data obtained from the two reactors and from the different O-atom production arrangements, as shown in these figures. A four-parameter fit was found to give the best fit to the data:

$$k_4(295-1127 \text{ K}) = 1.1 \times 10^{-12} \exp(-695 \text{ K/T}) + 1.5 \times 10^{-9} \exp(-7508 \text{ K/T}) \text{ cm}^3 \text{ molecule}^{-1} \text{ s}^{-1} \quad (6).$$

As in previous work^{4,7-10} the results of a covariance matrix analysis were combined¹⁴ to determine precision limits. 2σ precision limits obtained vary from a minimum of $\pm 3\%$ at 393 K to a maximum of $\pm 12\%$ at 1127 K. Allowing, probably exaggeratedly, for $\pm 20\%$ systematic errors leads to corresponding accuracy limits of $\pm 20\%$ to $\pm 23\%$. A three-parameter fit of the format $k(T) = a (T/K)^n \exp(-e \text{ K/T})$ was also attempted, but led to higher 2σ precision limits, varying from a minimum of $\pm 6\%$ at 541 K to a maximum of $\pm 16\%$ at 295 K.

There has been only one previous measurement of the O-atom trichloro-ethylene reaction. This relative room temperature measurement, as assessed in the evaluation of Cvetanovic,¹⁵ is shown in Fig. 4. and is in good agreement with the present work.

DISCUSSION

In Fig. 5 the rate coefficient plot of reaction (4) is compared to those of the other discussed ethylenic reactions. The trends that were observed⁴ are continued. Below about 700 K the plots have similar slopes, indicating that Cl-substitution does not strongly affect the activation energies. The rate coefficients of reactions (3) and (4) are approximately equal near room temperature and differ only slightly at higher temperatures. This confirms that rate coefficients do not change much with further Cl-substitution of an already mono-substituted C-atom. The sequence of rate coefficients can now be extended to read: $k_{C_2H_4}(T) > k_1(T) = k_2(T) > k_3(T) = k_4(T)$. The sharp curvature of the $k_4(T)$ plot above 700 K, similar to, but stronger than, that of $k_3(T)$, can again be attributed to H-abstraction and is shown below to be in agreement with the predictive method described in the Introduction.

The rate coefficient expression for the addition channel used is:⁶

$$k_{ADD}(T) = A T^{-0.5} [1 - \exp(-1.439 \omega/T)]^{-2} \exp(-E_0/RT) \quad (7),$$

Here A is a temperature independent pre-exponential factor, ω is the vibrational frequency of the degenerate bending mode in the O-olefin transition state, and E_0 is the energy barrier. The parameters A, ω and E_0 are selected such that the best fit is obtained with the experimental values of the rate coefficients at three temperatures in the 300-500 K range. This yields:

$$k_{ADD}(295-1460) = 1.0 \times 10^{-11} (T/K)^{-0.5} [1 - \exp(-423 \text{ K/T})]^{-2} \exp(-729 \text{ K/T}) \text{ cm}^3 \text{ molecule}^{-1} \text{ s}^{-1} \quad (8)$$

The previously described method for estimating rate coefficients for H-atom abstraction^{4,7} gives for O + trichloro-ethylene:

$$k_{ABS}(295-1460) = 2.4 \times 10^{-16} (T/K)^{1.55} \exp(-2801 \text{ K/T}) \text{ cm}^3 \text{ molecule}^{-1} \text{ s}^{-1} \quad (9).$$

In Fig. 6 the estimated rate coefficient values are compared to the experimental points. It may be seen that the addition channel expression alone yields at higher temperatures values lower than those measured, but that the sum of the $k_{ABS}(T)$ and $k_{ADD}(T)$ expressions again^{4,7} yields good agreement with experimental results.

CONCLUSIONS

Rate coefficients for the O + trichloro-ethylene reaction have been measured for the first time above room temperature. They follow the trends established for the O-atom reactions with the less substituted ethylenes and confirm the usefulness of our recently developed method for estimating high temperature rate coefficients for O-atom olefin reactions. It would appear that the method can be extended to other reactions of O-atoms with aliphatic hydrocarbons.

REFERENCES

- 1) Tsang, W.; *Combust. Sci. and Tech.* **1990**, *74*, 99
- 2) Oppelt, E. T.; *J. Air Poll. Contr. Assoc.*, **1987**, *37*, 558
- 3) Penner, S. S.; Report from NSF sponsored Workshop, **1988**, La Jolla, California
- 4) Hranisavljevic, J.; Adusei, G. Y.; Xun, Y.; Fontijn, A.; *Combust. Sci. and Tech.*, submitted
- 5) Klemm, R. B.; Sutherland, J. W.; Wickramaaratchi, M. A.; Yarwood, G.; *J. Phys. Chem.* **1990**, *94*, 3354
- 6) Singleton, D. L.; Cvetanovic, R. J.; *J. Am. Chem. Soc.* **1976**, *98*, 261
- 7) Adusei, G. Y.; Fontijn, A.; *J. Phys. Chem.*, submitted

- 8) Ko, T.; Marshall, P.; Fontijn, A.; *J.Phys.Chem.* **1990**,*94*,1401
- 9) Mahmud, K.; Kim, J. S.; Fontijn, A.; *J.Phys.Chem.* **1990**,*94*,2994
- 10) Marshall, P.; Ko, T.; Fontijn, A.; *J.Phys.Chem.* **1989**,*93*,1922
- 11) Fontijn, A.; Futerko, P. M.; in Fontijn, A. (Ed.), *Gas-Phase Metal Reactions*, North Holland, Amsterdam, 1992, Chapter 6.
- 12) Marshall, P.; *Comput.Chem.* **1987**,*11*,219
- 13) Ko, T.; Adusei, G. Y.; Fontijn, A.; *J.Phys.Chem.* **1991**,*95*,8745
- 14) Wentworth, W. E.; *J.Chem.Educ.* **1991**,*95*,8745
- 15) Cvetanovic, R. J.; *J.Phys.Chem.Ref.Data* **1987**,*16*,261

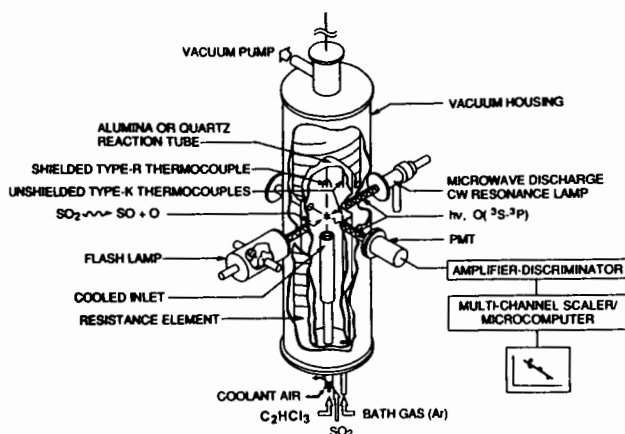


Figure 1. HTP reactor - older design (reactor A), for details see Ref. 8

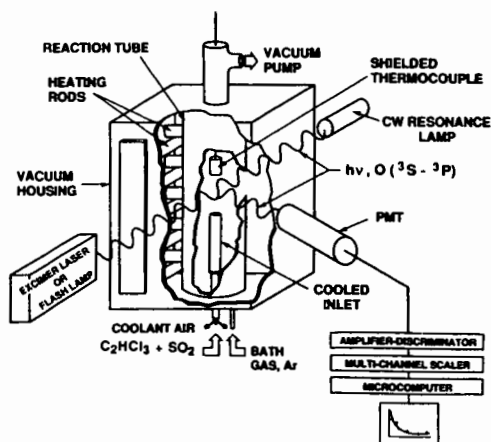


Figure 2. HTP reactor - newer design (reactor B), for details see Ref. 9

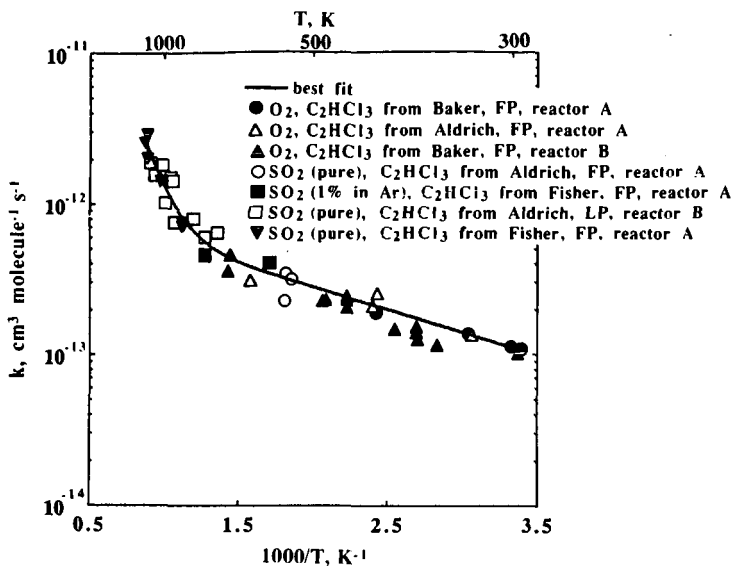


Figure 3. Summary of the rate coefficient measurements for the O + trichloro-ethylene reaction

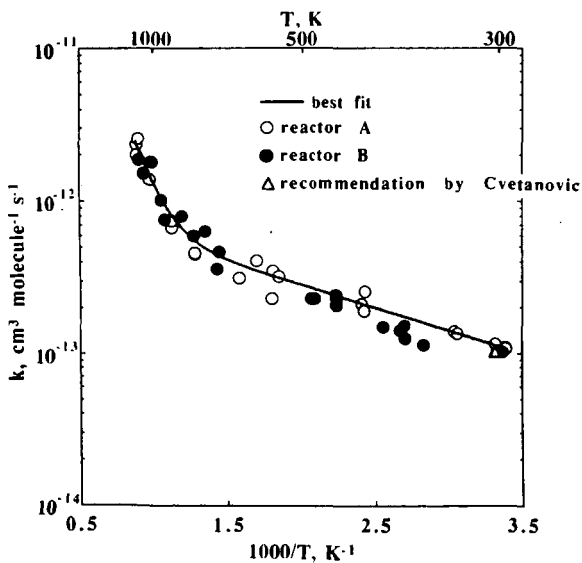


Figure 4. Rate coefficient measurements for the O + trichloro-ethylene reaction differentiated by the reactor

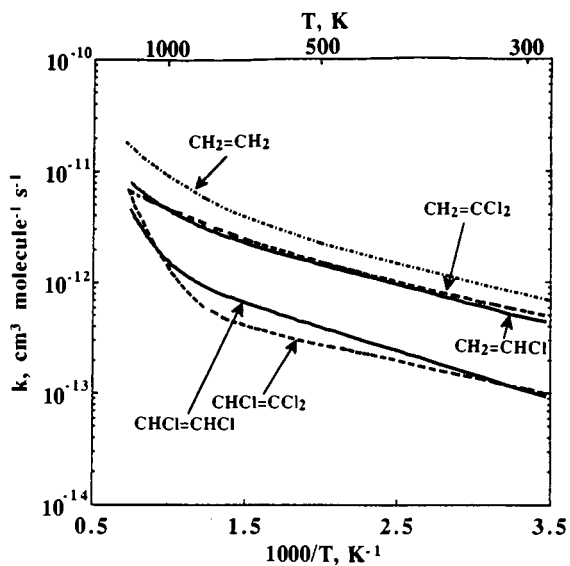


Figure 5. Comparison of ethylenic reactions

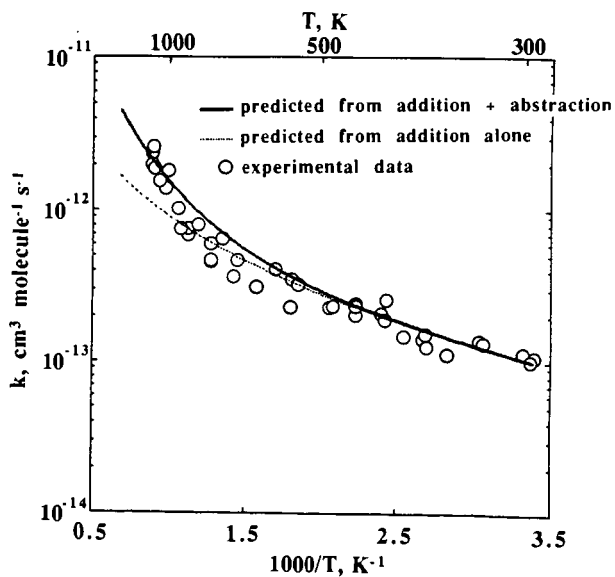


Figure 6. Comparison of the predicted and measured rate coefficients for the O + trichloro-ethylene reaction

HIGH-TEMPERATURE STUDY OF $O + H_2CO \rightarrow OH + HCO$

Jan P. Hessler,¹ Hong Du,² and Paul J. Ogren³

¹Chemistry Division, Argonne National Laboratory, 9700 S. Cass Ave.,
Argonne, Illinois 60439

²Present address: Physical Sciences Inc., 20 New England Business Center,
Andover, Massachusetts 01810

³Department of Chemistry, Earlham College, Richmond, Indiana 47374

Keywords: Elementary Chemical Kinetics, Gas Phase Rate Coefficients, Formaldehyde

In our previous studies of the reactions of the methyl radical with molecular oxygen, we noticed that after the methyl radical has been consumed the reactions which control the concentration of hydroxyl are the hydroxyl-hydroxyl self reaction, the title reaction, and the reaction between hydroxyl and formaldehyde. From the long-time temporal behavior of hydroxyl we have been able to extract the rate coefficient for the title reaction over the temperature range 1580 to 2250 K. When we combine our data with the low temperature data of Klemm et al [J. Chem. Phys. 1980, 72, 1256-1264] we obtain the rate expression

$$k(T) = 2.6 \times 10^{-16} T^{1.67} \exp(-891/T(K)) \text{ cm}^3 \text{ s}^{-1}$$

This result is consistent with the earlier recommendation of Herron [J. Phys. Chem. Ref. Data 1988, 17, 967-1026] which is based on a Bond-Energy-Bond-Order calculation adjusted to agree with the experimental results at 700 K.

INTRODUCTION

The reactions of formaldehyde represent an important set of secondary reactions in the combustion of hydrocarbon fuels. Unfortunately, above 1000 K, very few rate coefficients of reactions with formaldehyde have been measured. All of these high-temperature measurements, by different groups or techniques, differ significantly. Previously, only three high-temperature shock-tube studies of the reaction of formaldehyde with atomic oxygen have been published. Izod et al¹ estimated a rate coefficient of $1.0 \times 10^{-10} \text{ cm}^3 \text{ s}^{-1}$ from 1400 to 2200 K, Bowman² deduced $8.3 \times 10^{-11} \exp(-2300/T(K)) \text{ cm}^3 \text{ s}^{-1}$ from 1875 to 2240 K, and Dean et al³ concluded the coefficient is $3.0 \times 10^{-11} \exp(-1552/T(K)) \text{ cm}^3 \text{ s}^{-1}$ from 1905 to 3045K.

While we were measuring the primary reactions of the methyl radical with molecular oxygen we noticed that as the radical is consumed a formaldehyde molecule and a hydroxyl radical are created. This is independent of the reaction chain which produces formaldehyde. We have taken advantage of this observation to extract the rate coefficient at high temperatures for the reaction of formaldehyde with atomic oxygen from the long-time behavior of our measured profiles of the hydroxyl concentration.

EXPERIMENTAL

The experiments were performed in an ultra-high purity stainless-steel shock tube fitted with two 2"-long windows for optical observations and six pressure transducers for measurements of the shock velocity. The tube has a diameter of 25 mm and the expansion section is 1.5 m long. The methyl precursor, azomethane, was synthesized by the standard method⁴ and purified by bulb-to-bulb distillation. High-purity oxygen (99.998%), xenon (99.999%), and helium (99.9999%) were purchased from commercial vendors and used as supplied. Samples were prepared manometrically in a three-liter stainless-steel mixing vessel and introduced into the shock tube from the expansion end of the tube. The purity and composition of each batch of samples were checked by mass spectrometric analysis.

The temporal dependence of the hydroxyl radical was monitored by the tunable-laser flash-absorption technique.⁵ The wavelength of the doubled light from a high-resolution (0.02 cm^{-1} at 618 nm) pulsed dye laser was tuned to the $Q_{11}(13/2)$ [$^{AN}\Delta F_{v-p}(J'')$ notation] transition of the (0,0) band of hydroxyl at 32381 cm^{-1} . An absorption profile at 2200 K is shown in figure 1.

ANALYSIS

In any analysis of a complex chemical system the reduction of experimental data is only as good as the mechanism used to describe the chemistry. A high-speed parallel-processor (Alliant Concentrix 2800) allows us to use a relatively large reaction mechanism for this description. We have constructed a reaction mechanism which contains 25 species and 89 reactions. The mechanism presented by Frenklach et al.⁶ was used as the starting point. Most of the rate coefficients are from the recent review by Baulch et al.⁷ The rate coefficients for the major reactions under our experimental situation are given in Table I. At high temperatures the primary reactions which remove the methyl radical and

Produce formaldehyde, hydroxyl, and atomic oxygen are



Since reaction 76 is relatively fast, for every methyl radical removed a formaldehyde molecule is formed. This is independent of the relative rates of reactions 49 and 51. Also, because reaction 7 is fast a hydroxyl radical is formed for every formaldehyde molecule. Although the concentrations of formaldehyde and hydroxyl are independent of the relative rates of reactions 49 and 51, the concentration of atomic oxygen will depend upon this ratio. Therefore, this approach is only suited for the high-temperature region where the rate of reaction 49 dominates that of reaction 51. The secondary reactions which control the long-time behavior of the hydroxyl radical are



To demonstrate that we can obtain information on the rate of reaction 32 by monitoring the temporal behavior of the hydroxyl radical we used our complete reaction mechanism to perform a sensitivity analysis⁸ for hydroxyl at the experimental conditions of the profile shown in figure 1. In figure 2, we plot the square of the reduced sensitivity coefficients with respect to hydroxyl. From this figure we see that immediately after the methyl radical is depleted reaction 32 determines the kinetic behavior of the hydroxyl radical. Reaction 32 produces another hydroxyl radical. Therefore, at long times the profile is controlled by reaction 11. To quantitatively determine the relative importance of each reaction⁹ we integrate the squared sensitivity coefficients in figure 2 between 0 and 30 μs . From this calculation we conclude that over the initial 30 μs interval the relative weight of reaction 32 is 26%, for reaction 11 the weight is 53%. The total weight for the sum of all of the reactions which remove methyl is 9.1%. At this high temperature the relative weight for reaction 33 is only 2.7%. A relative weight of 26% is more than sufficient to extract a rate coefficient from an experimental profile. For this analysis we use the recently measured rate coefficient of Wooldridge et al.¹⁰ for the hydroxyl-hydroxyl self reaction and vary only the incubation time, the cross section for optical absorption, and the rate coefficient for reaction 32 to fit the experimental profiles. The result of the non-linear least-squares analysis for the profile of figure 1 is shown in figure 3.

As we change the experimental conditions to produce lower temperatures the sensitivity of hydroxyl with respect to the rate coefficient of reaction 32 becomes less important while that of reaction 33 becomes more important. By reformulating the procedure for non-linear least-squares analysis in terms of dimensionless parameters¹¹ we are able to estimate the relative importance of reactions 32 and 33 for each experimental profile. With this approach we have been able to determine the rate coefficient for reaction 32 from the highest temperature of 2250 K down to 1580 K. Below 1580 K the relative weight of reaction 32 is not large enough to allow us to determine its rate. The results of our non-linear least-squares reduction of the experimental profiles are summarized in Table II.

DISCUSSION

At 2000 K our results are a factor of 1.8 lower than those of Izod et al., a factor of 2.1 higher than Bowman's, and a factor of 3.9 higher than those of Dean et al. All of the above scientists, including ourselves, have numerically integrated the set of differential equation which result from a complex reaction mechanism to deduce the rate coefficient for the $\text{O} + \text{H}_2\text{CO}$ reaction. From our analysis we know that our best-fit values for the rate coefficient of reaction 32 are correlated with the value for the rate coefficient for the hydroxyl-hydroxyl self reaction. This correlation may be expressed as

$$\delta k_{32} = 0.6726k_{11}$$

where δk_j is the fractional change in the rate coefficient of the j^{th} reaction. The numerical coefficient was determined by a correlation analysis⁹ of the reduced sensitivity coefficients shown in figure 2. It should be obvious that similar correlations may also exist in the previous experiments. These correlations could account for the observed discrepancies. However, before precise statements about correlations can be made it is necessary to carefully compare the mechanisms used for each experiment and perform both a sensitivity and correlation analysis for each set of experimental conditions. Such a detailed discussion is beyond the scope of this preprint.

The rate coefficient for reaction 32 has been measured by Klemm *et al*¹² between 250 and 750 K. Their results along with ours are shown in figure 4. We have fit both sets of data to the general expression $\ln[k(T)] = \ln A + \beta \ln T - \Delta E/kT$ and obtain

$$\ln[k(T)] = -(35.9 \pm 3.7) + (1.67 \pm 0.47) \ln T - (891 \pm 342)/T(K) \text{ cm}^3\text{s}^{-1}.$$

The confidence limits are at the 95.4% or 2- σ level. These apparently large confidence limits are due to the correlation between the parameters. This correlation may be expressed by the vector

$$S_1 = 0.103\epsilon_{\ln A} + 0.281\epsilon_{\beta} - 0.382\epsilon_{\Delta E/k}$$

where the ϵ_j s represent unit vectors in the 3-dimensional fractional parameter space. The physical interpretation of this vector is that if we change $\ln A$ by 10.3%, β by 28.1%, and $\Delta E/k$ by -38.2% we will move from the minimum value of χ^2 to a point on the $\Delta\chi^2$ surface which defines the 2- σ confidence limits and produces the largest change in all of the parameters. The two curves at the 2- σ confidence limit are shown by the dashed lines in figure 4.

Our analytic expression for the rate coefficient compares favorably with the recommendation of Herron,¹³ $5.5 \times 10^{-17} T^{1.84} \exp\{-522/T(K)\}$ which is based upon a Bond-Energy-Bond-Order calculation adjusted to give agreement between experiment and calculation at 700 K. Our expression differs significantly with the recommendation of Baulch *et al*⁷ of $6.85 \times 10^{-13} T^{0.57} \exp\{-1390/T(K)\} \text{ cm}^3\text{s}^{-1}$.

ACKNOWLEDGEMENTS

We wish to thank Chris C. Walker, an undergraduate student from Earlham College, for help with the analysis of the hydroxyl profiles. He participated in the Fall 1993 Science and Engineering Research Semester program. This program is coordinated by the Division of Education Programs. This work was performed under the auspices of the U. S. Department of Energy, Office of Basic Energy Sciences, Contract No. W-31-109-ENG-38.

REFERENCES

- (1) Izod, T. P.; Kistiakowsky, G. B.; Matsuda, S. *J. Chem. Phys.* 1971, 55, 4425-32.
- (2) Bowman, C. T. *Proc. 15th Symp. (Int.) on Combust. (1975)*, pp. 869-82. Pittsburgh: Combustion Inst.
- (3) Dean, A. M.; Johnson, R. L.; Steiner, D. C. *Combust. Flame* 1980, 37, 41-62.
- (4) Renaud, R.; Leitch, L. C. *Can. J. Chem.* 1954, 32, 545-49.
- (5) VonDrasek, W. A.; Okajima, S.; Kiefer, J. H.; Ogren, P. J.; Hessler, J. P. *Applied Optics* 1990, 29, 4899-906.
- (6) Frenklach, M.; Wang, H.; Rabinowitz, M. J. *Prog. Energy Combust. Sci.* 1992, 18, 47.
- (7) Baulch, D. L.; Cobos, C. J.; Cox, R. A.; Esser, C.; Frank, P.; Just, T.; Kerr, J. A.; Pilling, M. J.; Troe, J.; Walker, R. W.; Warnatz, J. *J. Phys. Chem. Ref. Data* 1992, 21, 411-752.
- (8) Lutz, A. E.; Kee, R. J.; Miller, J. A. "SENKIN: A Fortran Program for Predicting Homogeneous Gas Phase Chemical Kinetics With Sensitivity Coefficients," Sandia National Laboratories, 1989.
- (9) Hessler, J. P.; Ogren, P. J. *J. Chem. Phys.* 1992, 97, 6249-58.
- (10) Wooldridge, M. S.; Hanson, R. K.; Bowman, C. T. *A Shock Tube Study of the OH + OH + H2O + O Reaction*, paper 92-93. 1992 Fall Technical Meeting, Western States Section, The Combustion Institute, 12-13 October 1992, Berkeley, CA.
- (11) Hessler, J. P.; Current, D. H.; Ogren, P. J. *to be published*.
- (12) Klemm, R. B.; Skolnik, E. G.; Michael, J. V. *J. Chem. Phys.* 1980, 72, 1256-64.
- (13) Herron, J. T. *J. Phys. Chem. Ref. Data* 1988, 17, 967-1026.

Table I. Rate Coefficients for some of the reactions of the mechanism.

REACTIONS CONSIDERED	$A(\text{cm}^3 \text{s}^{-1})$	β	$E/k(\text{K})$
7. $\text{H}+\text{O}_2 \rightleftharpoons \text{OH}+\text{O}$	$1.62\text{E}-10$	0.0	7474
11. $\text{OH}+\text{OH} \rightleftharpoons \text{H}_2\text{O}+\text{O}$	$4.00\text{E}-11$	0.0	3080
32. $\text{CH}_2\text{O}+\text{O} \rightleftharpoons \text{HCO}+\text{OH}$		This work	
33. $\text{CH}_2\text{O}+\text{OH} \rightleftharpoons \text{HCO}+\text{H}_2\text{O}$	$1.25\text{E}-11$	0.0	84
49. $\text{CH}_3+\text{O}_2 \rightleftharpoons \text{CH}_3\text{O}+\text{O}$	$2.20\text{E}-10$	0.0	15800
51. $\text{CH}_3+\text{O}_2 \rightleftharpoons \text{CH}_2\text{O}+\text{OH}$	$5.50\text{E}-13$	0.0	4500
76. $\text{CH}_3\text{O}(\text{+M}) \rightleftharpoons \text{CH}_2\text{O}+\text{H}(\text{+M})$	$1.00\text{E}+15$	0.0	17223
Low pressure limit: $0.432\text{E}-09$ 0.0 11065.			

Table II. High-temperature rate data for $\text{O} + \text{H}_2\text{CO} \rightarrow \text{OH} + \text{HCO}$.

Mach #	P(kPa)	T(K)	$t_{\text{max}}(\mu\text{s})$	N	rmsd(m^{-1})	$k(10^{-12} \text{cm}^3 \text{s}^{-1})$	$\sigma(\text{pm}^2)$
5.081	186.6	2251	30	271	0.55	66.8	6306
5.072	174.7	2244	60	561	0.51	88.9	5958
4.880	193.2	2100	40	373	0.58	54.3	6087
4.813	188.3	2047	62	547	0.35	69.3	4222
4.689	221.9	1956	68	617	0.61	61.3	4880
4.587	221.1	1891	33	280	0.61	27.4	5450
4.458	221.3	1797	50	438	0.41	46.3	5341
4.321	217.5	1705	58	488	0.44	22.6	5739
4.128	207.8	1580	40	311	0.37	19.0	4749

For all profiles: $X_{\text{Xe}} = 0.49785$, $X_{\text{C}_2\text{H}_6\text{N}_2} = 0.00015$, $X_{\text{He}} = 0.198$, $X_{\text{O}_2} = 0.304$

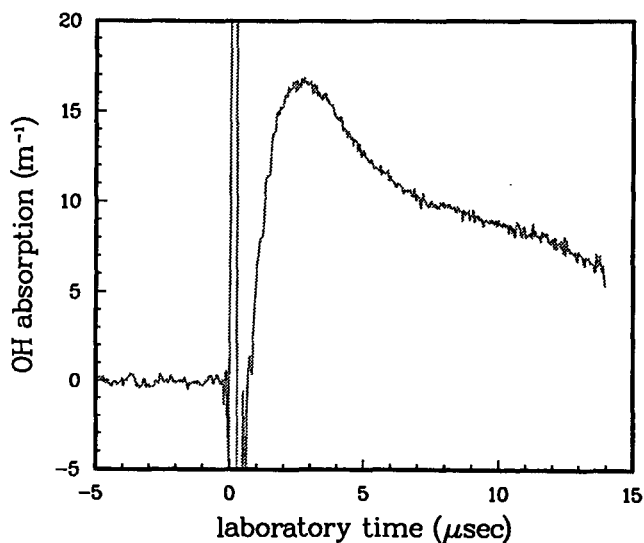


Figure 1. Absorption profile of hydroxyl at 2244 K and 174.7 k(Pa). The compression ratio, ρ_2/ρ_1 , gives $t_{\text{particle}} \approx 4.07t_{\text{lab}}$.

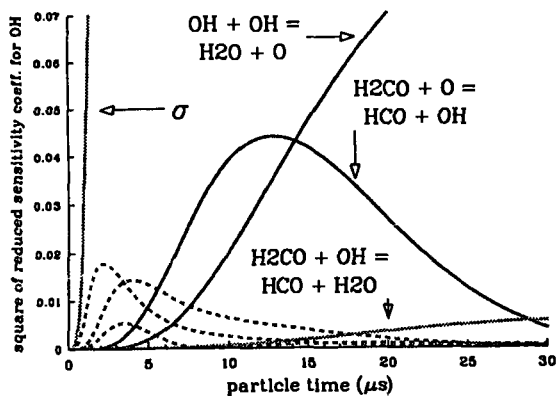


Figure 2. Square of the reduced sensitivity coefficients for the profile in figure 1.

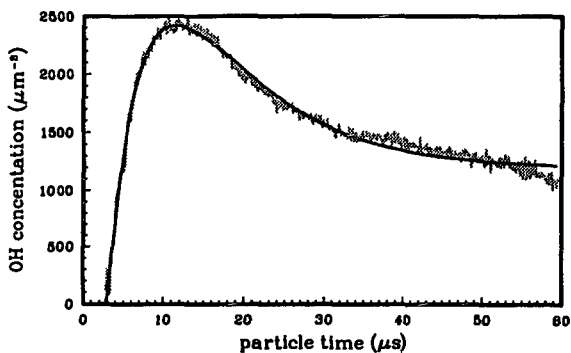


Figure 3. Non-linear least-squares fit of the profile in figure 1.

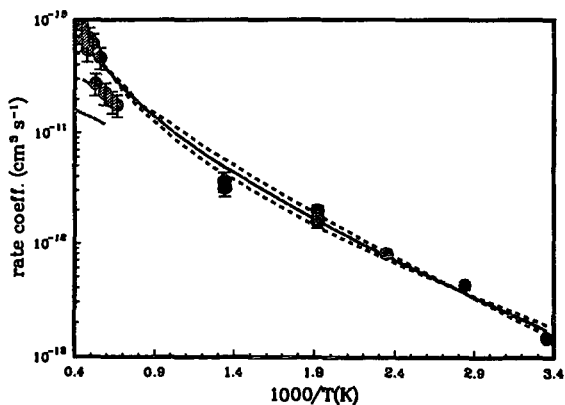


Figure 4. Rate coefficient for the $O + H_2CO \rightarrow OH + HCO$ reaction. The solid line is the best fit to the data and the dashed lines represent the 2σ boundary.

Thermal Decomposition Studies of Chlorocarbon Molecules
in a Shock Tube using the Cl-atom ARAS Method

K. P. Lim and J. V. Michael
Chemistry Division
Argonne National Laboratory
Argonne, IL 60439

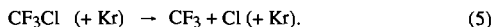
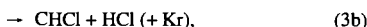
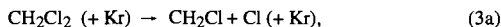
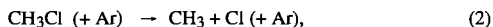
Keywords: Rate constants, Shock tubes, Chlorocarbon dissociations

ABSTRACT

Because of needs for understanding the chemical kinetic mechanism in chlorocarbon molecule incineration, we have recently completed studies on the thermal decompositions of COCl_2 , CH_3Cl , CH_2Cl_2 , CCl_4 , and CF_3Cl . The shock tube technique combined with atomic resonance absorption spectrometry (ARAS), as applied to Cl atoms, has been used to obtain absolute rate data for these reactions. In all cases, the decompositions are nearly in the second-order regime. Theoretical calculations, using the Troe formalism, have been performed. In these calculations, both the threshold energies for decomposition, E_0 , and the energy transferred per down collision, ΔE_{down} , are varied parametrically for best fitting to the data. The latter quantity determines the collisional deactivation efficiency factor, β_c .

INTRODUCTION

This article discusses thermal decomposition results obtained with the shock tube technique for five chlorocarbon molecules. One motivation is to supply thermal rate data for understanding the chemical destruction mechanisms in incinerators for this important class of compounds. The atomic resonance absorption spectrometric (ARAS) method is used to monitor the production of Cl atoms as they form during the decompositions. The reactions studied are:



We have attempted to rationalize the results on these reactions with Troe type theoretical fits that are based on C—Cl bond strengths and the average energy transferred per down collision.¹⁻³ The results of these comparative theoretical calculations are discussed.

EXPERIMENTAL

The shock tube methods that are used in the present studies are traditional⁴ and have been described in detail previously.⁵⁻⁹ Therefore, only a brief description will be given here. Experiments in both incident and reflected shock waves have been carried out on these systems. In both instances, corrections for non-ideal shock wave behavior have been applied.¹⁰ The tube has an optical path length of 9.94 cm, and the resonance radiation from a Cl-atom resonance lamp traverses the tube at a distance of 67 or 6 cm from the endplate for incident or reflected shock wave experiments, respectively.

In order to use the method, it was necessary to measure the curve-of-growth for Cl atoms. In experiments on CH_3Cl ,⁶ the curve-of-growth was determined; however, the results were slightly perturbed by secondary chemistry. We have checked the curve-of-growth by carrying out additional experiments with CF_3Cl where no such complications are present.⁹ The results are shown in Fig. 1 where they are compared to the dashed line determined previously.^{5,6} This result demonstrates that the perturbing secondary chemistry in the CH_3Cl case was adequately being described because the present agrees with the earlier result within experimental error. The line shown in the figure can be expressed in modified Beer's law form as:

$$-\ln(I/I_0) \equiv (\text{ABS}) = \sigma \ell [\text{Cl}]^\alpha = 4.41 \times 10^{-9} [\text{Cl}]^{0.581} \quad (6)$$

when $[\text{Cl}]$ is expressed in molecules cm^{-3} . Hence any value of $(\text{ABS})_i$ can be converted into $[\text{Cl}]_i$ thereby giving a Cl-atom concentration profile for any experiment.

RESULTS

The thermal decomposition results were obtained at three loading pressures in either incident or reflected shock wave experiments. Bimolecular rate constant values, $k/[\text{M}]$, were determined in each instance. The data were then plotted in Arrhenius form as shown in Figs. 2 to 7. Essentially no pressure effects could be documented in any of the cases within experimental error suggesting that the decompositions were near to the low pressure values. We then performed linear least squares analysis on the entire data base for each reactant. The results are given as equations (7) to (13) in units of $\text{cm}^3 \text{ molecule}^{-1} \text{ s}^{-1}$.

$$\text{Reaction (1a):} \quad k/[\text{Kr}] = 7.24 \times 10^{-8} \exp(-30594 \text{ K}/T) \quad (7)$$

$$\text{Reaction (1b):} \quad k/[\text{Kr}] = 7.60 \times 10^{-9} \exp(-30594 \text{ K}/T) \quad (8)$$

$$\text{Reaction (2):} \quad k/[\text{Ar}] = 1.09 \times 10^{-8} \exp(-29325 \text{ K}/T) \quad (9)$$

$$\text{Reaction (3a):} \quad k/[\text{Kr}] = 6.64 \times 10^{-9} \exp(-28404 \text{ K}/T) \quad (10)$$

$$\text{Reaction (3b):} \quad k/[\text{Kr}] = 2.26 \times 10^{-8} \exp(-29007 \text{ K}/T) \quad (11)$$

$$\text{Reaction (4):} \quad k/[\text{Ar}] = 1.19 \times 10^{-7} \exp(-25050 \text{ K}/T) \quad (12)$$

$$\text{Reaction (5):} \quad k/[\text{Kr}] = 1.73 \times 10^{-7} \exp(-33837 \text{ K}/T) \quad (13)$$

DISCUSSION

We have used the semi-empirical form of Troe theory¹⁻³ to calculate theoretical rate constants for these reactions. Since there are no potential energy surface calculations for the present cases, as described earlier,⁶ the best choice of transition states are the Lennard-Jones (LJ) complexes where the LJ-distance between the combining species is taken to be the reaction coordinate, and all rotational degrees of freedom in each of the combining species are considered to be free. Using conventional transition state theory, this model will always give, as the high pressure limit for the recombination of the two species making up the complex, the collision rate constant with electronic degeneracy factors included. Hence,

$$k_{-1LJ} = (g^\ddagger/g_1g_2) \sigma_{12}^2 \Omega(2,2)^* (8\pi kT/\mu)^{1/2} \exp(\epsilon_{12}/kT). \quad (14)$$

With $g^\ddagger = 1$, $g_1 = g_{\text{radical}} = 2$, and $g_2 = g_{\text{Cl}} = 2 (2 + \exp(-hc(882.36 \text{ cm}^{-1})/kT))$, equation (14) has been evaluated for the various back reactions. The value for the high pressure dissociation rate constants are then calculated as $k_{\infty} = k_{-1LJ}K$ where equilibrium constants, K , have been directly calculated from molecular constants.

The theory of Troe and coworkers¹⁻³ has then been used to calculate the limiting low pressure rate constants, k_{sc}^0 , which are functions of the various threshold energies, E_0 . These values for k_{∞} and k_{sc}^0 , along with the LJ model for the transition states and values for the collisional deactivation efficiency factor, β_c , can then be used to calculate values for S_K , B_K , F_{cent} and finally, $k/[\text{M}] = k_{\infty} F_{LH} F(P_r)$ where F_{LH} is the Lindemann-Hinshelwood factor, $P_r/(1+P_r)$, and $F(P_r)$ is the broadening factor, a function of reduced pressure, $P_r = \beta_c k_{sc}^0 [\text{M}]/k_{\infty}$. The parameter, ΔE_{down} , determines β_c . In all of the present calculations, we parametrically vary both E_0 and ΔE_{down} . The final fitted theoretical results are compared to the data in Figs. 2-7.

For COCl_2 , parametric calculations were carried out with E_0 between 65.4 and 77.5 kcal mole⁻¹ and with respective ΔE_{down} values between 420 and 4897 cm^{-1} .⁵ Mutual values, (75.5, 2553), (75.0, 2169), (74.5, 1714), or (73.75, 1574), can explain the data shown in Fig. 2; however, the best overall fit is with the third set. This threshold value implies a heat of formation for COCl that is consistent with new thermochemical data¹¹ within experimental error. Similar parametric calculations were carried out for CH_3Cl , again yielding a range of acceptable values which are: (81.3, 866), (80.3, 761), (79.3, 638), (78.3, 560), or (77.3, 490). The calculation for the middle set is shown in Fig. 3. Using the heat of formation for CH_3Cl given in the JANAF tables,¹² the

implied E_0 value would be $82.32 \text{ kcal mole}^{-1}$. Since the heats of formation of Cl and CH_3 are not in doubt, the present results would suggest a $(-3.0 \pm 2.0) \text{ kcal mole}^{-1}$ modification to $(-15.1 \pm 2.0) \text{ kcal mole}^{-1}$ for the heat of formation of CH_3Cl at 0 K. It should be pointed out that the large ΔE_{down} value of 1600 cm^{-1} , reported earlier,⁶ is mostly due to the fact that E_0 was fixed at the JANAF value of $82.32 \text{ kcal mole}^{-1}$. Two thermal decomposition processes have to be considered in the thermal decomposition of CH_2Cl_2 .⁷ The one that gives Cl atoms is about one-third of the molecular elimination process. We have carried out parametric calculations on both processes. The Cl-atom process can be fitted with mutual values, (81.25, 560), (78.25, 394), and (75.25, 268) with the middle set being only slightly superior at all pressures. The best set for the molecular elimination process is (73.0, 630). These two best fits are shown in Figs. 4 and 5. Our conclusion is that the heat of formation for CH_2Cl at 0 K is $(28.5 \pm 3.0) \text{ kcal mole}^{-1}$, and this agrees with a recent evaluation.¹³ Several Troe calculations have been carried out for CCl_4 using only the ARAS data from this laboratory.⁸ Mutual values, (68.7, 1329), (67.7, 1049), (66.7, 735), (65.7, 560), or (64.7, 428), bracket the acceptable sets of fits. The lines shown in Fig. 6 are calculated from the middle set. Hence, the implied value for E_0 is $(66.7 \pm 2.0) \text{ kcal mole}^{-1}$, and this agrees with a recent thermochemical determination for the heat of formation of CCl_3 , $16.7 \text{ kcal mole}^{-1}$.¹⁴ Lastly, the acceptable parametric fits for the CF_3Cl experiments⁹ are: (87.0, 1049), (86.0, 857), (84.8, 700), or (84.0, 595). The best fit is with the second set implying that $E_0 = (86.0 \pm 2.0) \text{ kcal mole}^{-1}$, and this calculation is shown in Fig. 7. This suggests that the heat of formation for CF_3Cl at 0 K is $(-1.2 \pm 2.0) \text{ kcal mole}^{-1}$ lower than the JANAF value¹² at $(-169.2 \pm 2.0) \text{ kcal mole}^{-1}$. Therefore, the present value agrees with JANAF within experimental error. The findings from the theoretical calculations are summarized in Table I.

In four out of the five cases, the thermochemical conclusions from the present analysis are in agreement with earlier thermochemical data. The only exception is CH_3Cl where a downward modification of $3.0 \text{ kcal mole}^{-1}$ in the heat of formation would be more compatible with our results. Stronger thermochemical conclusions from the present results are simply not possible because, in each case, there are a number of acceptable fits spanning a range of threshold energies. In principal, this range could be narrowed if the temperature range were substantially expanded; however, with the present ARAS technique, a large increase in the temperature range is not possible. We point out that even if the temperature range was much greater, there is a strong coupling between E_0 and ΔE_{down} (i. e., they are strongly correlated). Hence, an uncertain knowledge in either parameter creates a significant uncertainty in the other quantity. Troe and coworkers have given a rationale for understanding the behavior of the collisional deactivation efficiency factor, β_c , in terms of the energy loss per collision with bath gas molecules. These factors decrease with increasing temperature thereby supplying a reason for the usual observation that apparent experimental activation energies are always lower than the bond strengths of the bond being broken in a dissociation. This is a significant advance in understanding; however, it is still true that there is really no first principles theory for *a priori* calculation of these quantities.¹⁵ Trends in β_c 's (or in the ΔE_{down} values that determine them) might be discovered if the thermochemistry is known perfectly. This may be the case in hydrocarbon chemistry; however, there are still uncertainties in the chlorocarbon thermodynamic functions. We believe that this is a partial explanation for the unrelated values for ΔE_{down} in Table I. With this state of affairs, continuing experimental studies on this type of molecule are absolutely necessary if the thermal rate behavior is desired for any reason. Theoretical calculations alone will not be predictive and therefore will not be helpful.

ACKNOWLEDGMENT

This work was supported by the U. S. Department of Energy, Office of Basic Energy Sciences, Division of Chemical Sciences, under Contract No. W-31-109-Eng-38.

REFERENCES

1. Troe, J., *J. Chem. Phys.* **65**, 4745 (1977); *ibid.*, 4758 (1977).
2. Troe, J., *J. Phys. Chem.* **83**, 114 (1979).
3. Troe, J., *Ber. Bunsenges. Phys. Chem.* **87**, 161 (1983).
4. Bradley, J. N., *Shock Waves in Chemistry and Physics*, Wiley, New York, 1962.
5. Lim, K. P., and Michael, J. V., *J. Phys. Chem.*, in press.
6. Lim, K. P., and Michael, J. V., *J. Chem. Phys.* **98**, 3919 (1993).
7. Lim, K. P., and Michael, J. V., *Symp. (Int.) Combust.*, [Proc.] **25**, submitted.
8. Michael, J. V., Lim, K. P., Kumaran, S. S., and Kiefer, J. H., *J. Phys. Chem.* **97**, 1914 (1993).
9. Kiefer, J. H., Sathyanarayana, R., Lim, K. P., and Michael, J. V., *J. Phys. Chem.*, submitted.
10. Michael, J. V., and Sutherland, J. W., *Int. J. Chem. Kinet.* **18**, 409 (1986).
11. Nicovich, J. M., Kreutter, K. D., and Wine, P. H., *J. Chem. Phys.* **92**, 1429 (1992).
12. Chase, M. W. Jr., Davies, C. A., Downey, J. R. Jr., Frurip, D. J., McDonald, R. A., and Syverud, A. N., *J. Phys. Chem. Ref. Data* **14**, Supplement No. 1 (1985).
13. Manion, J. A., and Rodgers, A. S., *Thermodynamic Tables, Non-Hydrocarbons*, Thermodynamics Research Center, Texas A & M University Press, College Station, TX, June 30, 1993, p. r-7250 - r-ref-7251.
14. Hudgens, J. W., Johnson, R. D. III, Timonen, R. S., Seetula, J. A., and Gutman, D., *J. Phys. Chem.* **95**, 4400 (1992).
15. Michael, J. V., and Lee, J. H., *J. Phys. Chem.* **83**, 10 (1979); Michael, J. V., *ibid.*, 17 (1979).

Table 1. Theoretical Results

Reaction	$\Delta E_{down}/\text{cm}^{-1}$	$E_0/\text{kcal mole}^{-1}$	Comments	Ref.
$\text{COCl}_2 (+ \text{Kr}) \rightarrow \text{COCl} + \text{Cl} (+ \text{Kr})$	1714	74.5 ± 1.0	75.6 implied by	11,12
$\text{CH}_3\text{Cl} (+ \text{Ar}) \rightarrow \text{CH}_3 + \text{Cl} (+ \text{Ar})$	638	79.3 ± 2.0	compared to 82.3	12
$\text{CH}_2\text{Cl}_2 (+ \text{Kr}) \rightarrow \text{CH}_2\text{Cl} + \text{Cl} (+ \text{Kr})$	394	78.25 ± 3.0	79.0 implied by	12,13
$\rightarrow \text{CHCl} + \text{HCl} (+ \text{Kr})$	630	73.0 ± 3.0	79 or 70.1, from	12 or 13
$\text{CCl}_4 (+ \text{Ar}) \rightarrow \text{CCl}_3 + \text{Cl} (+ \text{Ar})$	735	66.7 ± 2.0	67.7 implied by	12,14
$\text{CF}_3\text{Cl} (+ \text{Kr}) \rightarrow \text{CF}_3 + \text{Cl} (+ \text{Kr})$	857	86.0 ± 2.0	compared to 84.8	12

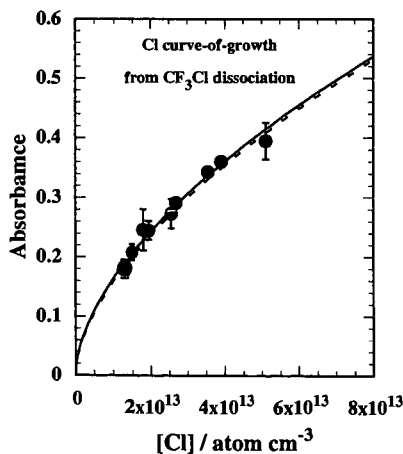


Fig. 1

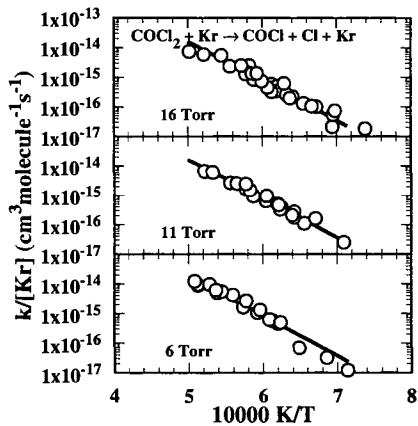


Fig. 2

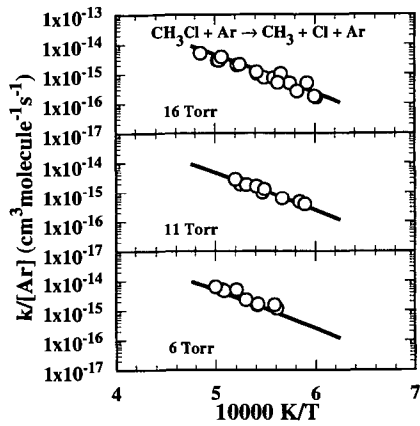


Fig. 3

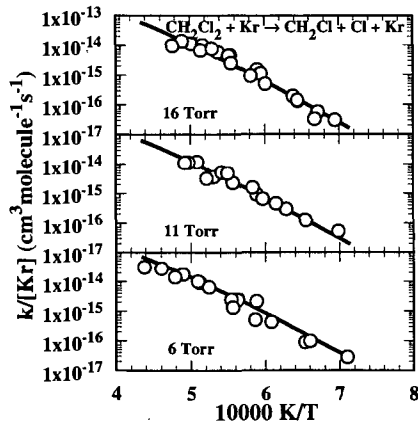


Fig. 4

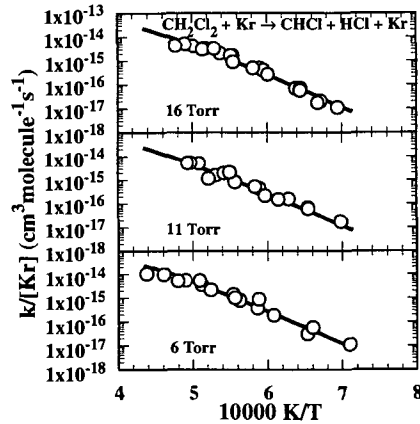


Fig. 5

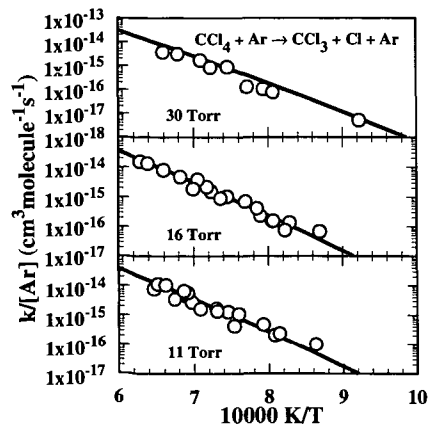


Fig. 6

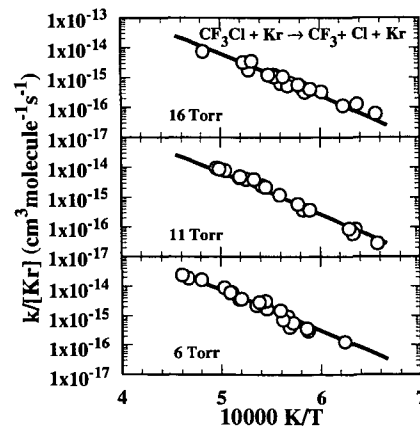


Fig. 7

SINGLE PULSE SHOCK TUBE STUDIES ON THE UNIMOLECULAR
DECOMPOSITION OF LARGE UNSATURATED MOLECULES:
TRANS-1-PHENYL-1-PENTENE

Wing Tsang and James A. Walker
Chemical Kinetics and Thermodynamics Division
National Institute of Standards and Technology
Gaithersburg, MD 20899

Keywords: 1-phenyl-1-pentene, decomposition, shock tube

Introduction

Decomposition kinetics represent an important component of combustion chemistry. A challenging aspect of this chemistry involves the building up, breakdown and rearrangements of large and unsaturated structures. In this paper experiments that lead to quantitative information on the thermodynamic and kinetic properties of these large unstable species will be described. The aim is to provide a base of information upon which predictions can be made. Thus the concentration on single step thermal reactions. Previously, the methodology has been employed to determine unimolecular rate constants (at the high pressure limit) for the decomposition of a large variety of alkenes, alkynes and benzyl compounds. These have also led to a determination of the heat of formation of the large radicals that are formed. A summary of earlier results can be found in Table 1.

	Rate Expressions	Constants (1100)
	s^{-1}	
1-hexene \rightarrow allyl+n-propyl ¹	$8 \times 10^{15} \exp(-35600/T)$	70
\rightarrow 2 propene	$4 \times 10^{12} \exp(-28900/T)$	16
1-hexyne \rightarrow propargyl+n-propyl ¹	$8 \times 10^{15} \exp(-36300/T)$	37
\rightarrow allene+propene	$5 \times 10^{12} \exp(-28400/T)$	31
phenylpentane \rightarrow benzyl+n-butyl ²	$1 \times 10^{16} \exp(-36500/T)$	39
c-hexene-2 \rightarrow t-hexene-2 ³	$4 \times 10^{14} \exp(-33333/T)$	37
t-1,3pentadiene- \rightarrow c-1,3pentadiene ⁴	$4 \times 10^{13} \exp(-26700/T)$	287

Table 1. Earlier Data on the Decomposition of Unsaturated Compounds

The present study is concerned with a molecule that contains both aromatic and olefinic groups, trans 1-phenylpentene (TPP). Possible mechanisms for decomposition can be found in Figure 1. They involve the cleavage of the resonance weakened C-C bond (2) leading to the formation of 3-methylallyl radical and ethyl, a retroene reaction (1) that forms ethylene and allylbenzene directly and trans to cis(CPP) isomerization (3). All of these reactions have their counterparts in the simpler compounds. Some of the results are listed in Table 1. The quantitative results will bear on a number of interesting issues. In the case of trans-cis isomerization, it will be possible to determine the effect of benzyl resonance. From the rate expression for bond breaking, the activation energy will lead directly to the heat of formation of the 3-phenylallyl radical and in turn its resonance energy. The A-factor can be compared with that for reactions of the 1-olefins, thus leading to information on the effect of the addition to the phenyl group to the vinyl structure. Of particular interest will be the fate of the 3-phenylallyl radical. It can undergo beta bond scission to form phenyl allene or internal displacement to form indene. The latter is especially interesting since it represents the formation of the second ring in such systems. We have observed indene formation in the hydrogen atom induced decomposition of 1-phenylpropene and for the purposes of determining abstraction rate constants it is important to demonstrate that the conversion is quantitative. Similarly, it will be possible to determine how the rate constants for the molecular, retroene, process will be effected in the more complex environment of this molecule.

Single pulse shock tube studies have unique capabilities for

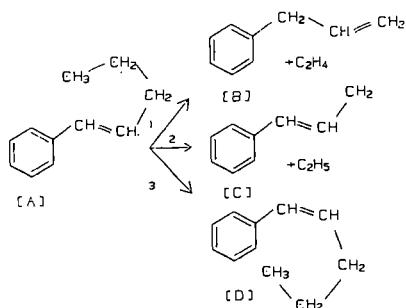


Figure 1. Mechanism for the decomposition of trans-1-phenyl-1-pentene. A=Trans-1-phenyl-1-pentene, B=Allylbenzene, C=3-phenylallyl, D=Cis-1-phenyl-1-pentene

determining the thermal decomposition properties of large organic molecules. There is no chance of surface processes. Final product analysis using gas chromatography with flame ionization detection offers the possibility of detecting all reactants and products. Multiple reaction channels can thus be quantitatively investigated. By working at dilute concentrations, in the presence of a chemical inhibitor, all chain processes can be suppressed. The high temperatures are an important factor in assuring that practically all large organic radicals are decomposed in a time scale such that only the initial and subsequent unimolecular decomposition processes can occur. This is an important aid in the interpretation of the results. The isolation of individual reactions for study means that it is possible to study a number of unimolecular decompositions simultaneously. This is the basis of the internal standard method and removes the uncertainty in the reaction temperature, an important contributing factor to errors in single pulse shock tube experiments. The general technique has been successfully used to determine the rate expression for unimolecular decomposition of many organic compounds. For bond breaking reactions, these lead directly to heats of formation of the organic radicals that are formed. It is by this technique that the first indications were obtained regarding the need for an upgrading of the then generally used heats of formation of simple alkyl radicals⁵.

There have been no previous study on the decomposition of TPP. Robaugh and Stein⁶ have studied in VLLP experiments the decomposition of 1-phenyl-1-butene. Assuming an A-factor of $2 \times 10^{15} \text{ s}^{-1}$, they find an activation energy of 282 kJ/mol leading to an "extra" resonance energy in comparison to that for benzyl of 23 kJ/mol. From the data in Table 1 it can be seen that the breaking of the C-C bond in these cases are characterized by A-factor near 10^{16} s^{-1} and resonance energies near 45 kJ/mol. The former is a factor of 3 smaller than the characteristic values for alkanes while the latter is directly reflected in the activation energy. The smaller A-factor for alkene and alkyne decomposition can be attributed to the tightened structure of the resonance stabilized radical that is formed and contrasts with the alkyl radicals formed during alkane decomposition. Overall, the unimolecular rate constants are increased by factors ranging from 20 to 30 as a result of allylic and benzyl substitution at the present temperatures. For the 3-phenylallyl radical, the structure compared to the molecule is even tighter since two weakly hindered rotors will in the radical become torsions. At these temperatures, retroene reactions are competitive with the bond breaking reaction for the alkenes and alkynes (see Table 1) but apparently does not occur for the benzyl compounds. The recommended rate expressions for the cis \leftrightarrow trans isomerization demonstrate that the full value of the resonance energy is manifested in the transition state. There appears to be

surprisingly large differences in the A-factors. Nevertheless, the changes are in the proper direction.

Experimental

Experiments are carried out in a heated single pulse shock tube. The entire shock tube and the gas handling system is maintained at 100°C. This permits the introduction and withdrawal from the shock tube of quantitative mixtures of low-volatility compounds. Details of the apparatus and the procedures can be found in earlier papers¹. Analysis is by gas chromatography with flame ionization detection. Two columns are used for the analysis. The light hydrocarbons, principally ethylene are separated with a 12 foot Poropak N⁷ column operated at 50 C. For the heavier species, from C₄ on up, a wide bore 30 meter dimethylsiloxalane column in the programmed temperature mode is used for analysis. Toluene is used as the chemical inhibitor. The ratio of toluene to the TPP is maintained at 200 to 1. This guarantees that all the reactive radicals will react with toluene in preference to the TPP. Stable benzyl radicals are formed. Under the conditions of the shock tube experiments they can only recombine with itself or other radicals that are present. They have insufficient time to react with the TPP. As a result the initial unimolecular decomposition reaction is isolated for study. For the determination of rate expressions, the use of an internal standard as the reference reaction¹ ($k(1\text{-methylcyclohexene} = \text{isoprene} + \text{ethylene}) = 10^{15} \exp(-33500/T) \text{s}^{-1}$) permits the calculation of the reaction temperature on the basis of the extent of reaction and the heating time (500 microseconds).

Results

The important products formed from the thermal decomposition of dilute concentrations of TPP in large excesses of toluene are listed in Table I. Also present are considerable amounts of methane and smaller quantities of ethane and ethylbenzene. These are the expected products from the hydrogen atom induced decomposition of toluene. These were not needed for the quantitative analysis of the data. Excellent mass balances are realized and it is clear that the mechanism outlined in Figure 1 fully accounts for the decomposition processes. Benzene is from the reaction of hydrogen atom with toluene and the amount that is formed is in reasonable agreement from that which would have been predicted on the basis of earlier determinations of hydrogen atom attack on toluene. Note that the benzene formed is a measure of all the hydrogen that can be formed in the reactive system. This can include impurities or small quantities from the decomposition of toluene, the inhibitor itself. Ethylene is formed from the decomposition of the ethyl radical and directly from the retroene reaction. From the allylbenzene yields, it is apparent that the latter is only a minor reaction channel. Unfortunately allylbenzene is present as an impurity in the reaction mixture.

Table 2: Typical Product Distribution from the Decomposition of 100 ppm Phenyl-1-Pentene in 2% Toluene at 2 atm. pressure

Compounds	Temperature (K)		
	1057	1080	1149
ethylene	2.7	4.9	27.3
benzene	1.7	3.0	17.2
allylbenzene		.62	1.3
indene	2.2	4.3	24.5
cis-phenyl-1-pentene	4.4	6.6	13.1
trans-phenyl-1-pentene	93.9	88.2	60.4

Thus it proved impossible to make a high accuracy determination of the rate expression of the retroene reaction. Nevertheless it is interesting that, as required, the sum of the allylbenzene and indene concentration is close to that of the ethylene found. Indene and the cis isomer are the major large reaction products.

The former is more important at high extent of reaction. The satisfactory mass balance indicates that all the 3-phenylallyl radical formed is converted into indene. Further confirmation is offered by the absence of any of the phenyl butenes, the expected product from the addition of methyl radicals to 3-phenylallyl. This radical should exist in the cis and trans conformation and it is only from the cis isomerization that indene can be formed. The present results demonstrate that under high temperature conditions this isomerization must be quite rapid. No phenyl allene is detected. Beta bond cleavage is not competitive with internal displacement. This is not surprising since it is expected that the activation energy for the ejection of a beta hydrogen bond in this system will have an activation energy of 260 kJ/mol.

A small uncertainty is introduced into the quantitative interpretation of the results in terms of bond breaking by the simultaneous conversion of TPP to the cis-isomer with the bond breaking reaction. The cis-isomer can of course also undergo the retro-ene and bond breaking reactions. At the high temperatures of these experiments the properties of the cis and trans isomers are very similar. It should be possible to speak of a single average entity. Furthermore, the concentration of the cis compound is never more than 20% of the trans species. On this basis and using the relation $k = \log(1 - X \cdot \text{indene}/(\text{TPP})) / X \cdot t$ where t is the residence time of about 500 microseconds and $X = 1 + \text{allylbenzene}/\text{indene}$ and represents the contribution from the retroene channel, an Arrhenius plot of the data can be found in Figure 1. This leads to the following rate expression for the bond breaking reaction $k(\text{TPP} \rightarrow 3\text{-phenylallyl} + \text{ethyl}) = 4 \times 10^{15} \exp(-34010/RT) \text{ s}^{-1}$ over the temperature range of 1000-1180 K. and at a pressure of argon of approximately 2 atms.

As noted earlier, accurate determination of the concentration of allylbenzene is made difficult by its presence as an impurity. The consequence is that it is necessary to subtract two numbers. Thus as can be seen in Figure 1, the data show considerable scatter. The rate expression that is obtained $k(1\text{-PP} \rightarrow \text{allylbenzene} + \text{C}_2\text{H}_4) = 1.9 \times 10^{11} \exp(-25640/T) \text{ s}^{-1}$ has parameters that are much lower than that listed above. Nevertheless, it is probably not an accident that at 1100 K the rate constant is 14 s^{-1} or very close to the value for hexene decomposition to form two propene. It is suspected that the expression in Table 1 is more likely to be the correct one.

From the yields of cis-1-phenylpentene (CPP), the rate expression for trans \rightarrow cis isomerization can be obtained. The rate relation is $k_3 = \log(1(\text{CPP}/\text{TPP})) / (1 + K_{\text{eq}}) \exp(k_1 + k_2)t / (1 + K_{\text{eq}}) t = k_3$ where $K_{\text{eq}} = k_3/k_{-3}$ and is derived from the observed convergence of the ratio of the trans and cis compounds as the temperature is increased. This ratio, 3.9 implies the greater stability of the trans compounds and is contrary to the published results for the analogous phenylpropenes⁹. An Arrhenius plot of the results can also be found in Figure 1. This leads to the rate expression $1.5 \times 10^{13} \exp(-27400/T) \text{ s}^{-1}$.

Discussion

The experimental rate constants are only slightly larger than that determined by Robaugh and Stein. Since their study involves the ejection of a methyl group instead an ethyl the differences should be somewhat larger. It is suspected that the discrepancies are about a factor of 1.5 to 2. High pressure rate constants are not directly determined from VLPP studies and this type of differences may arise from the extrapolational procedure.

Assuming that combination rate constants involving 3-phenylallyl and ethyl radical have no temperature dependence, the enthalpy of reaction at 1100 K is 291 kJ/mol. From known thermodynamics⁸ this is equivalent to a resonance energy of the 3-phenylallyl radical of 66 ± 6 kJ/mol and can be compared with that for allyl and benzyl of about 50 ± 4 kJ/mol¹. The heat of formation of the 3-phenylallyl radical is 228 ± 6 kJ/mol. The A-factor is an

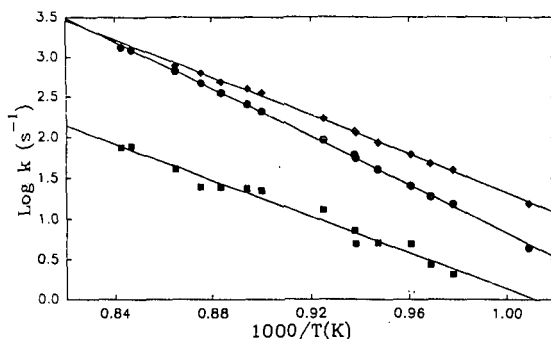


Figure 2: Arrhenius Plots for the Decomposition of t-1-phenylpentene to form 3-phenylallyl + C₂H₅, (●); cis-1-phenylpentene, (◆); and allylbenzene + C₂H₄, (■).

order of magnitude and half an order of magnitude lower than those for alkanes and alkenes, respectively and is consistent with the very stiff radical (no free rotors) that is formed. At lower temperatures rate constants for cis isomerization are larger than that for bond cleavage. They are consistent with an activation energy that feels the full effect of the benzyl resonance energy. The retroene reaction is slower than for bond cleavage. It appears that phenyl substitution does not have much effect on the rate constants. The satisfactory mass balance also means that there are no other processes that make contributions to the decomposition process as the molecular complexity is increased.

The formation of indene from 3-methylallyl must involve an internal addition followed by the displacement of the hydrogen atom. This is an endothermic process. From the heat of formation of 3-methylallyl and indene⁹ the enthalpy of reaction is 63 kJ/mol. When this is coupled with the estimated barrier for addition of hydrogen to indene leading to the breaking of the olefinic ring structure one obtains an overall barrier for cyclization of 89 kJ/mol. This barrier is made up of a barrier to addition and then that for ejection of hydrogen. An actual rate expression could be derived if there are reliable values for the entropies of indene. In its absence, a typical value of the A-factor, 10¹¹s⁻¹, coupled with the barrier for cyclization will lead to rate constants near 0.5 microseconds at 1100 K. Quantitative conversion to indene must occur.

References

1. Tsang, W., "Comparative Rate Single Pulse Shock Tube in the Thermal Stability of Polyatomic Molecules," Shock Tubes in Chemistry, A. Lifshitz ed., Marcel Dekker, pg. 59, 1981.
2. Walker, J. A. and Tsang, W., J. Phys. Chem., 94, 3324, 1990
3. Bauer, S. H., Yadava, B. P. and Jeffers, P., J. Phys. Chem., 76, 770, 1974
4. Marley, W. N. and Jeffers, P., J. Phys. Chem., 79, 2085, 1975
5. Tsang, W., J. Amer. Chem. Soc., 2873, 1985
6. Robaugh, D. A. and Stein S. E., J. Amer. Chem. Soc., 108, 3224, 1985
7. Certain commercial materials and equipment are identified in this paper in order to specify adequately the experimental procedure. In no case does such identification imply recommendation or endorsement by the national Bureau of Standards, nor does it imply that the material or equipment is necessarily the best available for the purpose.
8. Stull, D. R., Westrum, E. F., and Sinke, G. C., "The Chemical Thermodynamics of Organic Compounds" John Wiley and Sons, New York, 1969.
9. Cox, J. D. and Pilcher, G. "Thermochemistry of Organic and Organo-Metallic Compounds", Academic Press, New York, 1970

FLUORINATED HYDROCARBON FLAME SUPPRESSION CHEMISTRY

D. Burgess, Jr., W. Tsang, and M.R. Zachariah
Chemical Science and Technology Laboratory
National Institute of Standards and Technology
Gaithersburg, MD 20899

and
P.R. Westmoreland
Department of Chemical Engineering
University of Massachusetts
Amherst, MA 01003

Keywords: Combustion Chemistry; Reaction Mechanism; Flame Inhibition

ABSTRACT

A comprehensive, detailed chemical kinetic mechanism was developed for fluorinated hydrocarbon destruction and flame suppression. Existing fluorinated hydrocarbon thermochemistry and kinetics were compiled and evaluated. For species where no/incomplete thermochemistry was available, this data was calculated through application of ab initio molecular orbital theory. Group additivity values were determined consistent with experimental and ab initio data. For reactions where no or limited kinetics was available, this data was estimated by analogy to hydrocarbon reactions, by using empirical relationships from other fluorinated hydrocarbon reactions, by ab initio transition state calculations, and by application of RRKM and QRRK methods. The chemistry was modeled considering different transport conditions (plug flow, premixed flame, opposed flow diffusion flame) and using different fuels (methane, ethylene), equivalence ratios, agents (fluoromethanes, fluoroethanes) and agent concentrations. An overview of this work is presented.

INTRODUCTION

During the past year a major effort was conducted at NIST to rate potential replacements (FCs, HFCs, HCFCs) for Halon 1301 (CF₃Br). Halon 1301 has been widely used as a chemical extinguisher in sensitive/critical environments where it is necessary to use fire suppressants that are clean (minimal residue & reactivity), non-toxic, and non-conductive. These environments include aircraft, nuclear reactors, computer rooms, and libraries. Halon 1301 has all of these desirable properties and is extremely effective for fire suppression. Unfortunately, it is also extremely effective for depleting stratospheric ozone (attenuates damaging UV radiation from the sun). Consequently, production and use of Halon 1301 and other high ODP chemicals are being banned on a worldwide level.

The chemical kinetic modeling work presented here is a small part of larger, short term intensive program at NIST evaluating potential replacements for Halon 1301 for the U.S. Air Force, Navy, Army and Federal Aviation Administration. The modeling effort complemented the many experimental measurements in the overall NIST program characterizing the effectiveness of various potential replacements. Our work focused on agent chemistry. However, there are also many physical effects relating to mass and heat transport processes. Many of these issues were addressed by other work in the overall project. This included measurements of PVT properties, discharge dynamics, dispersion mechanics, as well as measurements of extinction effectiveness for more realistic geometries than can be modeled. In our work, we attempted to consider indirectly these physical effects in order to provide a framework for transfer of the results of our simulations to more realistic conditions.

FLUORINATED HYDROCARBON SYSTEM

The major objective of this work was to provide a chemical basis for rationalizing the relative degree of effectiveness of each candidate agent. In order to accomplish this objective, it was necessary to develop a chemical mechanism based on elementary reaction steps for their destruction, their participation in and influence on hydrocarbon flame chemistry, as well as prediction of potential by-products of incomplete combustion. The focus of this work was restricted to chemistry involving only fluoromethanes and fluoroethanes. This included both agents specifically considered in the overall NIST project as replacements (CH₂F₂, CF₃-CH₂F, CF₃-CHF₂, CF₃-CF₃), as well as all other possible fluoromethanes and fluoroethanes. The chlorine-substituted (CHF₂Cl, CF₃-CHF₂Cl) and larger fluorinated hydrocarbon (C₃F₈, C₃F₇H, C₄F₁₀, cyclo-C₄H₈) candidates were not considered in our study because they would significantly increase the complexity of the chemistry. However, the effectiveness of each can be estimated to some degree by analogy to

other agents that were studied using qualitative trends observed and a fundamental understanding of the chemistry.

The complete set of fluoromethanes and fluoroethanes were studied for two basic reasons.

First, when the four considered candidate agents decompose in the flame, they generate a pool of fluorinated hydrocarbon stable species and radicals, which results in the formation of many other fluoromethanes and fluoroethanes. Consequently, in order to adequately describe the decomposition of these four agents (and resultant chemistry), it is necessary to describe the chemistry of all intermediates and products that are created, including most of the other fluoromethanes and fluoroethanes. For example, the lowest energy and primary decomposition pathway for one of the agents, $\text{CF}_3\text{-CF}_3$, involves dissociation of the C-C bond to form (two) CF_3 radicals. The CF_3 radicals then react with methyl radicals (CH_3), which are present in significant concentrations in hydrocarbon flames. This radical-radical combination has two channels whose relative importance depend upon temperature. These channels result in the formation of both a fluoroethylene, $\text{CH}_2=\text{CF}_2$ (and HF), and another fluoroethane, $\text{CH}_3\text{-CF}_3$. In order to correctly predict flame products, the magnitude and rate of heat release in the flame, and ultimately the effectiveness of the added agent, it is also necessary to correctly describe the decomposition of these additional stable fluorinated hydrocarbon species ($\text{CH}_3\text{-CF}_3$, $\text{CH}_2=\text{CF}_2$). When one considers decomposition channels for these molecules, other reaction channels for CF_3 , and relevant chemistry for other candidates, most of the fluoromethanes and fluoroethanes must also be considered.

Second, since there was no directly related experimental work, it was imperative to provide a level of self-consistency by considering a range of modeling parameters, including a variety of reactor/flame geometries, fuels, and (potential) agents. This provided a level of confidence and some validation of the qualitative trends that we observed. Quantitative prediction of the absolute or even relative effectiveness of the specific agents will require benchmarking of the simulations with experimental measurements. It is anticipated that this will be done in the near future.

SPECIES THERMOCHEMISTRY

A large comprehensive reaction set or "mechanism" for fluorinated hydrocarbon chemistry was constructed including C_1 and C_2 stable and radical hydrocarbon species, as well as partially oxidized fluorinated hydrocarbons. Existing thermochemical data was compiled and evaluated. A number of general sources were used [1-5], as were compilations/evaluations [6,7] and individual sources [8-11] for fluorinated hydrocarbons. Where little or no data existed for species of interest (most radicals), we estimated that thermochemistry using either empirical methods (e.g. group additivity) or through applications of ab initio molecular orbital theory. In all cases (experimental, empirical, ab initio), an effort was made to use thermochemistry consistent with data for all species.

Standard hydrogen/oxygen and hydrocarbon thermochemistry was used, most of which can be found in the JANAF tables [2], as can data for F, F_2 , and HF. FO^* , FOO^* , FOF , and HOF species were initially considered, but later excluded, because their concentrations were found to be negligible in the high temperature hydrocarbon flames.

Thermochemical data for the fluoromethanes (CH_3F , CH_2F_2 , CHF_3 , CF_4) can be found in the JANAF tables [2] and has also been reexamined more recently [12]. Thermochemical data for the perfluoromethyl radical ($^*\text{CF}_3$) can be found in the JANAF tables. Reliable, experimentally derived heats of formation for the other fluoromethyl radicals ($^*\text{CH}_2\text{F}$, $^*\text{CHF}_2$) and a more recent value for $^*\text{CF}_3$ can be found in other evaluated sources [9,11,13]. Ab initio calculations of thermochemical data [14-16] for the fluoromethanes and fluoromethyls are consistent with the experimentally derived values. In this work we employed thermochemical data for the fluoromethylenes ($:\text{CHF}$, $:\text{CF}_2$) from the JANAF tables. However, there is some uncertainty (± 10 - 20 kJ/mol) in heats of formation for these important species. Furthermore, there have been recent measurements and evaluations [8,10,17,18] and ab initio calculations [14,15] that need to be evaluated. Thermochemical data for $\text{CHF}=\text{O}$, $\text{CF}_2=\text{O}$, $^*\text{CF}=\text{O}$, and $^*\text{CF}$ can be found in the JANAF tables. However, there is some uncertainty (± 10 - 20 kJ/mol) in the heats of formation for $\text{CHF}=\text{O}$ and $^*\text{CF}=\text{O}$ as their heats of formation were calculated using average

bond dissociation energies from other compounds. Our ab initio calculations [15] of thermochemistry for these carbonyl fluorides are consistent with the indirect, experimentally derived values. However, given the uncertainty in all of the data, further mechanism refinement will require critical evaluation of these data.

Experimentally derived thermodynamic properties for six fluoroethanes have been compiled and critically evaluated [6]. Data for other fluoroethanes can be found in the DIPPR compilation [5]. There are experimentally derived thermochemical data [8] for only a few fluoroethyl radicals ($\text{CH}_3\text{-CH}_2^\bullet$, $\text{CF}_3\text{-CH}_2^\bullet$, $\text{CF}_3\text{-CF}_2^\bullet$). However, thermochemistry for all fluoroethyl radicals have been calculated using ab initio molecular orbital theory by Tschuikow-Roux et al [19] and for a few fluoroethyl radicals by other workers [14-16]. For consistency, we have used the Tschuikow-Roux et al values. Experimentally derived thermochemistry is available for $\text{CF}_2=\text{CF}_2$ in the JANAF tables [2] and for $\text{CH}_2=\text{CHF}$ and $\text{CH}_2=\text{CF}_2$ in the DIPPR compilation [5]. For the other fluoroethylenes: $\text{CHF}=\text{CHF}(\text{E})$, $\text{CHF}=\text{CHF}(\text{Z})$, $\text{CHF}=\text{CF}_2$, we relied upon ab initio calculations [14]. We are not aware of any experimentally derived thermochemistry for fluorovinyl radicals and, consequently, used our ab initio calculated values [15]. Further mechanism refinement would involve benchmarking ab initio calculations with the experimental data (using bond and group additivity methods) to provide a consistent set of data for the fluoroethanes, -ethyls, -ethylenes, and -vinyls.

REACTION SET DEVELOPMENT

The literature on reaction kinetics for fluorinated hydrocarbons was compiled, reviewed, and evaluated. A large part of our work is based on the pioneering work of Biordi et al [20] and Westbrook [21]. Due to the limited nature of this paper, the reaction set that we developed can only be outlined here. Many of the rate constants can be found in the NIST Chemical Kinetics Database [22].

Utilizing species identified as potentially important, we constructed a grid of possible reactions. Existing chemical rate data involving these fluorinated species were then compiled and evaluated. Where rate data was available over a limited temperature range or at different pressures (for unimolecular or chemically activated steps), RRKM and QRRK methods were used to estimate the rate constant temperature (and pressure) dependence and to predict relative rates where multiple product channels were possible. Where no rate data were available for potential reactions, the rate constants were estimated by analogy to hydrocarbons or substituted hydrocarbons. The rate constant prefactors were adjusted for reaction path degeneracy and activation energies were adjusted empirically based on relative heats of reaction or bond energies.

Initially, upper limits were used for estimated rate constants. If as a result of simulation under a variety of conditions, it was observed that a specific reaction contributed to the chemistry and its rate constant was an upper limit estimate, then its value was reexamined and possibly refined. For important contributing reactions, where no good analogy was available, where significant uncertainty existed in the barrier (generally reactions with tight transition states and modest-to-large barriers), or where energetically similar product channels were possible, ab initio methods were used to calculate the geometries and energies of the transition states. RRKM methods were then applied to obtain the temperature (and pressure) dependence of the rate constant.

CONTRIBUTING REACTIONS

The hydrocarbon and hydrogen/oxygen reaction subsets of the mechanism were derived from the Miller/Bowman mechanism [23]. This reaction subset consists of about 30 species and 140 reactions. A number of species important in fuel rich flames (e.g. C_2H) were eliminated from the mechanism. A number of species important in fuel lean flames (e.g. CH_3OH) were added using kinetics from other validated mechanisms [20]. Rate constants for a few reactions (e.g. CH_3+OH) were also adjusted to provide correct fall-off and product channel ratios. The hydrogen/oxygen/fluorine reaction subset consists of only 3 species and about 8 reactions, although many more were initially considered. Three reactions were determined to be most important: combination of H and F atoms to form HF and H atom abstractions from H_2 and H_2O by F radicals.

The C_1 reaction subset consists of about 15 species and 200 reactions. Both thermally- and chemically-activated fluoromethane decompositions are included (e.g. $\text{CH}_2\text{F}_2 \Rightarrow \text{:CHF} + \text{HF}$ and $\bullet\text{CHF}_2 + \text{H}$

=> :CHF + HF). Fluoromethane decompositions via abstraction of H atoms by H, O, and OH radicals were also considered with abstractions by OH and H the major decomposition pathways. The fluoromethyls produced here were destroyed by several pathways whose relative importance were sensitive to conditions: reactions with H radicals, CH₃ radicals, and oxygen-containing species (O₂, O, OH). The products of the latter reactions consist of carbonyl fluorides (i.e. CF₂O, CHF=O, °CF=O) and HF or other elimination products (e.g. °CHF₂ + OH => CHF=O + HF). It was seen almost exclusively that any reaction channel with an HF product was the dominant channel. The fluoromethyls (:CHF, :CF₂) were largely created by combination of fluoromethyls and H radicals via chemically-activated fluoromethanes (and HF elimination). The fluoromethyls were predominantly destroyed similarly by combination with H radicals via chemically-activated fluoromethyls (and HF elimination creating °CH and °CF). °CF radicals created here were largely consumed by reactions with H₂O and O₂ resulting in CHF=O and °CF=O formation.

Typical reaction pathways for the decomposition of two potential agents, CH₂F₂ and CHF₃, are shown in Figure 1.

The C₂ reaction subset consisted of about 40 species and 400 reactions. Due to the limited nature of this paper, this reaction set cannot be described here in detail. Briefly, the fluoroethane destruction pathways (like fluoromethanes) consist of thermally- and chemically-activated decompositions and H atom abstraction reactions. Fluoroethyl radicals can react with H radicals (like fluoromethyls) creating fluoroethylenes (via chemically activated fluoroethanes and HF elimination). Fluoroethyl radicals can also react with oxygen-containing species (O₂, O, OH) resulting in the formation of oxidized fragments (e.g. CF₂-CF₂° + O => °CF₂ + CF₂=O). Fluoroethylenes (produced from thermally- and chemically-activated fluoroethane decompositions) are predominantly destroyed via reaction with O radicals resulting in the formation of oxidized fragments (e.g. CH₂=CF₂ + O => °CH=O + °CHF₂). Fluoroethylenes are also destroyed to a lesser degree through H atom abstraction by radicals such as OH, resulting in formation of fluorovinyl radicals (e.g. CH₂=CF₂ + OH => CF₂=CH° + H₂O). Fluorovinyl radicals (like fluoromethyl and fluoroethyl radicals) are destroyed via reactions with H radicals, as well as with oxygen-containing species. However, it was observed that the fluorovinyl radicals established a dynamic equilibrium with the parent fluoroethylenes, irrespective of the specific creation and destruction pathways.

PREMIXED FLAME CALCULATIONS

Adiabatic, freely-propagating, premixed flame calculations [25] were performed utilizing the reaction mechanism briefly outlined above. Typically, fuel lean CH₄/air conditions were modeled in order to be most sensitive to flame speed changes and (in a practical sense) since agents are added to the air supply. More realistic would be to simulate agent effects in a diffusion flame. We have performed a few opposed flow diffusion flame calculations; however, those results are preliminary and ongoing.

A summary of the effects on adiabatic flame temperature and speed are shown in Figure 2 for addition of a variety of "agents" to a CH₄/air flame (equivalence ratio of 0.65). In addition to potential fluorinated hydrocarbon agents: CF₄, CHF₃, CH₂F₂, CF₃-CF₃, CF₃-CF₂H, and CF₃-CFH₂, other species were added to investigate the effect of heat capacity and heat release on flame speed changes. These reference "agents" include N₂, H₂O, CO₂, HF, and CH₄. In order to correct for differences in heat capacities for the different "agents", the amount of added "agent" was normalized to an equivalent amount of N₂, adjusting for relative heat capacities at 1500K. For example, addition of 1% CF₄ (with C_p=105 J/mol/K) would be roughly equivalent to addition of 3% N₂ (with C_p=35 J/mol/K). Using heat capacities at other temperatures (1000-2000K) had little impact on the relative normalized mole fractions.

In Figure 2a, it can be seen that the effect of the various agents on flame temperature can be bracketed by addition of inert molecules (N₂, H₂O, CO₂, HF), where there is decrease in flame temperature, and by addition of more fuel (CH₄), where there is an increase in flame temperature. The decrease in flame temperature upon addition of the inerts is due to dilution and increased heat capacity of the mixture. The increase in flame temperature upon addition of more fuel is due to increased heat release as the mixture becomes more rich. Addition of agents which are more fuel-

like results in a larger increase in flame temperature. All of the fluorinated hydrocarbons are fuels since they all eventually decompose, burn, and form CO_2 , H_2O , and HF (liberating heat). At one extreme is CF_4 , very little of which decomposes in the flame, and consequently, there is only a small increase in flame temperature relative to addition of inerts. On the other extreme is CH_2F_2 , which completely burns forming highly exothermic products CO_2 and HF. In Figure 2b, a range of effects on flame speed for the various added agents can be observed. For the inert molecules and the nearly inert fluorinated hydrocarbons (CF_4 , $\text{CF}_3\text{-CF}_3$), a decrease in flame speed is observed consistent with dilution of the mixture. On the other extreme, for CH_4 (the fuel) and CH_2F_2 (a slightly poorer fuel), an increase in flame speed is observed.

Of the various agents considered, only CHF_3 was seen to have any chemical effect in flame suppression. Figure 2 shows that although there is an increase in flame temperature upon CHF_3 addition, there is also a decrease in flame speed relative to inert molecule addition. Inspection of reaction pathways for CHF_3 and other agents (see Figure 1) reveals that a significant amount of decomposed CHF_3 results in the formation of the relatively unreactive perfluorocompound carbonyl fluoride ($\text{CF}_2=\text{O}$). Decomposition of $\text{CF}_2=\text{O}$ occurs only very slowly via reaction with either H radicals (H addition + HF elimination) or with H_2O (through a hot fluoroformic intermediate). For all other agents, this $\text{CF}_2=\text{O}$ bottleneck is avoided.

SUMMARY

These simulations are consistent with qualitative trends observed in experimental measurements of agent effectiveness in the work by others in other parts of the overall project at NIST. In order to quantitatively predict agent effectiveness, experimental validation of the mechanism will be necessary and is currently underway.

REFERENCES

1. D.R. Stull, E.F. Westrum, Jr., and G.C. Sinke, The Chemical Thermodynamics of Organic Compounds, John Wiley, NY, 1969.
2. D.R. Stull and H. Prophet, JANAF Thermochemical Tables, NSRDS-NBS 37, 1971.
3. J.B. Pedley, R.D. Naylor, and S.P. Kirby, Thermochemical Data of Organic Compounds, Chapman and Hall, NY, 1986.
4. A.S. Rodgers, TRC Thermodynamics Tables, Texas A&M University, College Station, TX, 1989.
5. T.E. Daubert and R.P. Danner, DIPPR Data Compilation of Pure Compound Properties, NIST Standard Reference Data, 1985.
6. S.S. Chen, A.S. Rodgers, J. Chao, R.C. Wilhoit, and B.J. Zwolinski, *J. Phys. Chem. Ref. Data* 4, 441 (1975).
7. S.A. Kudchadker and A.P. Kudchadker, *J. Phys. Chem. Ref. Data* 7, 1285 (1978).
8. A.S. Rodgers, *ACS Symp. Ser.* 66, 296 (1978).
9. D.F. McMillen and D.M. Golden, *Ann. Rev. Phys. Chem.* 33, 493 (1982).
10. S.G. Lias, Z. Karpas, and J. F. Liebman, *J. Am. Chem. Soc.* 107, 6089 (1985).
11. W. Tsang, *J. Phys. Chem.* 90, 414 (1986).
12. A.S. Rodgers, J. Chao, R.C. Wilhoit, and B.J. Zwolinski, *J. Phys. Chem. Ref. Data* 3, 117 (1974).
13. J.M. Pickard & A.S. Rodgers, *Int. J. Chem. Kinet.* 15, 569 (1983).
14. C.F. Melius, private communication, 1992.
15. M.R. Zachariah, unpublished results, 1993.
16. M.R. Nyden, private communication, 1993.
17. D.S. Hsu, M.E. Umstead & M.C. Lin, *ACS Symp. Ser.* 66, 128 (1978).
18. G.O. Pritchard, W.B. Nilsson, and B. Kirtman, *Int. J. Chem. Kinet.* 16, 1637 (1984).
19. Y. Chen, A. Rauk, and E. Tschuikow-Roux, *J. Chem. Phys.* 94, 7299 (1991); and prior references.
20. J.C. Biordi, C.P. Lazzara, and J.F. Papp, *J. Phys. Chem.* 82, 125 (1978).
21. C.K. Westbrook, *Combust. Sci. Technol.* 34, 201 (1983).
22. W.G. Mallard, F. Westley, J.T. Herron, R.F. Hampson, and D.H. Frizzel, NIST Chemical Kinetics Database, NIST Standard Reference Data, Gaithersburg, MD, 1993.
23. J.A. Miller and C.T. Bowman, *Prog. Energy Comb. Sci.* 15, 287 (1989).
24. C.K. Westbrook and F.L. Dryer, *Combust. Sci. Technol.* 20, 125 (1979).
25. R.J. Kee, J.F. Grcar, M.D. Smooke, and J.A. Miller, A Fortran Program for Modeling Steady Laminar One-Dimensional Premixed Flames, SAND85-8240, Sandia National Laboratories, 1985.

FIGURE 1. Typical Reaction Pathways for CH_2F_2 and CHF_3

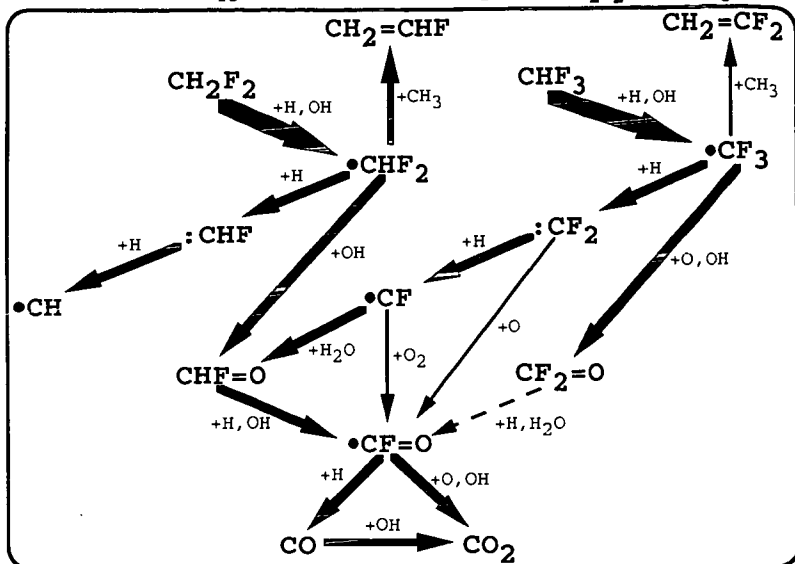
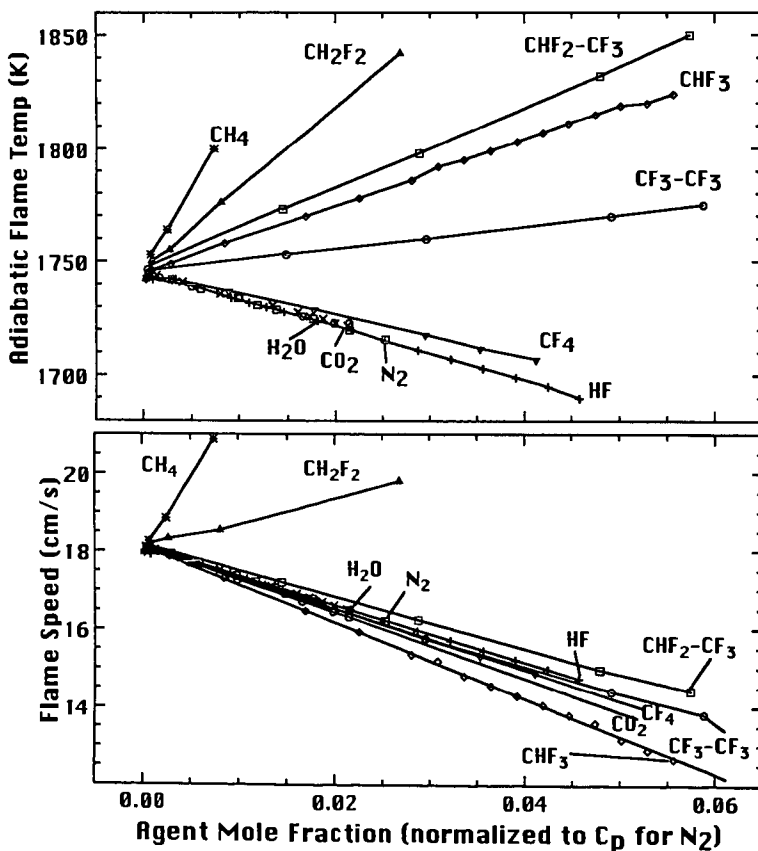


FIGURE 2. Effect of Agents on Flame Temperature and Speed



FORMATION OF AROMATIC COMPOUNDS AND SOOT IN FLAMES

R.P. Lindstedt and G. Skevis
 Mechanical Engineering Department,
 Imperial College of Science, Technology and Medicine,
 Exhibition Road, London SW7 2BX, UK.

Keywords: Soot Formation, PAH Formation in Flames, HACA Sequence

ABSTRACT

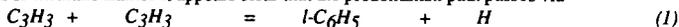
The formation of aromatic compounds such as toluene, naphthalene and phenylacetylene is discussed in the context of soot nucleation in flames. Detailed kinetic reaction steps have been reviewed and a reaction mechanism has been constructed. It is shown that good quantitative agreement between computations and measurements can be obtained for minor aromatic compounds in premixed benzene flames with the notable exception of naphthalene. Benzene flames have been preferred on the grounds that the uncertainties associated with the formation of the first ring can be avoided and as a detailed reaction mechanism for benzene oxidation has recently been proposed. Special attention has been given to species and processes, such as the HACA sequence, which are generally considered essential to the soot nucleation process.

INTRODUCTION

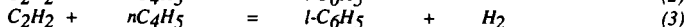
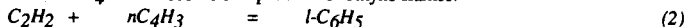
To develop a predictive capability for the formation of PAH and soot in laminar and turbulent flames is of fundamental scientific and practical interest. For diffusion flames with C_1 - C_3 fuels it has been shown [1] that predictions of soot are insensitive to the exact nature of the nucleation process for a wide range of conditions. For example, an *ad hoc* approximation assigning a C_{60} shell as a typical particle size where mass growth becomes dominant over nucleation, has been shown [1] to be satisfactory, provided that nucleation occurs close to the correct location in the flame structure. By contrast, it is reasonable to expect that in premixed flames the dynamics of the nucleation process becomes more important due to shorter time scales. Thus while the use of benzene [1], or even ethyne [2], as indicative species has been shown to be satisfactory in diffusion flame environments, this situation is unlikely to prevail for premixed or partially premixed combustion. Furthermore, many practical fuels, e.g. kerosene, contains a spectrum of aromatic fuel components. Clearly, for these cases current simplified approaches require refinement. The most obvious way of introducing improved descriptions of soot nucleation leads to the introduction of reaction steps for the formation of the second and subsequent aromatic rings. Modelling of the formation of the second ring requires accurate predictions of the underlying flame structure. For benzene flames this has proved difficult in the past. However, recently a benzene oxidation mechanism has been proposed [3] which gives good quantitative agreement for the flame features of relevance to the present study.

CHEMISTRY

Uncertainties have long prevailed regarding the benzene formation steps in flames burning C_1 - C_4 fuels. For methane flames it appears clear that the predominant path passes via

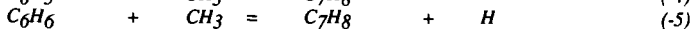
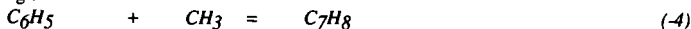


with the subsequent cyclization of the linear C_6H_5 species [3,4]. The situation for higher hydrocarbons is not as firmly established. However, there is some evidence [5] to suggest that reactions via the C_4 chain become competitive for ethyne flames.

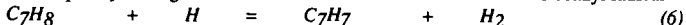


To by-pass the uncertainty associated with the formation reactions for the first ring the present work considers benzene flames. The reaction mechanism used is that proposed by Lindstedt and Skevis [3] which has been shown to predict the MBMS data by Bittner and Howard [6] well.

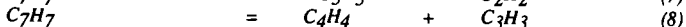
The reaction sequence adopted for toluene, phenyl-acetylene and naphthalene (the second ring) formation is outlined below. Toluene is produced by methyl radical attack on the benzene ring according to



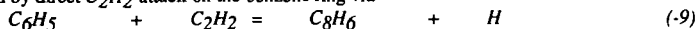
Toluene subsequently undergoes H atom attack on the side chain to form the benzyl radical



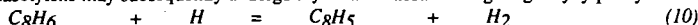
The benzyl radical further dissociates by ring opening either to cyclopentadiene and acetylene or to vinylacetylene and the propargyl radical thus feeding into the C_5 and C_4 chains respectively. Both reactions are assumed to be uni-molecular



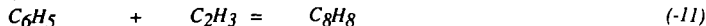
The phenylacetylene mechanism used here is adopted from the work of Herzler and Frank [7] who obtained data in a shock tube at temperatures in the range 1500 - 1900 K. Phenylacetylene is formed by direct C_2H_2 attack on the benzene ring via



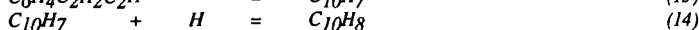
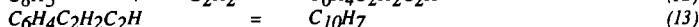
Phenylacetylene may subsequently undergo aryl H atom abstraction giving ethynylphenylene.



Styrene formation was also considered and postulated to occur via vinyl radical attack on the benzene.



The plausibility of naphthalene formation via the building blocks of the HACA sequence [8,9] is here investigated further. In the $C_{10}H_8$ formation sequence ethynylphenylene undergoes a further acetylene attack on the free site thus forming a di-substituted aromatic compound which subsequently isomerises to naphthyl radical. Naphthalene is then formed by a second H attack on the ring.



The above mechanism may readily be written in a generalised form for the formation of higher PAH [8] and soot. For the latter only the equivalent of reaction (10) is treated as reversible while reactions (12) and (13) are written in a slightly different form. Table 1 provides a listing of the most important reactions and rate coefficients in the present mechanism. The thermodynamic data was mainly obtained from the CHEMKIN database [10]. Toluene and naphthalene were assigned ΔH_f values of 12 kcal/mole and 36 kcal/mole respectively, while the heat of formation of the benzyl radical was set at 51.9 kcal/mole. Styrene was assigned a heat of formation of 35.5 kcal/mole. The heats of formation of phenylacetylene, 78.2 kcal/mole, and ethynylphenylene, 133.6 kcal/mole, were adopted from the work of Herzler and Frank [7]. For $C_6H_4C_2H_2C_2H$ the heat of formation was adopted from Frenklach et al [19]. Group additivity [11] was employed to estimate thermodynamic data for species not found in the literature.

RESULTS AND DISCUSSION

The first flame considered in this study was the rich, laminar, low-pressure 21.8% C_6H_6 , 68.2% O_2 , 10% Ar flame studied by McKinnon [12]. The flame was assumed to be burner stabilised and the experimental temperature profile was imposed on the calculations. However, it was found necessary to shift the temperature profile by 2 mm with respect to the species concentration profiles in order to account for probe effects. Profiles of the major species are shown in Figures 1 and 2. Clearly, major species are predicted well and the benzene consumption rate is matched. Also the model gives excellent agreement for acetylene and methane concentration levels as shown in Figure 3. The second flame considered was the rich, laminar, near-sooting 13.5% C_6H_6 , 56.5% O_2 , 30% Ar flame of Bittner and Howard [6], which has been studied extensively elsewhere [3]. Predictions of toluene and phenylacetylene levels are within a factor of 2 or better as shown in Figure 4. Computations using a lower heat of formation for C_8H_6 - 75.2 kcal/mole as suggested in [10] leads to equally acceptable phenylacetylene levels. Good agreement, again within a factor of 2, was also observed for styrene levels in the flame. Toluene and phenylacetylene profiles are also shown in Figure 5 for the 14.8% C_6H_6 , 55.2% O_2 , 30% Ar flame studied by McKinnon [12]. The agreement is again acceptable. Naphthalene chemistry is important because it provides the first step for PAH mass growth in flames. Initial computations using the above sequence [8,9] led to severe under-prediction of $C_{10}H_8$ levels - by a factor of 15 or more. In order to partially resolve the issue, the reaction sequence was retained but reactions (12) and (14) were postulated to proceed with a collision efficiency of 5%. This led to an increase of naphthalene levels by a factor of 3, as shown in Figure 6. Even assigning a collision efficiency of 1, unreasonable for a gas phase reaction, results in under-predictions by a factor of 4. Given the accuracy of predictions of other minor aromatic species this is of concern for quantitative predictions of soot nucleation based on the above reaction sequence.

CONCLUSIONS

It has been shown that good agreement between measurements and predictions may be obtained for small aromatic compounds in benzene flames and that consequently improved soot nucleation models may be developed. However, it has also been shown that significant uncertainties surround the reaction sequence for the second aromatic ring. It appears that either the reaction rates in the formation sequence [9] have to be assigned collision efficiencies similar to those used for soot mass growth [8] or that the whole mechanism for second ring formation has to be refined. For gas phase reactions the latter is clearly preferable. This may involve distinguishing between active sites, accounting for steric effects, incorporating attacks by a variety of radicals and exploring supplementary reaction paths.

ACKNOWLEDGEMENT

The Authors Gratefully Acknowledge the Financial Support of British Gas plc.

REFERENCES

- [1] Lindstedt, R.P., in *Mechanisms and Models of Soot Formation* (H. Bockhorn, Ed.), Springer-Verlag, To Appear.
- [2] Leung, K.M., Lindstedt, R.P. and Jones, W.P., *Combustion and Flame* 87, p.289 (1989)
- [3] Lindstedt, R.P. and Skevis, G., Submitted to the *Twenty-Fifth Symposium (International on Combustion)* Nov. 1993
- [4] Leung, K.M. and Lindstedt, R.P., *Comb. and Flame*, To Appear.
- [5] Vovelle, Ch., Delfau, J.-L. and Doute, Ch., *Proc. of Anglo-German Comb. Symp.*, Cambridge 1993, p. 148.
- [6] Bittner, J.D. and Howard, J.B., *Eighteenth Symposium (International) on Combustion*, The Combustion Institute, 1980, p.1105
- [7] Herzler, J. and Frank, P., in *Mechanisms and Models of Soot Formation* (H. Bockhorn, Ed.), Springer-Verlag, To Appear.
- [8] Frenklach, M. and Wang, H., *Twenty-third Symposium (International) on Combustion*, The Combustion Institute, 1990, p.1559
- [9] Frenklach, M. and Warnatz, J., *Comb. Sci. and Tech.* 51:265 (1987)
- [10] Kee, R.J., Rupley, F.M. and Miller, J.A., *The CHEMKIN Thermodynamic Database*, Sandia National Laboratories Report No. SAND87-8215, 1987
- [11] Benson, S.W., *Thermochemical Kinetics*, Wiley, New York, 1976
- [12] McKinnon, J.T., Jr., *Ph.D. Thesis*, Chemical Engineering Department, MIT, 1989
- [13] Miller, J.A. and Melius, C.F., *Combust. Flame.* 91:21 (1992)
- [14] Westmoreland, P.R., Dean, A.M., Howard, J.B. and Longwell, J.P., *J. Phys. Chem.* 93:8171 (1989)
- [15] Emdee, J.L., Brezinsky, K. and Glassman, I., *J. Phys. Chem.* 96:2151 (1992)
- [16] Braun-Unkoff, M., Frank, P. and Just, Th., *Twenty-second Symposium (International) on Combustion*, The Combustion Institute, 1988, p.1053
- [17] Brouwer, L.D., Muller-Markgraf, M. and Troe, J., *J. Phys. Chem.*, 92:4905 (1988)
- [18] Colket III, M.B., Seery, D.J. and Palmer, H.B., *Combust. Flame.*, 75:343 (1989)
- [19] Frenklach, M., Clary, D.W. and Yuan, T., Gardiner, W.C., Jr and Stein, S.E., *Comb. Sci. and Tech.* 50, p. 79 (1986)

Table 1. Reaction Mechanism Rate Coefficients in the Form $k = A T^n \exp(-E_a/RT)$. Units are kmole, cubic metres, seconds, Kelvin and KJ/mole

Reaction	A	n	E _a	Reference
C ₃ H ₃ + C ₃ H ₃ → l-C ₆ H ₅ + H	3.00e10	0.00	0.00	13
l-C ₆ H ₅ → n-C ₄ H ₃ + C ₂ H ₂	1.00e14	0.00	163.72	3
n-C ₄ H ₅ + C ₂ H ₂ → C ₆ H ₆ + H	1.90e04	1.47	20.54	14
C ₇ H ₈ → C ₆ H ₅ + CH ₃	1.14e15	0.00	417.56	15
C ₇ H ₈ + H → C ₆ H ₆ + CH ₃	1.20e10	0.00	21.54	15
C ₇ H ₈ + H → C ₇ H ₇ + H ₂	5.00e11	0.00	52.30	16
C ₇ H ₇ → c-C ₅ H ₅ + C ₂ H ₂	1.66e10	0.00	187.00	17
C ₇ H ₇ → C ₄ H ₄ + C ₃ H ₃	2.00e15	0.00	349.60	17
C ₈ H ₆ + H → C ₆ H ₅ + C ₂ H ₂	2.00e11	0.00	40.58	7
C ₈ H ₆ + H → C ₈ H ₅ + H ₂	4.00e10	0.00	40.58	7
C ₆ H ₅ + C ₂ H ₂ → C ₈ H ₈	5.01e09	0.00	0.00	18
C ₈ H ₅ + C ₂ H ₂ → C ₆ H ₄ C ₂ H ₂ C ₂ H	2.00e11	0.00	0.00	9, pw
C ₆ H ₄ C ₂ H ₂ C ₂ H → C ₁₀ H ₇	1.00e10	0.00	0.00	9
C ₁₀ H ₇ + H → C ₁₀ H ₈	5.00e11	0.00	0.00	9, pw

Figure 1 - Comparison between computed (lines) and experimental (points) profiles for C6H6, H2 and H2O
 Experimental data are from McKinnon [12]

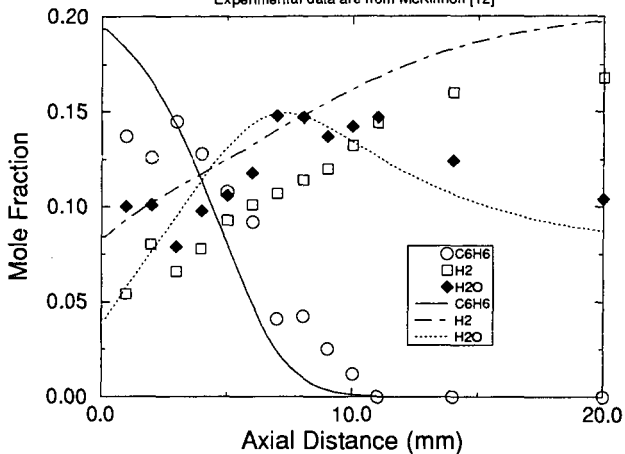


Figure 2 - Comparison between computed (lines) and experimental (points) profiles for O2, CO and CO2
 Experimental data are from McKinnon [12]

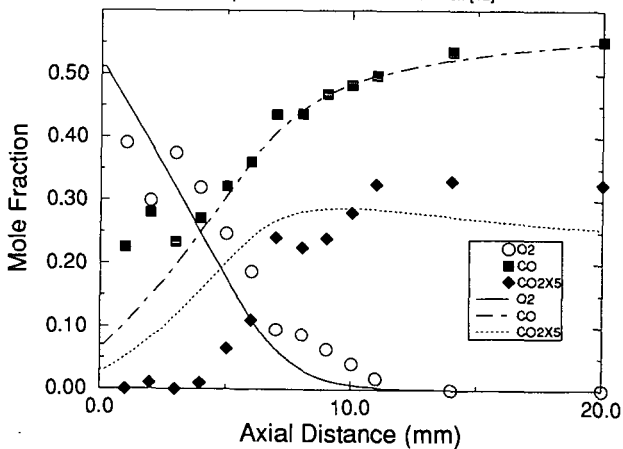


Figure 3 - Comparison between computed (lines) and experimental (points) profiles for C2H2 and CH4
 Experimental data are from McKinnon [12]

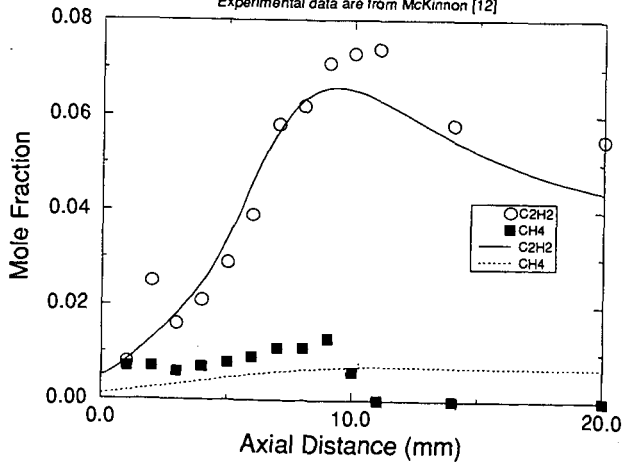


Figure 4 - Comparison between computed (lines) and experimental (points) profiles for C7H8 and C8H6
 Experimental data are from Bittner and Howard [6]

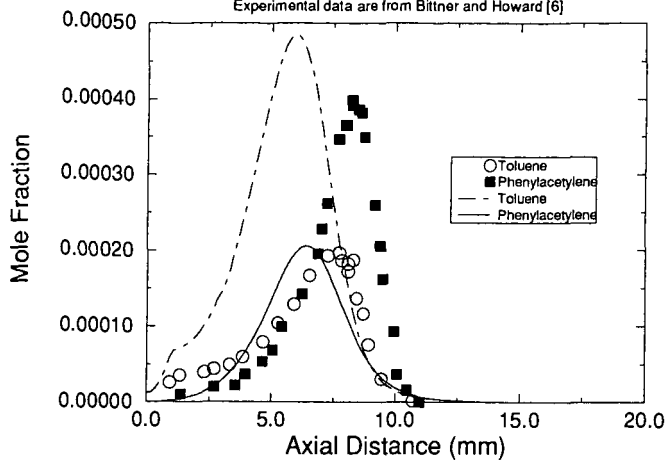


Figure 5 - Comparison between computed (lines) and experimental (points) profiles for C7H8 and C8H6
 Experimental data are from McKinnon [12]

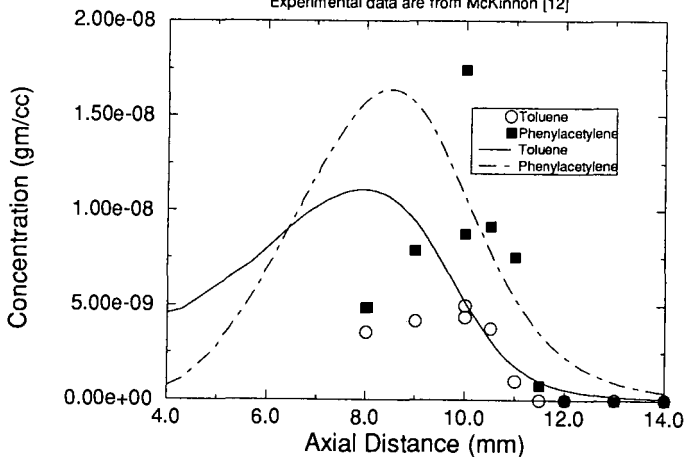
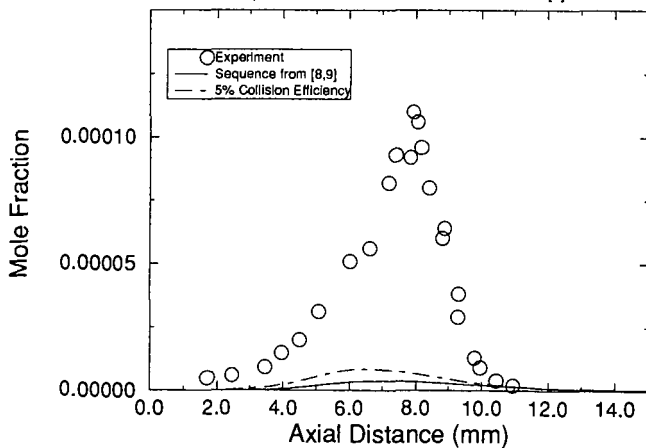


Figure 6 - Comparison between computed (lines) and experimental (points) profiles for C10H8
 Experimental data are from Bittner and Howard [6]



ENHANCED SOOT FORMATION IN FLICKERING CH₄/AIR DIFFUSION FLAMES

Christopher R. Shaddix, Joel E. Harrington, and Kermit C. Smyth
Building and Fire Research Laboratory
National Institute of Standards and Technology
Gaithersburg, MD 20899

ABSTRACT

Optical methods are used to examine soot production in a co-flowing, axisymmetric CH₄/air diffusion flame in which the fuel flow rate is acoustically forced to create a time-varying flowfield. For a particular forcing condition in which tip clipping occurs (0.75 V loudspeaker excitation), elastic scattering of vertically polarized light from the soot particles increases by nearly an order of magnitude with respect to that observed for a steady flame with the same mean fuel flow rate. Peak soot volume fractions, as measured by time-resolved laser extinction/tomography at 632.8 and 454.5 nm and calibrated laser-induced incandescence (LII), show a factor of 4-5 enhancement in this flickering flame. A Mie analysis suggests that most of the enhanced soot production results from the formation of larger particles in the time-varying flowfield.

Keywords: soot formation, laser diagnostics, laminar diffusion flames

INTRODUCTION

A critical assumption in applying chemical models developed in laminar flames to turbulent combustion is that the limited combinations of residence times, temperature histories, local stoichiometries, and strain rates sampled in laboratory-scale steady laminar flames are sufficient to quantitatively describe chemical processes in turbulent environments. In order to critically evaluate the validity of this assumption, an experimental facility for performing optical measurements in time-varying, laminar diffusion flames has been developed at NIST [1].

Under a wide variety of conditions, axisymmetric diffusion flames and pool fires exhibit a natural flickering behavior, with a frequency dependence on the fuel tube or pool diameter expressed as $f \sim 1.5/(D)^{1/2}$ (for f in Hz and D in meters) [2,3]. Previous researchers have found that this flickering tendency may be locked near the natural flicker frequency by applying a small periodic perturbation to the fuel flow [4-7]. In the present investigation optical diagnostics are phase-locked to a sinusoidal variation of the fuel flow velocity at the 10 Hz repetition rate of a Nd³⁺:YAG laser, allowing phase-specific measurements.

In a preliminary study of OH^{*} laser-induced fluorescence and elastic scattering from soot in steady and time-varying CH₄/air diffusion flames, it was found that the scattering intensity in the time-varying flame was significantly greater than that observed for the steady (i.e., unforced) flame with the same mean fuel and air flow rates [1]. In order to better quantify the observed soot enhancement for a forcing condition in which flame tip clipping occurs, we have applied laser light extinction and laser-induced incandescence (LII) to determine the soot volume fraction fields in these CH₄/air flames. In addition, laser energy-corrected imaging of soot scattering in the steady and flickering flames has been performed using vertically polarized incident light, supplementing previous measurements using horizontal polarization [1]. The OH^{*} fluorescence and soot scattering fields for the flickering flame studied here and its steady counterpart are shown in Fig. 1, to aid in the interpretation of the experimental results to follow.

EXPERIMENTAL METHODS

Figure 2 shows a schematic diagram of the burner and phase-locked imaging setup, which has been described in detail previously [1]. A coannular axisymmetric burner with a 1.1 cm diameter fuel tube surrounded by a 10.2 cm air annulus supports an unconfined laminar flame. The mean methane cold flow velocity and air coflow are 7.9 cm/s for both the steady and forced flames; the steady flame has a visible height of 79 mm. A loudspeaker attached to the fuel plenum locks the frequency of the flickering flame to the 10.13 Hz repetition rate of the Nd³⁺:YAG pumped dye laser system. The flickering flame data presented here were taken with 0.75 V peak-to-peak sine wave forcing, which is an intermediate excitation amplitude of those studied earlier [1].

Laser Extinction

Laser light extinction has traditionally been used to measure soot volume fraction. However, both absorption from large molecules, such as polycyclic aromatic hydrocarbons (PAH), and soot scattering interfere with the signal from soot absorption. For the CH₄/air flames studied here, soot scattering should represent a minor portion of the extinction, since the primary soot particles are small [8] and the extent of soot agglomeration in our relatively short residence time flames is expected to be limited. On the other hand, the contribution of molecular absorption to the measured extinction is of concern, particularly at low soot loadings. Consequently, extinction measurements were performed using the longest wavelength cw laser readily available in our laboratory (632.8 nm - HeNe). In most cases extinction was also measured using a shorter wavelength laser source (454.5 nm - Ar⁺), where molecular absorption is expected to be much stronger [9].

In order to perform accurate extinction measurements in these lightly sooting flames, a laser power stabilizer was used to reduce the noise in the input laser beams to $\sim 0.1\%$, allowing measurement of extinction levels as small as 0.01% after averaging. The line-of-sight nature of extinction necessitates data collection along multiple chords and subsequent tomographic inversion to yield locally resolved values of extinction. To obtain acceptable signal-to-noise, 200 consecutive time records of the amplified photodiode output were averaged using a digital oscilloscope. Extinction records were obtained for radial chords spaced by 0.25 mm across the width of the flames and were tomographically inverted with a 3-point Abel routine as implemented by Dasch [10]. For the time records in the flickering flame a Pascal-encoded version of Dasch's routine [11] was employed to yield phase-specific extinction profiles.

Laser-Induced Incandescence

Laser-induced incandescence (LII) has recently been developed as an alternative method for both relative [12,13] and quantitative [14] measurement of soot volume fraction. We employed LII as a second means of quantifying the soot volume fraction in both the steady and flickering CH_4 /air flames, in order to identify possible contributions from molecular absorption to the measured extinction and to avoid noise difficulties in the extinction signal which arose from flame wobble at heights above 60 mm in the flickering flame. For the LII measurement the fundamental dye laser beam at 560 nm was focused with a 300 mm focal length lens at the center of the flame. In order to minimize signal variations with shot-to-shot laser energy fluctuations, the LII data were obtained at sufficiently high energies ($\sim 7 \times 10^8$ W/cm²) to lie well within the plateau region where the LII signal varies little with laser energy [13,14]. Single-shot, 1-D line images were recorded on the ICCD camera, with a glass filter providing a detection bandwidth of 300 – 480 nm. To improve the signal-to-noise, 10 consecutive frames were collected at each height and averaged after verifying that the peak signal levels were consistent from frame to frame. Higher in the flickering flame the consecutive images often displayed side-to-side flame wobble. In these instances the LII frames were aligned radially and aberrant profiles were discarded (typically 2–3 out of 10, from $H = 60$ mm to $H = 110$ mm) before averaging. Flame luminosity signals were ~ 10 times weaker than the LII signals and were accounted for by taking a duplicate set of line images without laser light and subtracting these from the LII images. Further experimental details of the extinction and LII measurements are given in Ref. 15.

Soot Scattering

Scattering measurements were made with the same basic experimental setup and data collection procedure used for the earlier OH \cdot and soot imaging, in which dye laser light at 567 nm was frequency doubled to 283.50 nm [1]. To image scattering from vertically polarized light, a variable retardation plate (Babinet-Soleil compensator) rotated the incident beam to a vertical polarization relative to the detection axis. Shot-to-shot spatial profiles of the laser energy were recorded via on-camera imaging of a reflection from the incident laser sheet (see Fig. 2).

RESULTS

The soot volume fraction was calculated from the tomographically inverted extinction measurements using the Lambert-Beer transmissivity law and the Mie extinction formula in the Rayleigh limit [16–18]. An index of refraction $\bar{m} = 1.57$ – $0.56i$ was used for both HeNe and Ar^+ wavelengths in order to make direct comparisons with the results of Santoro and coworkers [18,19]. Figure 3 shows the symmetrized (averaged about the centerline), steady flame HeNe results; the maximum soot volume fraction is $3.2 (\pm 0.3) \times 10^{-7}$ at $H = 60$ mm above the fuel tube exit. Above $H = 30$ mm in the steady flame, peak soot volume fractions determined from the Ar^+ measurements are greater than the HeNe results by ~ 5 – 10% , which is within the 15% uncertainty estimated for the extinction measurements. Lower in the flame and along the inner edge of the soot profile, Ar^+ extinction yields a significantly larger soot volume fraction than HeNe extinction, consistent with the expectation of greater absorption by PAH in these regions [18,20,21]. Figure 3 also includes the comparison of symmetrized LII signals with the extinction-determined soot volume fractions in the steady methane flame. The peak HeNe soot volume fraction at $H = 50$ mm was used to calibrate the LII signal, since at this height and radial location one expects the smallest relative contribution of molecular absorption to the observed extinction [20]. The similarity in location and magnitude of the peak values of the extinction and LII results at different heights indicates that the LII signal closely follows the soot volume fraction. Differences in the two signals towards the center of the profiles may be due to significant molecular absorption at 632.8 nm at these locations, as well as the increased error in the tomographic inversion procedure towards the flame centerline [10].

In Fig. 4 the tomographically inverted, time-resolved HeNe extinction data for the flickering flame are shown at $H = 40$ mm. The soot volume fraction fields higher in the flame are qualitatively similar, with a decreasing time duration of measurable extinction and greater "rippling" noise in the reconstructed annular soot layer. This noise arises from side-to-side flame wobble during the data collection process. The largest instantaneous soot volume fraction (f_v) is $1.3 (\pm 0.3) \times 10^{-6}$, observed at $H = 120$ mm; this value is four times greater than the maximum f_v in the corresponding steady flame. Ar^+ extinction measurements were completed only to $H = 100$ mm in the flickering flame and yield somewhat greater ($\sim 30\%$) soot volume fractions than the HeNe extinction. Fig. 5 presents the area-integrated and time-averaged (for the flickering flame) soot volume fraction measurements as a function of height. The area under the HeNe flickering flame curve, a volumetric measure of the soot in the flame, is four times greater than its steady counterpart. This figure also shows the consistently larger Ar^+ signals in the flickering flame (up to $H = 100$ mm) and the convergence of the Ar^+ measurement

with the HeNe result higher in the steady flame. As in the steady flame, the increased Ar⁺ signals are attributed to enhanced PAH absorption.

LII signals were measured in the flickering flame up to H = 110 mm for the ten phase angles shown in Fig. 1. The maximum signal gives a soot volume fraction of $1.5 (\pm 0.2) \times 10^{-6}$ at H = 110 mm (80% phase), which is 5 times larger than that observed in the steady flame. Figure 6 shows the symmetrized LII signals compared with the extinction-derived soot volume fraction for 50% phase. Above H = 60 mm in the flickering flame the extinction-derived profiles are generally wider and shorter than their LII counterparts, consistent with the observed flame wobble and the time-averaged nature of the extinction measurement at each radial chord.

For vertically polarized incident light the maximum local soot scattering intensity in the flickering flame is ~ 8 times greater than that measured in the corresponding steady flame and occurs in the annular soot region of the clipped-off flame for phases of 80 and 90%. At the same locations the enhancement in peak scattering of horizontally polarized light is approximately a factor of 20. Flame tip burnout is complete at about 17 cm in the flickering flame, so it is certainly possible that even greater soot scattering intensities would be found at heights above the current limit for imaging of 13.4 cm.

Uncertainties quoted are one standard deviation, derived from signal variations in repeat measurements of scattering and LII; random errors in the extinction measurements are estimated from noise in the profiles. Calibration of LII in the steady flame may lead to small systematic errors for the time-varying flame results, due to changes in soot particle morphology. Long time-scale movements of the flames remain as a possible source of unquantified error.

DISCUSSION

The dramatic enhancement in soot formation observed when a steady CH₄/air flame is induced to flicker may provide a demanding test of the ability of recently formulated integrated soot models [e.g., 22-25] to accurately predict soot formation and oxidation rates in complex combustor flowfields. Changes in residence times, temperatures, and/or local stoichiometries are most likely responsible for the increased soot production, but differences in these variables have not been determined in these flames. Rayleigh and Mie analyses have been conducted on our scattering and soot volume fraction data in order to estimate the mean soot particle sizes and number densities as a useful first step in elucidating why soot production is enhanced in the flickering flames.

The vertically polarized scattering measurements were indirectly calibrated [15] by comparison with the data of Richardson and Santoro in the same nominal flame [19]. Rayleigh and Mie theory calculations were then performed on the calibrated LII and scattering signals using a FORTRAN code with the Mie-solution subroutine (BHMIE) given by Bohren and Huffman [26]. Number densities were calculated assuming a monodisperse size distribution at each measuring location. An index of refraction of 1.57-0.56i was used both to calibrate the LII signals to the HeNe extinction results in the steady flame and for the Mie analysis of the scattering at 283.5 nm. Calculations with other values for the index of refraction show similar trends.

Table I presents only a small subset of the calculated results: the soot volume fraction, particle diameter, and number densities are given at the point of maximum soot scattering for each measurement height in the steady flame and in the flickering flame at 50% phase. In lieu of velocity measurements, the contour of maximum scattering is used as a rough guide to the time history of soot particles in the steady flame. The Mie diameters in the steady CH₄/air flame increase up to H = 50 mm, and the calculated number densities decrease slightly as soot particle mass growth occurs, possibly reflecting the effect of soot particle agglomeration. The larger number densities at H = 60 mm and H = 70 mm in the steady flame may result from soot particle inception towards the centerline of the flame, or may also arise from the failure of the monodisperse Mie analysis to account for the high degree of polydispersion in the particle field anticipated at these locations (due to primary particle or agglomerate breakup during oxidation). At 50% phase in the flickering flame the derived soot particle diameter increases monotonically with height, while the number densities remain roughly constant until oxidation occurs at the top of the flame. In examining these results, however, recall that any given phase is a snap-shot in the time-history of the flickering flame. The Mie results shown in Table I, when combined with similar trends for all but the greatest heights of the flickering flame, show that particle number densities remain near $2-3 \times 10^9/\text{cm}^3$ through both the steady and flickering flames, whereas the effective particle diameters increase from a maximum of ~60 nm in the steady flame to ~90 nm in the flickering flame (using $\tilde{m} = 1.57-0.56i$). The extent of particle size increase shown here should not be over interpreted, since the particle size parameters ($x = \pi D/\lambda$) in the flickering flame are large (~1) and the deviation between agglomerate and Rayleigh or Mie analysis increases with increasing size parameter [27,28].

We thank Chris Cromer for loaning us the laser power stabilizer and George Mulholland and Robert Santoro for insightful discussion of soot formation processes and diagnostic techniques, particularly with regard to the calibration of LII signals.

REFERENCES

1. Smyth, K.C., Harrington, J.E., Johnsson, E.L., and Pitts, W.M., *Combust. Flame* 95:229-239 (1993).
2. Hamins, A., Yang, J.C., and Kashiwagi, T., *Twenty-Fourth Symposium (International) on Combustion*, The Combustion Institute, Pittsburgh, 1992, pp. 1695-1702.
3. Cetegen, B.M., and Ahmed, T.A., *Combust. Flame* 93:157-184 (1993).
4. Strawa, A.W., and Cantwell, B.J., *Phys. Fluids* 28, 2317-2320 (1985).

5. Lewis, G.S., Cantwell, B.J., Vandsburger, U., and Bowman, C.T., *Twenty-Second Symposium (International) on Combustion*, The Combustion Institute, Pittsburgh, 1988, pp. 515-522.
6. Pearson, I.G., and Proctor, D., in *Experimental Heat Transfer, Fluid Mechanics, and Thermodynamics 1991* (J.F. Keffer, R.K. Shah, and E.N. Ganic, eds.), Elsevier Science, 1991, pp. 316-322.
7. Vandsburger, U., Seitzman, J.M., and Hanson, R.K., *Combust. Sci. and Tech.* 59:455-461 (1988).
8. Puri, R., Santoro, R.J., and Smyth, K.C., *Combust. Flame*, in press.
9. Miller, J.H., Mallard, W.G., and Smyth, K.C., *Combust. Flame* 47:205-214 (1982).
10. Dasch, C.J., *Applied Optics* 31:1146-1152 (1992).
11. We thank J. Houston Miller for providing us with the base Pascal algorithm required to tomographically invert extinction records in time or frequency.
12. Dec, J.E., zur Loye, A.O., and Siebers, D.L., *SAE Technical Papers Series* SAE-910224, Society of Automotive Engineers, PA, 1991.
13. Tait, N.P., and Greenhalgh, D.A., *Proceedings of the "Optical Methods and Data Processing in Heat Transfer and Fluid Flow" Conference*, London, April 1992.
14. Quay, B., Lee, T.-W., and Santoro, R.J., *Combust. Flame*, in press.
15. Shaddix, C.R., Harrington, J.E., and Smyth, K.C., submitted to *25th Symposium (International) on Combustion*.
16. Kerker, M., *The Scattering of Light*, Academic Press, New York, 1969, pp. 31-39.
17. D'Alessio, A., in *Particulate Carbon: Formation During Combustion* (D.C. Siegla and G.W. Smith, Eds.), Plenum, New York, 1981, pp. 207-259.
18. Santoro, R.J., Semerjian, H.G., and Dobbins, R.A., *Combust. Flame* 51:203-218 (1983).
19. Richardson, T.F., and Santoro, R.J., private communication, 1993.
20. Prado, G., Garo, A., Ko, A., and Sarofim, A., *Twentieth Symposium (International) on Combustion*, The Combustion Institute, Pittsburgh, 1984, pp. 989-996.
21. Smyth, K.C., Miller, J.H., Dorfman, R.C., Mallard, W.G., and Santoro, R.J., *Combust. Flame* 62:157-181 (1985).
22. Syed, K.J., Stewart, C.D., and Moss, J.B., *Twenty-Third Symposium (International) on Combustion*, The Combustion Institute, Pittsburgh, 1990, pp. 1533-1541.
23. Leung, K.M., Lindstedt, R.P., and Jones, W.P., *Combust. Flame* 87:289-305 (1991).
24. Honnery, D.R., and Kent, J.H., *Twenty-Fourth Symposium (International) on Combustion*, The Combustion Institute, Pittsburgh, 1992, pp. 1041-1047.
25. Villasenor, R., and Kennedy, I.M., *Twenty-Fourth Symposium (International) on Combustion*, The Combustion Institute, Pittsburgh, 1992, pp. 1023-1030.
26. Bohren, C.F., and Huffman, D.R., *Absorption and Scattering of Light by Small Particles*, John Wiley & Sons, New York, 1983, pp. 477-482.
27. Charalampopoulos, T.T., and Chang, H., *Combust. Flame* 87:89-99 (1991).
28. Mountain, R.D., and Mulholland, G.W., *Langmuir* 4:1321-1326 (1988).

Table I: Mie Analysis of Soot Field Along Contour of Maximum Q_{vv}

Height Above Burner (mm)	Steady Flame			Flickering Flame (50% phase)		
	f_v (10^{-7})	D (nm)	N ($10^9/cc$)	f_v (10^{-7})	D (nm)	N ($10^9/cc$)
30	0.7 (0.2 ^a)	39 (5 ^b)	2.4 (1.3)	0.4 (0.1)	34 (4)	2.0 (1.4)
40	2.2 (0.4)	57 (6)	2.2 (1.1)	1.0 (0.2)	50 (6)	1.5 (0.9)
50	2.3 (0.3)	62 (6)	1.9 (0.8)	2.1 (0.2)	53 (5)	2.7 (1.0)
60	2.2 (0.4)	49 (5)	3.5 (1.8)	3.6 (0.3)	68 (5)	2.2 (0.7)
70	2.0 (0.5)	50 (7)	3.1 (2.2)	6.4 (0.5)	80 (6)	2.4 (0.7)
80				8.1 (0.5)	86 (6)	2.5 (0.7)
90				0.8 (0.2)	85 (11)	0.3 (0.2)

^a One standard deviation uncertainty estimates.

^b Diameter and number density uncertainties are the result of propagating volume fraction and scattering error estimates through Rayleigh analysis. These uncertainties agree well with the variation in Mie results over the range of uncertainty in f_v and Q_{vv} .

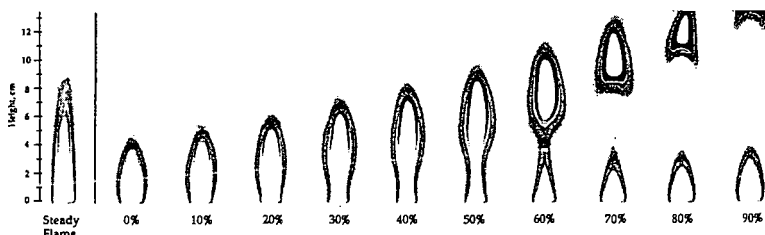


Figure 1. Laser energy-corrected OH^* laser-induced fluorescence and soot scattering images in a steady and time-varying laminar CH_4 /air diffusion flame using horizontally polarized light at 283.55 nm. The visible flame height of the steady flame is 79 mm above the fuel tube exit, which is located 1 mm above the bottom of the images. For the flickering flame, ten equally spaced phase increments are shown, corresponding to a time interval of 10 ms; zero phase is arbitrary. The OH^* fluorescence signals have not been corrected for local quenching rates and hence serve as a convenient, qualitative marker of the high-temperature reaction zone. For the full-height images presented here, 5 single-shot images (3.2 cm high) have been overlapped to compensate for reduced signal-to-noise at the upper and lower edges of the incident laser sheet. Several of the stacked images shown have been shifted slightly from side-to-side to compensate for flame wobble at higher flame locations.

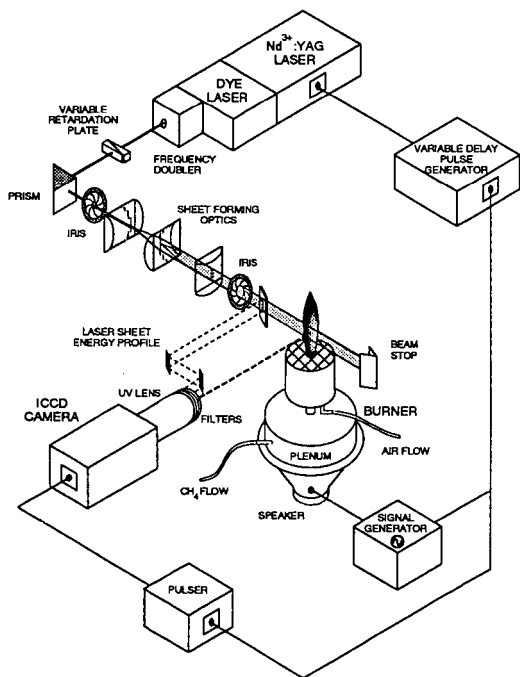


Figure 2. Experimental set-up for 1- or 2-D imaging of axisymmetric diffusion flames which are acoustically excited and phase-locked to the pulsed dye laser system operating at 10.13 Hz. For the laser-induced incandescence experiment, the frequency doubler and sheet-forming optics are removed, and a 300 mm focal length lens is used to focus the beam at the center of the flame. Images are recorded using an intensified charge-coupled device (ICCD) camera.

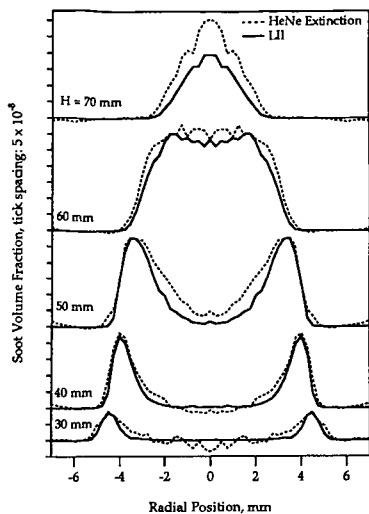


Figure 3. Soot volume fraction from symmetrized HeNe laser extinction (632.8 nm) and laser-induced incandescence (LII) signals at a series of heights in the steady CH_4 /air diffusion flame.

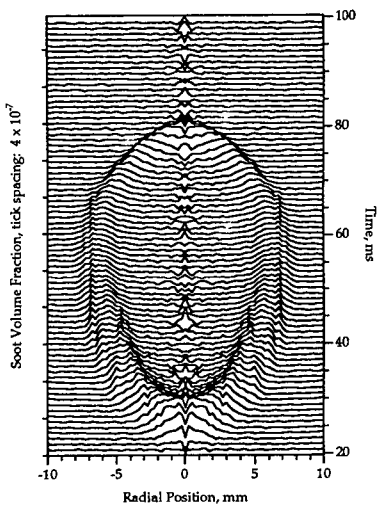


Figure 4. Time evolution of the soot volume fraction field at $H = 40$ mm in the flickering CH_4 /air diffusion flame (0.75 V loudspeaker excitation). Each line shown is separated by 1 ms in time and staggered by 6×10^{-8} in soot volume fraction. Time progresses from the bottom to the top of the figure, showing first the arrival of soot, the widening of the soot profile into an annular structure as time increases, the convergence of the soot profile to the centerline, and finally its disappearance as the bottom of the clipped-off portion of the flame passes above $H = 40$ mm.

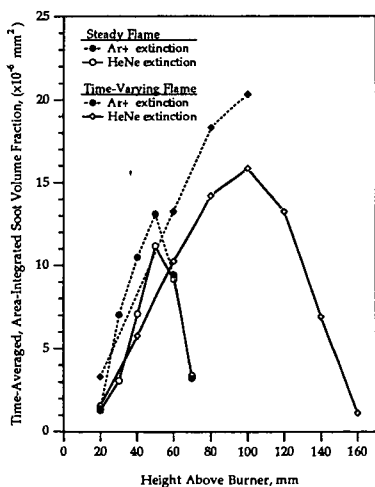


Figure 5. Area-integrated soot volume fraction from symmetrized HeNe (632.8 nm) and Ar^+ (454.5 nm) laser extinction measurements at a series of heights in CH_4 /air diffusion flames. The flickering flame measurements are expressed as time averages over a full cycle period. The area under the steady flame HeNe curve is $3.4 \times 10^{-4} \text{ mm}^3$; that under the flickering flame is $1.3 \times 10^{-3} \text{ mm}^3$.

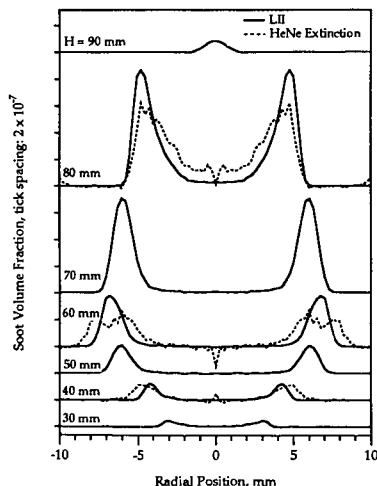


Figure 6. Laser-induced incandescence (LII) signals, interpreted as soot volume fraction, at a series of heights in the flickering CH_4 /air diffusion flame at 50% phase. Time-resolved, tomographically inverted HeNe extinction data are also shown at heights of 40, 60, and 80 mm above the burner.

REACTIONS OF $^1\text{CX}_2$ DURING CHLOROFLUOROCARBON PYROLYSIS

John J. DiFelice and Edward R. Ritter
Department of Chemical Engineering
Villanova University
Villanova, PA 19085

Keywords: fluorocarbon pyrolysis, difluoromethylene, chlorodifluoromethane

INTRODUCTION

Singlet carbenes are reactive intermediates which behave in a fashion quite different from radicals. In hydrocarbon and hydrochlorocarbon systems, radicals and radical chemistry typically dominate. However, in chlorofluorocarbon (CFC) and hydrochlorofluorocarbon (HCFC) systems, formation of perhalogenated singlet carbenes ($^1\text{CX}_2$) has been observed (DiFelice and Ritter, 1993; Westmoreland, 1993). While radicals undergo abstraction reactions and addition to double bonds, singlet carbenes can insert into single bonds. Singlet carbenes are species which have two paired nonbonded electrons; since paired electrons have opposite spin, singlet carbenes can insert into single bonds (March, 1992). Triplet carbenes, in contrast, contain unpaired electrons and behave essentially like radicals. Formation of perhalogenated triplet carbenes ($^3\text{CX}_2$) is less favorable in CFC and HCFC systems since the $^1\text{CX}_2$ singlet state is as much as 56 kcal/mol lower in energy than the triplet state (Melius, 1993).

The insertion of $^1\text{CX}_2$ into single bonds makes CFC and HCFC pyrolytic chemistry unique and interesting. However, there have been few studies on the combustion and pyrolysis chemistry of these compounds. Most experimental studies of CFCs and HCFCs are at conditions relevant to stratospheric ozone depletion (NIST, 1991a). These conditions are typically at much lower pressure and temperature than those encountered during incineration or pyrolysis. Recent combustion studies by Naegli, et al. (1991) and Tokuhashi, et al. (1990) demonstrate the need for further research on the incinerability and pyrolysis chemistry of these species. These studies focused on CF_2Cl_2 (Freon-12) and CHF_2Cl (Freon-22). They demonstrated that these species can be broken down in an incineration environment, and that significant quantities of by-products (PICs) are formed. These by-products have been neither completely classified, nor quantified.

Previous work (Ritter, 1993 and DiFelice and Ritter, 1993) has focused on the thermal reactions of $\text{CF}_2\text{Cl-CFCl}_2$ (Freon-113) and CHF_2Cl under pyrolytic conditions in helium and helium/hydrogen mixtures. These studies have characterized the pyrolysis under inert and reducing conditions. Studies have shown that formation and reaction of perhalogenated singlet carbenes ($^1\text{CX}_2$) are important during CHF_2Cl pyrolysis, while they are of questionable importance during $\text{CF}_2\text{Cl-CFCl}_2$ pyrolysis. The significance of various carbene insertion reactions are important for the mechanistic modeling of CHF_2Cl pyrolysis. Determination of their significance would also give insight into the $\text{CF}_2\text{Cl-CFCl}_2$ pyrolytic system. The carbene insertion reactions investigated include insertion into carbon-hydrogen (C-H) bonds and carbon-halogen (C-X) bonds. Other CFCs studied during the investigation include CF_2Cl_2 (Freon-12), CF_3Cl (Freon-13), and $\text{C}_2\text{HF}_4\text{Cl}$ (Freon-124).

EXPERIMENTAL

The experimental flow tube reactor consists of a quartz or alumina flow tube which passes through a 6 zone electrically heated tube furnace (see Figure 1). Typical reaction times range from 0.05 to 2 seconds with temperatures from 773 - 1098 K. In atmospheric pressure flow tube reactors, there is always the concern for significant wall reactions. Ritter et al. (1990) observed significant differences between experimentally determined rate constants for chlorobenzene decomposition when carried out in 0.4 and 1.0 cm id reactor tubes. However, they observed little difference between decomposition rates in 1.0 and 1.6 cm id reactors. In these studies 1.6 and 2 cm i.d. reactors are used to reduce the importance of possible surface reactions. Quartz flow tubes can be used for lower temperatures (less than 775°C), however, alumina is required at higher temperatures due to the rapid degradation of quartz by fluorides. The reactor operates isobarically near 1 atm total pressure. Liquid reagents such as $\text{CF}_2\text{Cl-CFCl}_2$ or CHCl_3 (chloroform) are admitted to the reactor by sparging helium gas through the liquid held at 0°C in an ice point impinger. Gaseous CFCs enter directly through calibrated rotameters. Calibration of the reactor temperature is performed using a 1/8" diameter Type-K thermocouple probe. This probe is moved axially to obtain the temperature of the reactor.

Helium is allowed to flow through the reactor to minimize radiation error from the furnace wall by cooling the bare-bead junction to the temperature of the gas.

Samples are drawn through a cold surface water cooled sampling probe by use of a vacuum pump. Gas leaving the probe passes through a heated line to a six port gas sampling valve equipped with a 1 mL sample volume for on-line analysis using GC/FID. Reactant and stable products are quantified using a GOW MAC model 750 P GC with dual flame ionization detectors. Gas chromatographic separations are carried out using a packed column Graphpac 60/80 mesh with 5% Fluorol (Supelco) or Carbowax with 5% Krytox (Alltech) which give excellent separation for complex mixtures of hydrocarbons, fluorocarbons, and CFCs. Accurate calibration of FID responses for parent CFCs are obtained by using a reactor bypass. GC/MS analyses are performed off-line for product identification. After initial identification, product responses are calibrated using standards prepared from the pure materials which are obtained from PCR Chemicals Inc, Gainesville, FL. Standards are prepared to determine GC response factors.

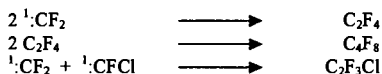
HCl and HF produced are quantified by diverting the total reactor effluent through a 2 stage impinger containing standardized NaOH solution and an appropriate indicator dye. Cl⁻ and F⁻ concentrations are measured directly using ion selective electrodes (Fisher Scientific). The electrodes are calibrated using standardized Cl⁻ and F⁻ solutions prepared at pH similar to the samples. All standards and samples contain the total ionic strength adjuster appropriate to the halide which is being measured. These measurements give total F⁻ and Cl⁻ only and do not speciate between halogen and hydrogen halide gases. They are used to check material balance on halogens.

RESULTS AND DISCUSSION

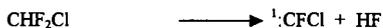
Results from CHF₂Cl pyrolysis in helium at 2 seconds reaction time suggest that CHF₂Cl conversion primarily follows first order kinetics at low temperatures (773 - 898K) via unimolecular HCl elimination:



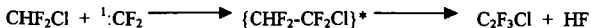
The major products of the pyrolysis in helium include perfluoroethylene (C₂F₄, the most abundant product), perfluoropropene (C₃F₆), octafluorocyclobutane (C₄F₈), and chlorotrifluoroethylene (C₂F₃Cl). Perfluoroethylene is formed by ¹CF₂ combination, C₄F₈ by dimerization of C₂F₄, and C₂F₃Cl by recombination of ¹CF₂ and ¹CFCl.



The product C₂F₃Cl is observed at temperatures only above 898K, suggesting either some degree of HF elimination from CHF₂Cl occurs at higher temperatures



or that ¹CF₂ inserts into CHF₂Cl followed by α, β HF elimination from the adduct:



Perfluoropropene (C₃F₆) most likely results from reaction of ¹CF₂ and C₂F₄. Although carbenes are believed to add to double bonds to form cyclopropanes (March, 1992), perfluorocyclopropane (cyC₃F₆) is not observed. This suggests that rapid isomerization to the perfluoropropene occurs, or some other mechanism is responsible for the production of this species.

The elimination of HCl from CHF₂Cl represents the lowest dissociation channel. However, at higher temperatures (above 898K) it becomes apparent that conversion of CHF₂Cl moves away from first order kinetics. When a first order assumption is applied over the entire temperature range (773 - 1023K), an Arrhenius plot yields an activation energy of 43 kcal/mol. This energy barrier, however, is lower than the ΔH of the reaction based upon the H_f of ¹CF₂ used by Paulino and Squire (1991). This suggests that there is a shift in reaction mechanism at higher temperatures.

923K. Results obtained at 973K, however, show a noticeable increase in CF_2Cl_2 conversion. This result suggests that $^1\text{CF}_2$ plays a role in CF_2Cl_2 conversion, under these conditions. This system is currently being investigated in more detail.

CONCLUSION

Insertion of $^1\text{CF}_2$ into C-H bonds appears to be important during the pyrolysis of CHF_2Cl and mixtures of CHF_2Cl and $\text{C}_2\text{HF}_4\text{Cl}$ at temperatures greater than 898K. Addition of H_2 to the CHF_2Cl pyrolytic system inhibits conversion by scavenging $^1\text{CF}_2$ by reaction with H_2 . Dichlorocarbene insertion into C-X appears to be an unfavorable reaction based upon experiments involving CHCl_3 and CF_3Cl . Similar reactions involving CF_2Cl_2 are currently being.

REFERENCES

- Buravtsev, N.N, Grigor'ev, A.S., and Kolbanovskii, Y.A. (1989) Kinet. Catal.
- DiFelice, J.J. and Ritter, E.R. (1993), presented at the Fall Technical Meeting of the Combustion Institute (Eastern States Section), Princeton, NJ, Oct. 1993.
- Ho, W., Yu, Q., and Bozzelli, J (1992), Comb. Sci. and Tech., 85, 22.
- March, Jerry (1992), Advanced Organic Chemistry, 2nd ed., John Wiley & Sons, NY.
- Melius, Carl F. (1993), BAC-MP4 Heats of Formation and Free Energies.
- Naglei, D.W., Robledo, R.C., and Erwin, J. (1991), Western States Combustion Institute Meeting, Los Angeles, CA, Paper No. 91-60.
- NIST (1991) Chemical Kinetics Database Version 3.0, NIST Standard Reference Database 17, 1991.
- Paulino, J.A. and Squires (1991), R.R., J. Am. Chem. Soc., 113, 5573-5580.
- Ritter, E.R., Bozzelli, J.W., and Dean (1990), A.M., J. Phys. Chem., 94, 2493.
- Ritter, E.R. (1993), Submitted to Combustion Science and Technology, (accepted, in press, 1994).
- Tokuashi, K., Urano, Y., Horiguchi, S. and Kondo, S., (1990) Combustion Science and Technology, 72, 117-129.
- Won, Y. S. and Bozzelli, J. W. (1992), Combust. Sci. and Tech., 85, 345.

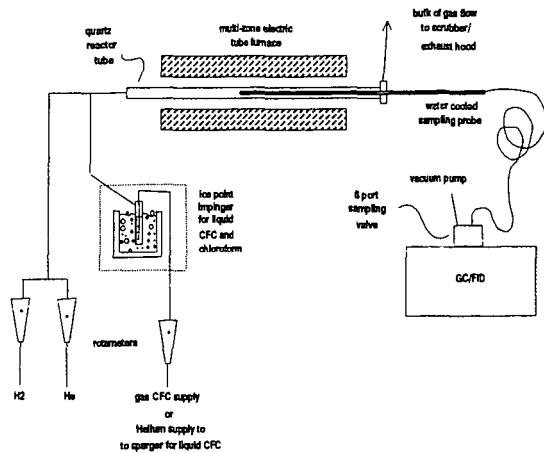


Figure 1. EXPERIMENTAL APPARATUS

C/Co vs. T(K); t=2 sec

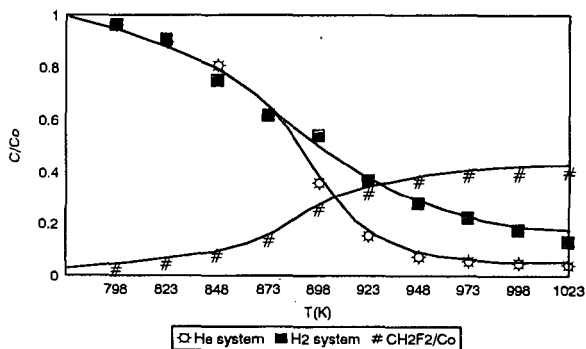


Figure 2. CHF₂Cl PYROLYSIS IN HE AND H₂

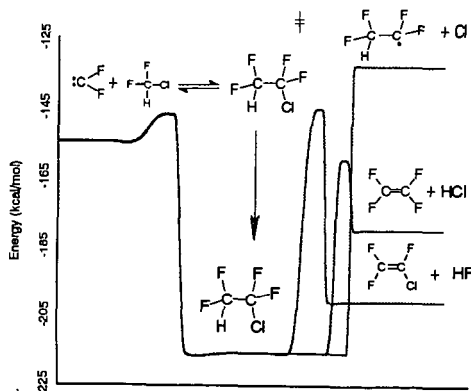


Figure 3. ¹:CF₂ INSERTION INTO CHF₂Cl

LAMINAR FLAMELETS, CONSERVED SCALARS, AND NON-UNITY LEWIS NUMBERS: WHAT DOES THIS HAVE TO DO WITH CHEMISTRY?

J. Houston Miller and Michael A.T. Marro
Department of Chemistry
The George Washington University
Washington, DC 20052

and

Mitchell Smooke
Department of Mechanical Engineering
Yale University
New Haven, CN

Keywords: conserved scalar, flamelet, combustion model

Abstract

In general, computation of laminar flame structure involves the simultaneous solution of the conservation equations for mass, energy, momentum, and chemical species. It has been proposed and confirmed in numerous experiments that flame species concentrations can be considered as functions of a conserved scalar (a quantity such as elemental mass fraction, that has no chemical source term). One such conserved scalar is the mixture fraction which is normalized to be zero in the air stream and one in the fuel stream. This allows the species conservation equations to be rewritten as a function of the mixture fraction (itself a conserved scalar) which significantly simplifies the calculation of flame structure. Despite the widespread acceptance that the conserved scalar description of diffusion flame structure has found in the combustion community, there has been surprisingly little effort expended in the development of a detailed evaluation of how well it actually works. In this presentation we compare the results of a "full" transport and chemical calculation performed by Smooke with the predictions of the conserved scalar approach. Our results show that the conserved scalar approach works because some species' concentrations are *not* dependent only on mixture fraction.

Introduction

The use of the laminar flamelet concept endures as an important tool in the analysis of turbulent combustion systems. In this technique, the occurrence of flamelet structures is determined probabilistically and then combined with structural information derived from either laminar flame calculations or experiments^{1,2,3,4}. A central criticism of the use of these laminar flamelet libraries to model turbulent systems centers on the interaction of small scale turbulent structures with flamelet structures.

In general, computation of laminar flame structure involves the simultaneous solution of the conservation equations for mass, energy, momentum and species. The latter may be solved in the Shvab-Zeldovich form⁵ as (Equation 1):

$$L(Y_i) \equiv \rho \frac{\partial Y_i}{\partial x} + \rho V \cdot \nabla Y_i - \nabla \cdot (\rho D_i \nabla Y_i) = w_i$$

where Y_i is the mass fraction of species i , w_i is the chemical production rate of species i , ρ is the total gas density, V is the convective velocity, and D_i is the molecular diffusivity.

Chemical elements (such as $i = C, H,$ or O) are conserved throughout the chemical reaction mechanism ($L(Z_i) = 0$). Linear combinations of elemental abundances, such as the mixture fraction, ξ , will also be conserved. Here we adopt Bilger's⁶ formulation of mixture fraction in terms of conserved scalars representing relative elemental concentrations for the fuel and oxidant streams in terms of atomic masses for $C, H,$ and O and their mass fractions.

It has been previously shown⁶ that flame species concentrations are only functions of ξ . This observation, combined with the assumption of equal diffusivities of all flame species, allows the species conservation equation (Eq. 1) to be rewritten as a function of the mixture fraction. The net chemical production rate for a species then can be written as (Equation 2):

$$w_i = -\left(\frac{1}{2}\right) \cdot \rho \chi \cdot \left(\frac{\partial^2 Y_i}{\partial \xi^2}\right)$$

with the instantaneous scalar dissipation rate, χ , defined as (Equation 3):

$$\chi = 2D \cdot (\nabla \xi^2)$$

It has been postulated that concentrations will depend exclusively on mixture fraction when chemical times are short with respect to transport times (i.e., large Damkohler number). It has been shown that this condition is not met for species whose chemistry of formation is slow^{7,8}. It has also been suggested that a second independent variable may be required to determine concentrations even for species whose chemistry is fast, and the scalar dissipation rate has been suggested as that variable^{9,10,11}. When a species' concentration is determined mostly by its mixture fraction dependence, molecular diffusion will occur preferentially along paths of the steepest mixture fraction gradients in space (Figure 1). We refer to these paths as diffusive trajectories in this paper.

Despite the widespread acceptance that the conserved scalar description of diffusion flame structure has found in the combustion community for the description of turbulent flame structure, there has been surprisingly little effort expended in the development of a detailed evaluation of how well it actually works^{12,13}. In this paper we analyze the validity of the conserved scalar approach to the analysis of laminar flame structures. Using the results of a flame structure calculation which has recently been reported¹², we evaluate the magnitude of the net chemical production rate, w_p , using Eq. 2 above and compare it to rates calculated from contributions of specific reactions in the flame code. The agreement between these two methods provides a test of the conserved scalar approach.

Flame Structure Calculations

The chemical structure of an unconfined, co-flowing, axisymmetric CH₄/air diffusion flame was computed with detailed transport and finite rate chemistry. C1 and C2 chemistry were included in a reaction mechanism which involved 83 reversible reactions and 26 species. Details of the calculation have been presented previously, and are summarized briefly below. The fuel was introduced into the flame through an inner tube of radius 0.2 cm and the coflow air through a concentric 5.0 cm diameter outer tube. The results of this flame calculation have been compared with an extensive data base of species concentrations and temperatures collected in a Wolfhard-Parker laminar diffusion flame. Concentration profiles of most flame species agree well for the calculations and the experiments. From calculated species concentrations, temperatures and their positions, ξ and χ can be calculated¹².

Figure 1 shows contours of mixture fraction in the calculated flame. Also shown are a number of diffusive trajectories through the flame. As stated earlier, these trajectories originate in the fuel rich regions of the flame and follow mixture fraction from rich to lean flame regions along pathways of the steepest gradient of ξ . As the data in this figure illustrate the mixture fraction gradients along these different vary dramatically, with those which cross the stoichiometric contour near the base of the flame having significantly steeper gradients than those that cross higher in the flame (for example the centerline trajectory).

Figure 2 illustrates the range of mixture fractions and scalar dissipation rates which are observed throughout the computed flame. This data show that at the stoichiometric surface ($\xi=0.055$) the value of the scalar dissipation rate (χ_{ST}) varies dramatically, from nearly 0 up to 5 s⁻¹. Extinction occurs in methane/air flames⁷ at $\chi_{ST}=12$ s⁻¹. Since the data shown in this figure include only locations as low as 0.64 mm above the burner surface, it is reasonable to expect that extinction occurs at lower flame heights.

Figure 3 shows concentrations of methane plotted as a function of mixture fraction for computational nodes throughout the flame. Except for positions very low in the flame, methane concentrations collapse onto a single curve when plotted in this way. Figure 4 shows a similar data presentation for hydrogen atom concentrations. In contrast to the data for methane, the peak shape as well as the peak location shows a dependence on flame location with data low in the flame having larger peak concentrations that occur at lower (leaner) mixture fractions.

Conserved Scalar Rates

Mass fractions of methane, Y_{CH_4} , were calculated and plotted against mixture fraction along each of the chosen trajectories of Figure 1. For these trajectories the dependence of Y_{CH_4} on ξ is largely independent of the trajectory chosen. These curves were numerically differentiated, and combined with local scalar dissipation rates to calculate the net production rate of methane

throughout the flame using Eq. 2. For this calculation we adopt Smooke's formulation for the diffusion coefficient⁴.

Figure 5 shows the results for all except the richest flame regions (for $\xi > 0.2$, w , rapidly approaches zero). Notice the sharp increase in CH_4 consumption near the stoichiometric surface. Because the methane concentrations show a common dependence on mixture fraction (Fig. 3), the magnitude of the conserved scalar rates is determined by the magnitude of the scalar dissipation rate which is largest near the base of the flame.

Chemical Rates

Of the 83 reactions in the mechanism used by Smooke six include methane as a reactant or product. The net rate of methane formation can be evaluated at each location in the flame by summing the contributions of these reactions. Figure 6 shows the dependence of these net rates on mixture fraction along the three diffusive trajectories. As the data in Figs 5 and 6 show, there is good agreement between rates calculated using the conserved scalar approach and that from an evaluation of the rate law. The six reactions that involve methane in the mechanism include it's abstraction reaction with hydrogen atoms. The data in Fig. 4 show that hydrogen atom concentrations, like the scalar dissipation rate, show a strong dependence on flame position with larger concentrations low in the flame.

Net chemical production rates for hydrogen atoms using the conserved scalar approach do not agree with those calculated using the hydrogen rate law in the mechanism. This result might have been anticipated given the non-collapse of the concentration versus mixture fraction data shown in Fig. 4.

Conclusions

In this paper we have compared the results of a "full" transport and chemical calculation performed by Smooke with the predictions of the conserved scalar approach. Our results show that the conserved scalar approach works because some species' concentrations are *not* dependent only on mixture fraction. For the latter species, the net chemical rates can not be evaluated from conserved scalar expressions. The current effort in this project focuses on the cause for the hydrogen atom concentration dependence on flame location. One possibility for this relationship is the fast diffusion velocity that exists for hydrogen atoms near the base of the flame because of its steep concentration gradients. For this species, transport times are short and of the same magnitude as chemical times. It is interesting to conjecture that this fast transport may be cast quantitatively as a dependence of concentration on scalar dissipation rates as has been proposed for flamelet modeling of turbulent combustion.

References

1. Williams, F.A. *Turbulent Mixing in Non-Reactive and Reactive Flow*; Plenum: New York, 1975, 198.
2. Peters, N. *Twenty-First Symposium (International) on Combustion*; The Combustion Institute: Pittsburgh, 1986, 1231.
3. Bilger, R.W. *Twenty-Second Symposium (International) on Combustion*; The Combustion Institute: Pittsburgh, 1988, 475.
4. Hermanson, J.C.; Vranos, A. *Combust. Sci. and Tech.*; 1991, 75, 339.
5. Williams, F.A. *Combustion Theory*; Addison-Wesley: Reading, MA, 1965.
6. Bilger, R.W. *Combust. and Flame*; 1977, 30, 277.
7. Smyth, K.C.; Taylor, P.H. *Chem. Phys. Lett.*; 1985, 122, 518.
8. Miller, J.H. *Twenty-Fourth Symposium (International) on Combustion*; The Combustion Institute: Pittsburgh, 1992, 131.
9. Drake, M.C. *Twenty-First Symposium (International) on Combustion*; The Combustion Institute: Pittsburgh, 1986, 1579.
10. Seshadri, K.; Maub, F.; Peters, N.; Warnatz, J. *Twenty-Third Symposium (International) on Combustion*; The Combustion Institute: Pittsburgh, 1990, 559.
11. Peters, N.; Kee, R.J. *Combust. and Flame*; 1987, 68, 17.
12. Norton, T.S.; Smyth, K.C.; Miller, J.H.; Smooke, M.D. *Combust. Sci. and Tech.*; 1993, 90, 1.
13. Smooke, M.D.; Lin, P.; Lam, J.K.; Long, M.B. *Twenty-Third Symposium (International) on Combustion*; The Combustion Institute: Pittsburgh, 1990, 575.
14. Smooke, M.D.; Giovangigli, V. *Reduced Kinetic Mechanisms and Asymptotic Approximations for Methane-Air Flames*; Lecture Notes in Physics, Springer-Verlag: Berlin, 1991, 384, 1.

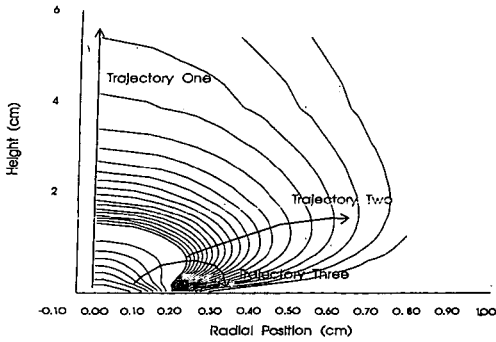


Figure One: Pictorial representation of the diffusive trajectories chosen across contours of mixture fraction, ξ .

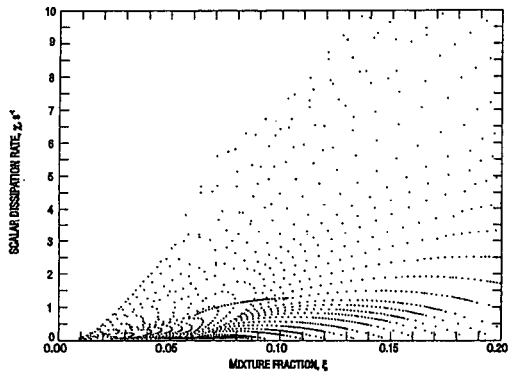


Figure Two: Plot of scalar dissipation rate, χ , versus mixture fraction, ξ . Values move from low to high in the flame from top to bottom.

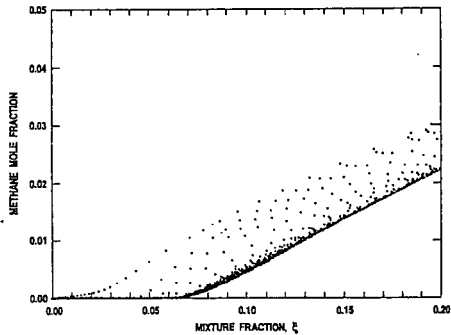


Figure Three: Plot of CH_4 mole fraction versus mixture fraction, ξ . (Positions low in the flame are on the left).

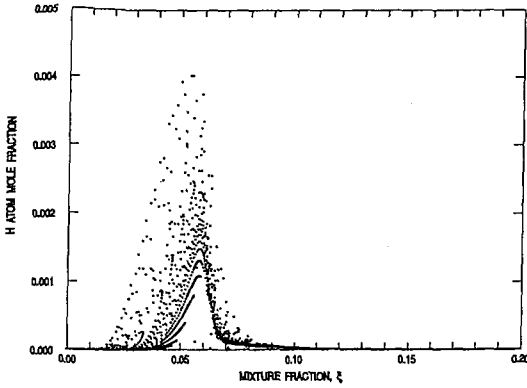


Figure Four: Plot of H atom mole fraction versus mixture fraction, ξ . (Values move from low to high in the flame from top to bottom).

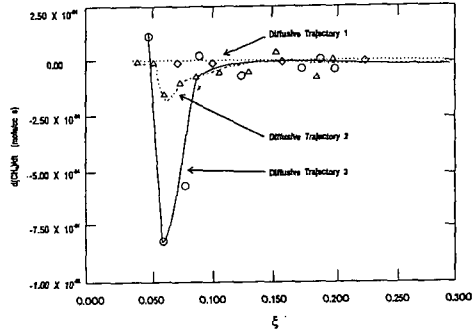


Figure Five: Conserved Scalar predicted rates of CH_4 production versus mixture fraction, ξ , along the diffusive trajectories chosen.

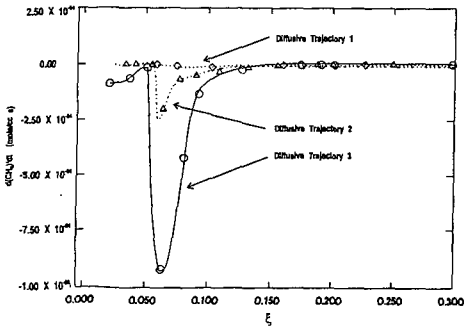


Figure Six: Chemical rate of CH_4 formation versus mixture fraction, ξ , along the chosen diffusive trajectories.

COMPUTER MODELING OF CHLORINE-CATALYZED INHIBITION REACTIONS IN C₂H₄/H₂/AIR/Cl₂ OXIDATION

C.R. Casias and J. Thomas McKinnon
Department of Chemical Engineering and Petroleum Refining
Colorado School of Mines
Golden, CO, 80401

Keywords: Chlorinated hydrocarbons, oxidation, chlorine inhibition

INTRODUCTION

This paper pertains to research currently underway in the area of chlorinated hydrocarbon combustion. The effects on combustion of chlorinated hydrocarbons or in the presence of chlorine is of practical importance, particularly as related to the incineration of hazardous wastes consisting of organic material containing chlorinated hydrocarbons. Overall, this effort has been undertaken in order to obtain a better understanding at the microscopic level of the oxidation process relating to free radical branching and inhibition of free radical branching. Additionally, this effort may provide insight for a better understanding of the conditions resulting in flame blow-out.

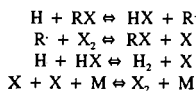
The effects on the concentration of free radicals such as H and OH in the presence of Cl have been previously studied by others. The principal reaction for the production of free radicals is given as



In the presence of chlorine, this reaction is generally considered to become inhibited by a reduced H atom concentration as a result of the formation of molecular hydrogen through the following net reaction,



The actual route through which H₂ is formed will vary depending on the temperature and concentration of species present. A generalized kinetic model for catalyzed recombination of H atoms (Westbrook, 1982) considers a cycle of reactions to result in the above net reaction. This cycle consists of the following reactions,



where X represents the halogen atom and R represents methyl, ethyl, or vinyl radicals.

This cycle of reactions will be of significance in recombining H atoms when the rates on each of the reactions are of the same relative order and particularly when no reaction significantly inhibits the ability of another reaction to proceed. For instance, if the first reaction of the cycle is limiting, the importance of following reactions dependent on the free radical R will be greatly reduced. Thus, the net recombination reaction must be rigorously analyzed by evaluation of each of the individual reactions involved in the cycle. These types of analyses are currently underway and preliminary findings are presented.

Additionally, conditions for blow-out are being assessed in order to establish the mechanism leading to this phenomena. The difficulty in assessing this is due primarily to the interdependency of temperature and the reaction mechanisms contributing to the rate of change of free radicals.

MODELING APPROACH

This study focuses on computer simulation predictions of the effects on ethylene oxidation by the introduction of chlorine in concentrations of less than 0.005 initial mole fraction, and under lean fuel conditions. Ethylene, being a hydrogen lean fuel, will produce a lower concentration of H atoms and changes in the concentration should therefore be more apparent.

The computational analysis was conducted using the Sandia CHEMKIN (Kee et al, 1989) and Perfectly-Stirred Reactor (PSR) (Glarborg et al, 1990) codes running on an IBM RISC 6000 computer. Calculations were performed adiabatically whereby inlet gas temperature and the mixture composition were specified.

The thermochemical data were acquired primarily from a Sandia National Laboratories report (Kee et al, 1992), although some estimations were conducted based on group additivity theory (Benson, 1976). The detailed chemical kinetic reaction mechanism consisting of 189 reversible and 77 irreversible elementary reactions was used. These elementary reactions were compiled from three different sources and account for the chlorinated hydrocarbon chemistry of trichloroethane (Chang and Senkan, 1986), inclusion of HCl and Cl₂ inhibiting reaction mechanisms (Westbrook et al, 1977), and premixed CH₃Cl/CH₄/air flames employing enhanced third-body effectivities (Lee et al, 1993).

For the adiabatic configuration, the fuel equivalence ratio of ethylene was approximately 0.75. The inlet temperature was set at 1650 K and chlorine was introduced in the form of Cl₂. To minimize the deviations of the inlet mole fractions of fuel and air, an initial mole fraction for H₂ of approximately 0.02 was included, and as the inlet mole fraction of Cl₂ was increased, the H₂ mole fraction was correspondingly decreased. The Cl₂ mole fraction was varied from 0.000 to 0.020; however, the primary region of interest was below 0.005 mole fraction Cl₂. The residence time was varied throughout the region of no conversion of C₂H₄ at the initial time to a time where the conversion was greater than 0.90. The residence time was increased as specified and then reduced to a time less than the time required for blow-out to occur. At the blow-out time, sensitivity analysis were conducted for the purpose of evaluating the dominant reactions at this point.

RESULTS

Results for exit mole fraction versus residence time are plotted in Figures 1 through 4 for varying inlet concentrations of Cl₂. These results agree with general expectations in that as the Cl₂ concentration is increased from 0.0025 to 0.01 mole fraction, the ignition and blow-out residence times increase. Below a value of 0.0025, the results from computer modelling indicate that ignition will not occur. This prediction also agrees with expectations since the more reactive Cl₂ possesses a greater tendency than H₂ to interact with other species in the reactor, particularly at lower temperatures.

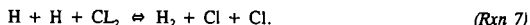
At the point just prior to blow-out, sensitivity analyses were conducted. Species evaluated included H, OH, O and H₂. The most significant reactions were the free radical chain branching reactions



Since the concentrations of the free radicals decreased as the Cl₂ concentration increased, this result is evidence that Cl₂ plays a role in the removal of OH and H radicals. In conjunction with Westbrook's findings, one mode of chlorine-catalyzed recombination consistent with the results obtained in this analysis would include the following reactions,



where the net reaction would yield,



Reactions 5 and 6 were among the more significant reactions as indicated from the sensitivity analysis. Preliminary assessment of the possibility of this pathway has included the evaluation of the forward and reverse rate constants and rates. Continued investigations will include in-depth analysis kinetics of this particular pathway as well as investigation into other possible pathways. Other such pathways under investigation include the set of reactions



and



where the net reaction results in H atom recombination. The rates for these sets of reactions are being evaluated at various temperatures and species concentrations to determine their relative order and role in H atom recombination.

ACKNOWLEDGEMENT

This work is supported by the National Science Foundation National Young Investigation Program (Grant Number CTS-9258149)

REFERENCES

- Benson, S.W., *Thermochemical Kinetics*, (1976), 2nd. Ed., John Wiley & Sons, New York.
- Chang, Wen-Dong, and Senkan, Selim M., Detailed Chemical Kinetic Modelling of Fuel-Rich $C_2HCl_2/O_2/Ar$ Flames, (1989), *Environ. Sci. Technol.*, **23**, 442-450.
- Glarborg, P., Kee, R.L., Grcar, J.F., and Miller, J.A., (1990), "PSR: A FORTRAN Program for Modeling Well-Stirred Reactors", Sandia National Laboratories, SAND86-8209.
- Kee, R.J., Rupley, F.M., and Miller, J.A., "The Chemkin Thermodynamic Data Base", (1992), Sandia National Laboratories, SAND-8215B
- Kee, R.J., Rupley, F.M., and Miller, J.A., (1989), "Chemkin-II: A Fortran Chemical Kinetics Package for the Analysis of Gas-Phase Chemical Kinetics", Sandia National Laboratories, SAND89-8009.
- Lee, K.Y., Yang, M.H., and Puri, I.K., (1993), Numerical Simulation of Stoichiometric Premixed Flames Burning $CH_3Cl/CH_4/Air$ Mixtures at Atmospheric Pressure with a Full and Short Mechanism and Comparison of the Flame Speeds with Experimental Results, *Combust. Flame*, **92**, 419-439.
- Westbrook, C.K., (1982), Inhibition of Hydrocarbon Oxidation in Laminar Flames and Detonations by Halogenated Compounds, *Nineteenth Symp. (Int'l) on Comb.*, The Combustion Institute, 127-141.
- Westbrook, C.K., Creighton, J. Lund, and Dryer, F.L., (1977), A Numerical Model of Chemical Kinetics of Combustion in a Turbulent Flow Reactor., *J. Phys. Chem.*, **81**, 2542.

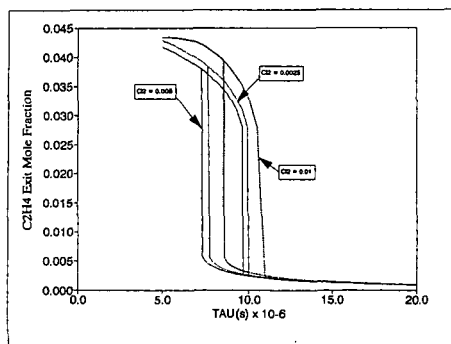


Figure 1. Ethylene Oxidation: Exit mole fraction of ethylene in a perfectly-stirred reactor for initial Cl_2 inlet mole fractions of 0.0025, 0.005, and 0.01.

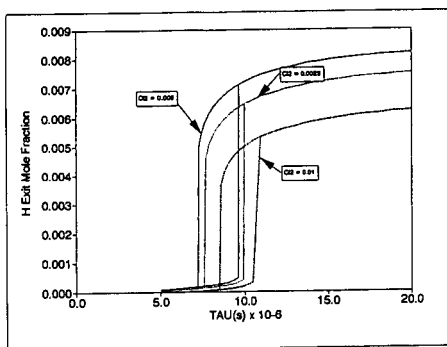


Figure 2. Ethylene Oxidation: Exit mole fraction of H in a perfectly-stirred reactor for initial Cl_2 inlet mole fractions of 0.0025, 0.005, and 0.01.

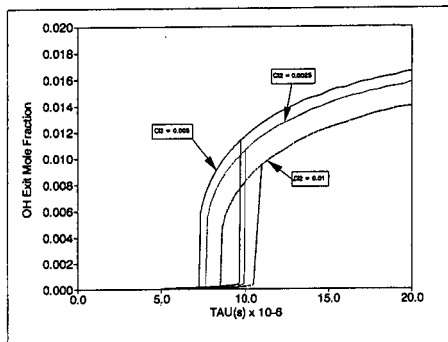


Figure 3. Ethylene Oxidation: Exit mole fraction of OH in a perfectly-stirred reactor for initial Cl_2 inlet mole fractions of 0.0025, 0.005, and 0.01.

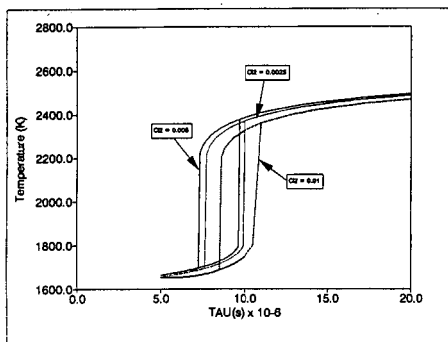


Figure 4. Ethylene Oxidation: Temperature profile in a perfectly-stirred reactor for initial Cl_2 inlet mole fractions of 0.0025, 0.005, and 0.01.

NUMERICAL CALCULATION OF SOOT FORMATION IN PREMIXED HYDROCARBON FLAMES

Fabian Mauss and Henning Bockhorn
Fachbereich Chemie, Universität Kaiserslautern
Erwin Schrödingerstraße, 67663 Kaiserslautern, Germany

Keywords: Soot formation, numerical simulation, hydrocarbon flames

Abstract

Numerical calculations including a chemical model for soot formation have been performed for premixed burner stabilized ethene-air flames at 0.1 and 1.0 MPa that have been investigated experimentally by Wagner et al. The maximum temperatures in the flames have been varied in the experiments by changing the mass flow rates of the mixture. In accordance with the experimental data the numerical calculations predict a bell shaped dependence of the final soot volume fraction on the maximum flame temperature.

The dependence of the final soot volume fraction on pressure between 0.1 and 1.0 MPa is calculated to be proportional $p^{1.5}$ to p^2 . This is slightly weaker than found experimentally in the experiments of Wagner et al. It is concluded that the pressure dependence of some gasphase reaction rates, in particular that for the formation of benzene and the PAH growth has to be validated.

Introduction

In sooting hydrocarbon flames fuel molecules are converted within few milliseconds into carbonaceous particles containing millions of carbon atoms. It is known that the formation of soot is mainly determined by particle inception, by coagulation of primary soot particles to larger aggregates, and by heterogeneous reactions of soot particles with the surrounding gasphase. Much progress has been made in understanding these processes, however, a number of problems are yet unsolved [1-4].

Phenomenologically, the final soot volume fraction f_v^∞ in premixed flames—that is the soot volume fraction attained shortly after the reaction zone—depends for a given fuel on pressure, mixture, composition and temperature. From numerous experimental work, e.g. [5-9] it is known that in a pressure range from 0.1 to 1.0 MPa the final soot volume fraction varies with the square of pressure. The temperature dependence of the final soot volume fraction reveals a bell shaped form, whereas the dependence on mixture composition may be given as $f_v^\infty \sim [(C/O) - (C/O)_{\text{sooting limit}}]^n$ with $2.5 \leq n \leq 3$, cf. [8].

The formation of soot in premixed flames is dominated by heterogeneous surface growth reactions, see e.g. [10,11]. Ethyne has been found to be the most likely chemical "growth specie", because ethyne is the most abundant hydrocarbon species in the soot forming region of premixed flames.

A mechanistic interpretation of surface growth reactions has been introduced by Frenklach [12]. Analogously to the planar growth of polycyclic aromatic hydrocarbons, surface growth of soot particles is, on the per-site basis, explained by a radical hydrogen abstraction carbon addition (HACA) mechanism. In addition oxidation of soot particles by OH and O₂ has been taken into account.

In the following the over-all temperature and pressure dependence of the final soot volume fraction is explained in terms of chemical reactions between gasphase compounds and the soot surface. This concept basically contains the competing processes in soot formation by surface reactions: carbon addition by adding ethyne and oxidation by oxygen and OH. Presuming a different temperature dependence of the three processes, the picture of the temperature dependence of the soot volume fraction is—in principle—understandable.

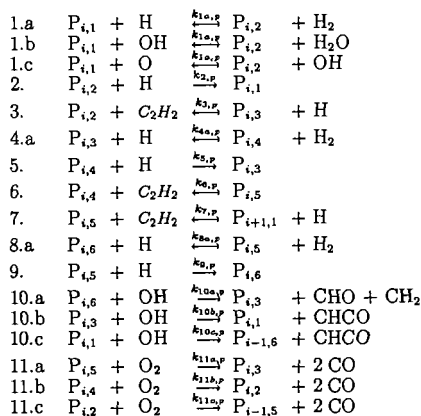
Model for soot formation

The model for soot formation that has been integrated into a numerical code for one-dimensional flat premixed flames, cf. [14], has been developed from the one discussed above. The PAH growth has been formulated with the help of fast polymerisation reactions [14] reducing the number of equations to be solved and the numerical effort. It should be emphasized that detailed models of the kind below depend essentially upon the quality of kinetic parameters and the knowledge of the reaction channels for the reactions of the species involved. Furthermore, it should be mentioned that these models reproduce only phenomena connected with the formation of the bulk of soot. Many phenomena, e.g. the formation of high molecular tarry structures that are observed in an early stage of soot formation or the "fine structure" of soot are not covered by these models.

The model is essentially subdivided into three parts — gas phase chemistry, polymerisation of PAH and formation and growth of soot particles.

The gas phase chemistry up to the first aromatic ring is calculated with the help of a detailed mechanism provided by Warnatz [15], consisting of about 250 elementary reactions between 52 chemical species. The first aromatic ring, viz. benzene, is formed via the reaction $C_3H_3 + C_3H_3 \rightleftharpoons c - C_6H_6$. The calculation of the growth reactions of benzene to small PAH follows the mechanism suggested by Frenklach and Warnatz [16]. Following Frenklach [17], the further growth of PAH is assumed to be a polymerisation process.

Within each polymerisation stage two aromatic rings are added to a given PAH. Each step from PAH to PAH involves several chemical reactions. The detailed growth and oxidation mechanism used for the calculations presented here is given below.



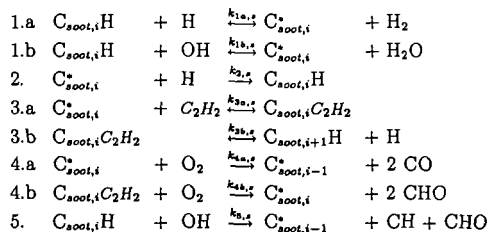
The growth mechanism is initiated by an H-abstraction step due to the attack of H, O and OH via reactions 1a-1c. The radicalic site of $P_{i,2}$ may be deactivated by the H-addition (reaction 2) or by the revers of reactions 1a-1c. Ethyne is taken up at the radicalic site of $P_{i,2}$ via reaction 3. The repetition of this reaction sequence (reactions 4-6) leads to the closure of an aromatic ring. Because $P_{i,5}$ has a radicalic site, ethyne may be added again and an other ring closure occurs (reaction 7). This second ring closure leads to the next polymerisation stage, where the reaction sequence is repeated. In analogy to the radical sites of $P_{i,2}$ and $P_{i,4}$ the radical site of $P_{i,5}$ can be deactivated by H-addition (reaction 9) or by the revers of reactions 8a-8c. PAH may be oxidized by reactions with OH (10.a-c) and t PAH with a radicalic site may be oxidized by reactions with O_2 (11.a-c).

The formulated reaction sequence is one possible reaction sequences leading to PAH-growth involving six-membered rings. Five-membered rings can be included by similar reaction sequences involving a larger number of intermediates without affecting, however, the basic ideas of the following approach.

Differently from the approach of Frenklach the growth of the PAH is assumed to be a fast polymerisation process. It follows that each PAH is in quasi steady state and that the concentrations of PAH can be calculated from an algebraic system of equations. Details of this analysis are given in [14].

The pathways to soot from PAH are particle inception and condensation of PAH on the surface of the soot particles. Both pathways are assumed to follow Smolouchowski's coagulation equations in the free molecular regime [12,18]. The equations are also used to calculate the coagulation of soot particles.

The heterogeneous surface growth and oxidation of soot particles follow the mechanism given below:



The mechanism is modified compared with the one introduced by Frenklach [12]. The reverse of reaction 1.b accounts for the radicalic site consuming influence of H_2O . Reaction 3 consists of two reactions—carbon addition, ring closure—, because it has been found recently that the reverse of reaction 3 accounts for the limitation of surface growth at high temperatures [19]. The more detailed analysis here shows, that the reverse of reaction 3.a is responsible for this effect, while reaction 3.b is approximately irreversible. If—in analogy to Frenklach's formulation and the planar PAH growth— $\chi(C_{soot,i}^*)$ and $\chi(C_{soot,i},C_2H_2)$ are replaced by the assumption of quasi stationarity, the appearance rate of soot can be expressed as follows. We first introduce a factor accounting for the progress of soot growth.

$$f3a = \frac{k_{3b,f}}{k_{3b,f} + k_{3a,b} + k_{4b}[O_2]} \quad (1)$$

If the ring closure via reaction $k_{3b,f}$ is fast compared with the radicalic site consuming and oxidation reactions then $f3a = 1$. If the radicalic site consuming and oxidation reactions are fast then $f3a = 0$. With this definition we write

$$\chi(C_{soot,i}^*) = \frac{k_{1a,f}[H] + k_{1b,f}[OH] + k_{3b,b}[H](1 - f3a)}{k_{1a,b}[H_2] + k_{1b,b}[H_2O] + k_2[H] + k_{3a,f}[C_2H_2]f3a} \cdot \chi(C_{soot,i}) \quad (2)$$

$$\chi(C_{soot,i},C_2H_2) = \frac{k_{3a,f}[C_2H_2]}{k_{3b,f} + k_{3a,b} + k_{4b}[O_2]} \cdot \chi(C_{soot,i}^*) + \frac{k_{3b,b}[H]}{k_{3b,f} + k_{3a,b} + k_{4b}[O_2]} \cdot \chi(C_{soot,i}) \quad (3)$$

$$\frac{df_0}{dt} = (k_{3a,f}[C_2H_2]f3a \cdot \chi(C_{soot,i}^*) - (k_{3b,b}[H](1 - f3a) + [OH]k_5) \cdot \chi(C_{soot,i})) \cdot S \quad (4)$$

In the soot forming limit ($f3a = 1$). In the radicalic site consuming limit, $f3a = 0$ the growth of soot is limited at high temperature because of the high activation energy of reaction $k_{3a,b}$.

The algebraic formulation of this model leads to an infinite number of partial differential equations for the number density of soot particles which is reduced to a limited number by using the method of moments (method 2 in [18]). Thermophoretical transport and size dependent diffusion of soot particles has been considered. The system of equations is solved numerically employing a Newton Method

Results and Discussion

Burner stabilized flat premixed ethene-air flames ($C/O = 0.72$) that have been investigated experimentally by Wagner et al. [8,20] have been numerically simulated at 0.1 and 1.0 MPa. The maximum flame temperature in the experiment has been varied by varying the mass flow rate of the unburnt mixture.

The temperature and soot volume fraction profiles of an ethene-air flame ($C/O = 0.72$) with a cold gas flow velocity of 4.5 cm/s are given in Fig.1. The soot volume fraction (cm^3_{soot}/cm^3_{gas}) is density related. Therefore, we have normalized the profile to a temperature of 1400 K. This is also demonstrated in Fig.1. It is obvious from this figure, that the final soot volume fraction is attained at a height of 35 mm above the burner. At larger heights the soot volume fraction increases with decreasing temperature and the normalized soot volume fraction remains constant. The agreement between calculated and measured data is reasonably good.

The calculated final soot volume fractions of all investigated flames at 0.1 MPa are shown in Fig. 2 in dependence on the flame temperature at 10 mm height above the burner. The final soot volume fraction: is given in the the normalized form. We prefer the normalized soot volume fraction, because this definition is not dependent on the shape of the temperature profile. The comparison of the model prediction with experimental data from Refs.[8,20] reveal that the calculations reproduce the soot volume fraction quite well at high flame temperatures. At lower flame temperatures the agreement between measured and calculated soot volume fractions is reasonable. In summary, the over-all dependence of soot formation on flame temperature can be understood with the help of the detailed chemistry soot model.

Most of the rate coefficients of reactions concerning the formation and growth of PAH or soot are unknown and have to be estimated from comparable gasphase reactions by analogy. However, the above discussed results clearly point out that within the framework of the presently available information the soot volume fraction can be predicted reasonably in terms of chemical reactions between gasphase compounds and the soot surface.

In addition to the calculations above the temperature dependence of soot formation in ethene/air flames at 1.0 MPa has been calculated. This is shown in Fig.3. It can be seen, that the model again predicts a bell shaped dependence of the soot volume fraction on flame temperature. However, the pressure dependence of the prediction as well as the temperature dependence at the higher pressure is weaker than found in the experiment [8]. The pressure

dependence of the final soot volume fraction is calculated to be proportional to p^2 at high flame temperatures. With decreasing flame temperature the pressure dependence reduces to proportional to $p^{1.5}$. A similar weak pressure dependence has been found experimentally [9] at pressures larger than 1.0 MPa where the final soot volume fraction varies linearly with pressure. We conclude that the decreasing pressure dependence of the soot volume fraction with increasing pressure is overestimated by the model used in this investigation. We note that the linear increase of the density related soot volume fraction just refers to the linear increase of the density with pressure. An analysis of the numerical results indicates, that the increasing partial pressure of H_2 is responsible for the limited rate of soot formation at high pressure. The increasing partial pressure of H_2 reduces the number of radicalic sites on the surface of the soot particles via the reverse of reaction (1.a.s).

Conclusions

A model that encompasses two pathways to soot from PAH, particle inception and condensation of PAH on the surface of the soot particles and that describes surface growth of soot similarly to the planar growth of PAH is employed to predict temperature and pressure dependence of soot formation in premixed ethene-air flames.

Within the framework of this model the experimentally measured final soot volume fraction and its temperature and pressure dependence are well reproduced.

Acknowledgement

This research was partially supported by the commission of the European Communities, the Swedish National Board for Technical Development (STU) and the Joint Research Committee of European car manufacturer (Fiat, Peugeot SA, Renault, Volkswagen and Volvo) within the IDEA programs.

References

- 1 Haynes, B.S. and Wagner, H.Gg.: Prog. Energy Combust. Sci. 7, p. 229 (1981).
- 2 Glassman, I.: Twenty-Second Symposium (International) on Combustion, p. 295, The Combustion Institute, 1988.
- 3 Howard, J.B.: Twenty-Third Symposium (International) on Combustion, p. 1107, The Combustion Institute, 1990.
- 4 Haynes, B.S. and Wagner, H.Gg.: Z. Phys. Chem. N.F. 133, p. 201, (1982).
- 5 Baumgärtner, L., Jander, H. and Wagner, H.Gg.: Ber. Bunsenges. Phys. Chemie 87, p. 1077, (1983).
- 6 Mätzing, H. and Wagner, H.Gg.: Twenty-First Symposium (International) on Combustion, P. 1047, The Combustion Institute, 1986.
- 7 Böhm, H., Hesse, D., Jander, H., Lüers, B., Pietscher, J., Wagner, H.Gg. and Weiss, M.: Twenty-Second Symposium (International) on Combustion, P. 403, The Combustion Institute, 1988.
- 8 Böning, M., Feldermann, Chr., Jander, H., Lüers, B., Rudolph, G. and Wagner, H.Gg.: Twenty-Third Symposium (International) on Combustion, P. 1581, The Combustion Institute, 1990.
- 9 Böhm, H., Feldermann, Ch., Heidermann, Th., Jander, H., Rudolf, G. and Wagner, H.Gg.: Twenty-Fourth Symposium (International) on Combustion, P. 991, The Combustion Institute, 1992.
- 10 Bockhorn, H., Fetting, F., Wannemacher, G. and Heddrich, A.: Twentieth Symposium (International) on Combustion, p. 879, The Combustion Institute, 1985.
- 11 Bockhorn, H., Fetting, F., Wannemacher, G. and Heddrich, A.: Ber. Bunsenges. Phys. Chemie 91, p. 819, (1987).
- 12 Frenklach, M. and Wang, H.: Twenty-Third Symposium (International) on Combustion, p. 559, The Combustion Institute, 1990.
- 13 Markatou, P., Wang, H. and Frenklach, M.: Combust. Flame 93, p. 467 (1993)
- 14 Mauss, F., Trilken, B. and Peters, N. in: Mechanisms and Models of Soot Formation, Bockhorn, H. (ed.); Springer Verlag, in press.
- 15 Warnatz, J. and Chevalier, C. in: Combustion Chemistry 2nd edition, Gardiner, W.C.jr.(ed.); Springer Verlag, in press.
- 16 Frenklach, M., Warnatz, J.: Combust. Sci. and Tech., 51, p. 265 (1987).
- 17 Frenklach, M.: Chemical Engineering Science, Vol. 40, No. 10, p. 1843 (1985).

STAGED COMBUSTION OF CHLORINE- AND NITROGEN-CONTAINING HYDROCARBONS FOR THE MINIMIZATION OF NO_x AND PIC'S

Fuhe Mao and Robert B. Barat
Dept. of Chemical Engineering, Chemistry, and Environmental Science
New Jersey Institute of Technology
Newark, NJ 07102

Keywords: combustion, nitrogen oxides, chlorinated hydrocarbons

This paper describes our current research in the area of staged combustion, wherein the overall fuel-lean system is divided into a fuel-rich (oxidant lean) first stage followed by a fuel-lean (oxidant rich) second stage. The first stage of our turbulent flow combustor is a jet-stirred, backmixed zone which can be modeled as a perfectly stirred reactor (PSR) under most conditions. The effluent from this zone enters a linear flow zone which can be modeled as a plug flow reactor (PFR). Industrial turbulent combustors, incinerators, and afterburners which employ a central fuel nozzle and swirled concentric air for flame stabilization can often be modeled with this sequence (Beer and Chigier, 1983).

This work utilizes an atmospheric pressure toroidal jet-stirred / linear flow two stage sequential combustor shown in Figure 1. The primary zone (torus) was first described by Nenniger et al., 1984. Premixed fuel gas and air are introduced at sub-sonic velocities into the torus around its outer circumference. The off-radial jets entrain the swirling bulk gas, causing a highly turbulent, backmixed condition. Residence times are typically 5-10 milliseconds in this 250 milliliter primary zone. The hot, reactive gases exit the torus, passing over a flow straightener into the secondary (linear) stage. Additional gases, typically air/ O_2 /steam in this work, are injected at this point. Second stage residence times are on the order of 20 milliseconds in this 30 centimeter long secondary zone. Stable species gas samples are withdrawn through two water-cooled probes. At present, all fuels are input to the reactor as gases. The primary fuel is C_2H_4 . Fuel-bound chlorine and nitrogen sources simulating hazardous wastes are CH_3Cl and CH_3NH_2 , respectively. A schematic of the entire facility is presented in Figure 2.

When CH_3Cl is burned, the sample gas is scrubbed of HCl in a gas-water countercurrent flow packed tower. The column is sufficiently oversized that effectively 100% HCl recovery from the inlet sample gas stream is achieved. The liquid effluent contacts chloride ion selective and reference electrodes used for HCl quantification.

The sample gas stream passes successively through a chilled bath for water vapor condensation, a droplet knockout, and a metal bellows pump, which provides the suction for sample withdrawal and the pressure head for sample passage to the various analyzers. The metered pump outlet sample gas is then split, with a portion flowing to O_2 , CO, and CO_2 continuous emission analyzers and a gas chromatograph. The gas chromatograph is equipped columns for separation of light hydrocarbons and chlorocarbons, CO, and CO_2 . The columns elute onto thermal conductivity and flame ionization detectors. The remainder of the sample gas passes through a gas drier, then flows to Total Hydrocarbon and NO_x analyzers.

There are three segments to the modeling of this combustor: elementary reaction mechanism, reactor simulation, and rate-of-production analyses. The first and second represent a major simplification of the turbulent fluid mechanics in favor of an emphasis on detailed chemistry. A favorable comparison of the experimental data and model predictions justifies the use of the third segment, which identifies the important chemical pathways.

For the experimental cases considered in this work, the reaction mechanism for the combustion of C₁/C₂ hydrocarbons and CH₃Cl is taken from Ho et al., 1992. The mechanism for CH₃NH₂ combustion and NO_x chemistry is taken from Miller and Bowman (1989), Sun et al. (1987), and Beer et al. (1981). Generated from the mechanism is ω_k , the net molar rate of production by reaction of species k, which is used in the reactor simulation equations.

The jet-stirred zone can be modeled under most conditions as a PSR, with the following governing species balance equations:

$$M(Y_k - Y_{k0}) = \omega_k W_k V \quad (1)$$

where M = mass flow rate, Y_k = mass fraction of species k (total of K species), W_k = molecular weight of k, and ω_k = net molar rate of production by reaction of k, V = reactor volume, and subscript 0 represents the feed condition. The linear flow zone can be modeled as a PFR, with the following governing species balance equations:

$$\frac{dY_k}{dt} = \frac{\omega_k W_k}{\rho} \quad (2)$$

where t = reaction (residence) time and ρ = mass density.

The mechanism is incorporated into a PSR+PFR reactor simulation program (driver code) which accesses the *CHEMKIN* package (Kee and Miller, 1986). The input to this driver includes composition, temperature, and mass rate of the PSR feed and post-PSR injection, reactor pressure, PSR volume and measured temperature, and PFR residence time and measured temperatures. Our driver program includes options to request net rate-of-production information for selected species to construct the chemical pathways involving reactants, intermediates, and products.

A series of runs were made to examine the effects of full staging on NO levels. A fuel-lean (equivalence ratio¹ $\phi = 0.86$) baseline was established. The feed to the primary stage was sequentially increased ($\phi = 0.86$ to 1.43) while the temperature was kept constant at 1760 K. The molar ratio of CH₃NH₂ to C₂H₄ in the feed was maintained at 0.058. For each fuel-rich PSR feed, air was injected into the secondary stage so as to achieve an overall combustor ϕ of 0.86. All concentrations reported for the PFR have been corrected upward for the dilution effect of the injected air.

¹ $\phi = [\text{fuel/air}]_{\text{actual}}/[\text{fuel/air}]_{\text{stoichiometric}}$

Measured temperature profiles for these runs are given in Figure 3. The PFR temperatures either decrease or increase along its length depending on the degree of additional combustion occurring. At higher primary stage ϕ values, the heat produced in the second stage more than overcomes sensible losses. The experimental operability advantage of these losses is now clear.

Figure 4 presents measured and model-predicted NO levels for these runs in the PSR. The highest levels occur for the fuel-lean feeds. As the primary stage ϕ increases, the NO concentration drops dramatically. However, as expected, the CO level increases with a drop in CO₂, as shown in Figures 5 and 6 respectively. The injection of the secondary air, though, enhances CO conversion. Figure 7 dramatically illustrates that a minimum in NO at the PFR outlet exists for a PSR feed ϕ of 1.35. Though the 700 ppm level is twice the 350 ppm PSR concentration, it is still much lower than the PFR outlet NO level of 1800 ppm for the all fuel-lean base case ($\phi = 0.86$).

Preliminary results have been obtained on the simultaneous staged combustion of C₂H₄/CH₃Cl/CH₃NH₂. The feed CH₃NH₂/C₂H₄ ratio, primary stage ϕ , and overall ϕ were kept constant, while the feed CH₃Cl/C₂H₄ ratio was varied. Increasing the CH₃Cl loading results in a drop in NO concentration (Figure 8), which cannot be explained by the negligible drop in reactor temperature profiles as the chlorine content increases. Rate-of-production analysis will be used to identify the responsible chemical pathways.

ACKNOWLEDGEMENT

The authors would like to thank the Hazardous Substances Management Research Center and the National Science Foundation for their financial support of this work.

REFERENCES

- Beer, J. M. and Chigier, N. A., Combustion Aerodynamics, Krieger Publishing, Malabar, FL (1983).
- Beer, J. M., Jacques, M. T., Farmayan, W., and Taylor, B. R., *18th Symposium (Int.) on Combustion*, The Combustion Institute, Pittsburgh, PA, p. 101 (1981).
- Kee, R. J. and Miller, J., Sandia National Laboratories Report, SAND86-8841, Livermore, CA (1986).
- Miller, J. and Bowman, C., *Progress in Energy and Combustion Science*, vol. 15, p. 287 (1989).
- Nenniger, J. E., Chomiak, J., Kridiotis, A., Longwell, J. P., and Sarofim, A. F., *20th Symposium (Int.) on Combustion*, The Combustion Institute, Pittsburgh, PA (1984).
- Sun, W. H., Longwell, J. P., and Sarofim, A. F., 193th National Meeting of the American Chemical Society (1987).

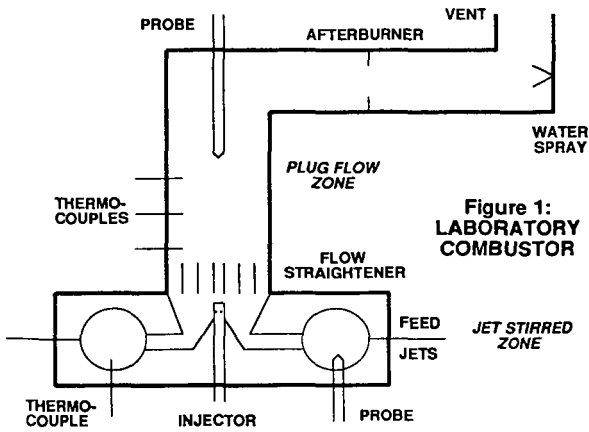


Figure 1:
LABORATORY
COMBUSTOR

Figure 2: STAGED COMBUSTION FACILITY

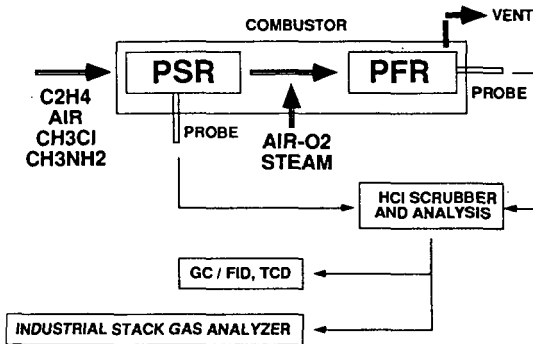


FIGURE 3

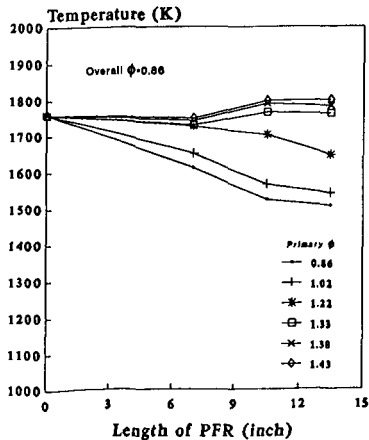
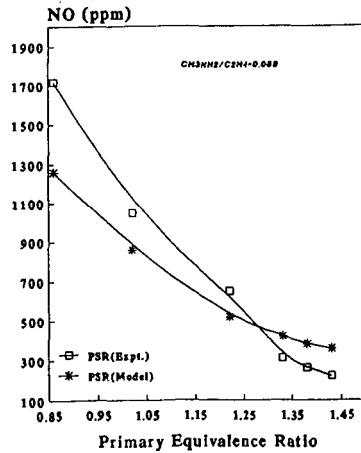


FIGURE 4



emissive factors less than 0.3 (9). Figure 3 compares the combustion reactivities of the suite of residual carbon samples to those of various laboratory-generated chars in the early-to-intermediate stages of combustion (20 - 60% char carbon conversion). To facilitate direct comparison, char combustion rates are presented at a common oxygen concentration of 6% and a gas temperature of 1500 K. The laboratory char data in Fig. 3 includes a set of previously published oxidation rates for a suite of ten U.S. coals of various rank (4). Char reactivity is seen to be a strong function of rank, represented here by the dry, ash-free carbon content of the parent coal. At any given rank the residual carbon samples are much less reactive than the laboratory chars by factors of 2 to 7. Also, in each case where chars were available from the same parent coal, the residual carbon samples are seen to be much less reactive (see Fig. 2). The residual carbon materials were also found to be significantly less reactive than the laboratory-generated chars in 7% oxygen at 500 - 700 °C, as determined by thermal gravimetric analysis.

Physicochemical properties: Carbon dioxide surface areas of the residual carbon sample investigated here range from 93 to 188 m²/g-organic-matter (on a dry, ash-free basis) and are roughly comparable to the areas of laboratory chars in the early and middle stages of combustion (8). The residual carbon samples have hydrogen to carbon ratios of 0.2 and 1.2 wt-% and oxygen to carbon ratios of 2 - 6 wt-%, also comparable to those of a variety of laboratory-generated chars in the intermediate stages of combustion (8).

Carbon structure: Fig. 4 shows two selected micrographs (HRTEMs); one of Illinois #6 char in the intermediate stages of combustion, after 72 msec residence time and a carbon conversion of approximately 45%, and one of Illinois #6 residual carbon. The images represent typical structures based on examination of at least ten fields for each sample. Individual graphitic layers are easily discernible in the images, often in parallel groupings with the nominal interlayer spacing characteristic of graphitic carbon, 0.34 nm. Curved structures are present in both images, as has been observed for other carbon materials (11). Indeed, there is evidence that curved structures are thermodynamically favored for graphitic carbon units below a certain size — flat graphitic layers of small size would necessarily possess high-energy dangling bonds at the edges (11). Fig. 4 clearly shows that the residual carbon samples possess a higher degree of crystalline order than the laboratory-generated chars at 72 msec residence time. The residual carbon sample in Fig. 4b shows numerous crystallites with stacking depths of 3 - 5 nm, or approximately 10 graphitic layers, and dimensions parallel to the basal planes of up to 10 nm.

DISCUSSION AND CONCLUSIONS

Despite the complexity of the boiler environment and the wide variety of boiler operating conditions and fuels examined here, the residual carbon samples, as a class of materials, exhibit consistent and unique properties. Particularly noteworthy is their low combustion reactivity relative to laboratory-generated chars in the early-to-intermediate stages of combustion. Here we attempt to relate the low reactivities to some measurable physicochemical property or properties of the residual carbon samples. In general, the high-temperature reactivity of a carbon material to oxygen is determined by 1) the amount of internal surface area available for reaction, 2) the pore structure which provides access to the particle interior, 3) the degree of encapsulation of carbon by mineral matter, 4) the intrinsic reactivity of the internal surfaces, governed by the chemistry and crystalline structure of the organic matrix and by the catalytic action, if any, of inorganic impurities [12]. The material characterizations performed provide some information on each of these factors and suggest that factor 4 is the likely explanation for the low reactivity of residual carbon.

High resolution TEM shows that residual carbon can possess a much higher degree of crystalline order than the laboratory-generated chars. The observed increase in order is likely the result of thermally induced lattice rearrangement (pregraphitization), possibly promoted by the oxidative removal of carbon. The importance of pregraphitization or "thermal annealing" on char reactivity has been noted by a number of researchers [13,14]. A recent study [15] has shown that a similar degree of turbostratic crystalline order is developed in coal chars over the course of 100 msec of combustion at particle temperatures of 1800 K. Pregraphitization and oxidation have similar time constants and thus occur to a large extent simultaneously under the conditions relevant to pulverized coal combustion. Because increased crystalline order in carbons is generally accompanied by a loss of reactivity due to a reduction in the number of reactive edge sites and basal plane defects, the low combustion reactivity of the residual carbon samples is not surprising.

Finally, we should consider what the residual carbon properties and reactivities may tell us about the combustion process in pulverized coal fired boilers. The boiler environment appears to induce significant crystalline order in chars, thereby reducing their oxidation reactivity relative to the chars formed in the laboratory. The primary differences between the two environments are (1) the much longer residence times in the boiler (approx. 1 sec vs. 70 msec), which leads both to more severe heat treatment and much higher extents of oxidation (> 99% vs. 20-60%) and (2) differences in peak particle temperature (1800 - 2400 K in boilers [16] vs. 1800 - 1900 K in the laboratory). The reactivity differences may also be influenced by differences in particle heating rates, although these are believed to be roughly similar in the two environments. The bulk of the residual carbon has been severely heat treated and oxidized — it is not a fraction of the feed that has bypassed high temperature regions due to poor mixing. Recent studies [8] have shown that subjecting the laboratory chars to further combustion to high conversions (> 80%), leads to loss of reactivity and near-extinction of the oxidation reaction. Low reactivities have thus been observed for highly reacted, highly heat-treated residues from both laboratory and commercial-scale combustors. This result implies that char combustion cannot be accurately modeled assuming a reactivity that is

phenomenon affecting the latter stages of combustion, and accounting for deactivation may be key to making more accurate predictions of unburned carbon levels in fly ash.

REFERENCES

1. Field, M. A. *Combustion and Flame* 1970 14 237
2. Smith I. W. *Combustion and Flame* 1971 17 303
3. Essenhigh R. H., in *Chemistry of Coal Utilization, Second Supp. Vol.* (M.A. Elliott ed.) John Wiley and Sons Inc., 1981
4. Hurt, R. H. and Mitchell R. E. *24th International Symposium on Combustion*, The Combustion Institute, Pittsburgh, PA, pp. 1243 - 1250, 1992
5. Walsh, P. M., Xie, J., Douglas, R. E., Battista, J. J., and Zawadzki, E. A. "Unburned Carbon Loss from Pulverized Coal Combustion," submitted to *Fuel* (1993).
6. Nandi, B. N., Brown, T. D., and Lee, G. K., *Fuel* 56 125 (1977).
7. Shibaoka, M. *Fuel* 64:263-269 (1985).
8. Hurt, R. H., Davis, K. A., and Hardesty, D. R. "Impact of Coal Quality on Coal Char Combustion, Final Report to EPRI". Sandia Technical Report June 1993
9. Mitchell R. E. *22nd International Symposium Combustion*, The Combustion Institute, p. 69, 1988.
10. Hurt, R. H. "Reactivity Distributions and Extinction Phenomena in Coal Char Combustion" submitted to *Energy and Fuels*, March 1993.
11. Ugarte, D. *Nature* 1992 359 707
12. Hecker, W. C., McDonald, K. M., Reade, W., Swensen, M. R., and Cope, R. F. *Twenty-Four (International) Symposium on Combustion*, The Combustion Institute, Pittsburgh, 1992, pp. 12 1231.
13. Smith, I. W., and Tyler, R. J., *Fuel* 51:312-321 (1972).
14. Suuberg, E. M. in *Fundamental Issues in Control of Carbon Gasification Reactivity*, Kluwer Academic Publishers, 1991, pp. 269-305.
15. Davis, K. A., Hurt, R. H., Yang, N. Y. C., and Headley, T. H., "Evolution of Char Chemistry, Crystallinity, and Ultrafine Structure during Pulverized Coal Combustion," submitted to the *Twelfth (International) Symposium on Combustion*, 1993.
16. Fletcher, T. H. personal communication, 1993.

ACKNOWLEDGMENTS

Financial support for this work is provided by the EPRI Office of Exploratory and Applied Research and the U.S. DOE Pittsburgh Energy Technology Center's Direct Utilization Advanced Research and Technology Development Program. The authors wish to acknowledge Hardarshan Valia of Inland Steel, Bruce Dyas of New England Power, John Sorge of Southern Company Services, and Donald Bull of Northern Indiana Public Service Co. for technical discussions and/or sample donation. The technical contributions of James Ross and Richard Yee are gratefully acknowledged.

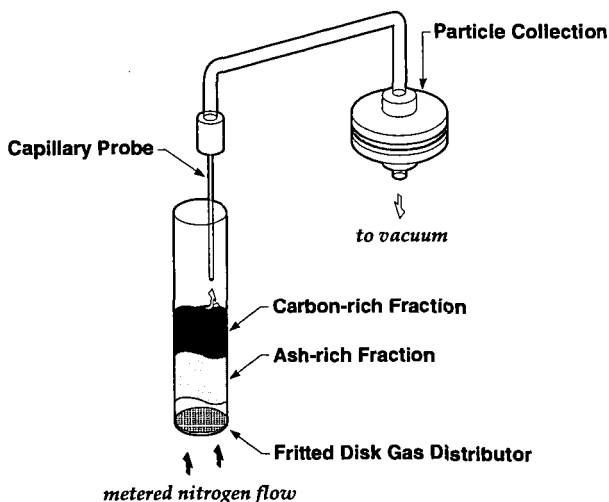


Figure 1. Residual carbon extraction by incipient fluidization.

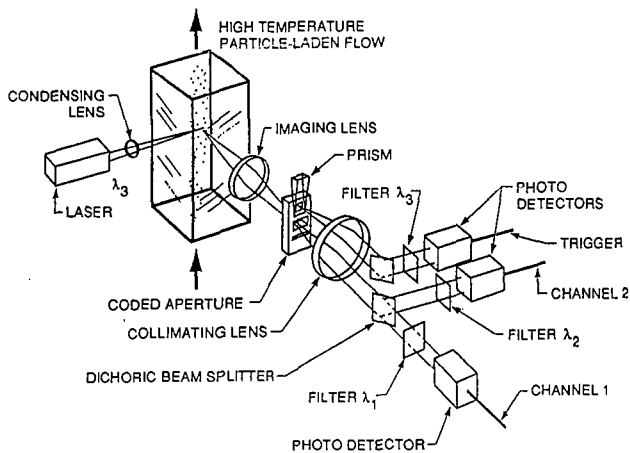


Fig. 2 The laminar flow reactor and optical diagnostic used for in situ measurement of particle size, temperature, velocity, and emissive factor.

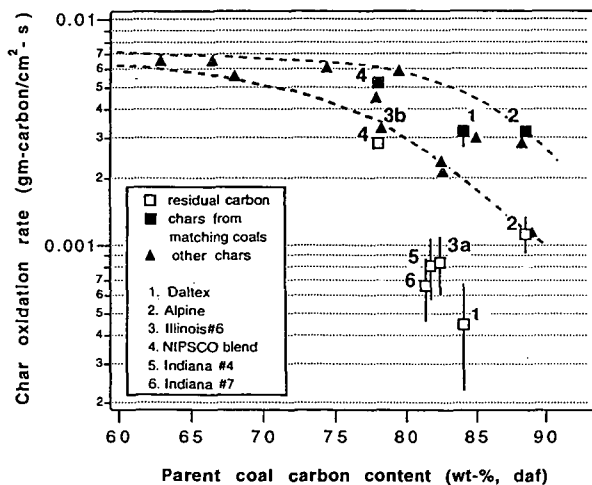


Figure 3 Combustion rates of various chars and residual carbon samples as a function of the carbon content of the parent coal. Gas temperature 1500 K; oxygen concentration 6 mol-%. Dashed curves indicate the range of reactivities observed for laboratory-generated chars at low-to-intermediate carbon conversion. Samples 3a and 3b both originate from Illinois #6 coals, but from two separate sources.

a.



b.



Figure 4 High-resolution transmission electron fringe images of Illinois #6 chars with different combustion histories. a) char samples from Sandia's high-temperature entrained flow reactor after 72 msec of combustion in 12 mole-% oxygen, b) residual carbon from commercial-scale pulverized-coal fired boiler. Magnification 2,000,000x.

FLAME STRUCTURE OF SANDWICH SYSTEMS BASED ON AMMONIUM PERCHLORATE, HMX AND POLYBUTADIENE RUBBER STUDIED BY PROBE MASS-SPECTROMETRY AND MODELING.

A.A. Chernov, V.M. Shvartsberg, N.E. Ermolin, O.P. Korobeinichev, V.M. Fomin
Institute of Chemical Kinetics and Combustion
Siberian Branch Russia Academy of Science,
630090 Novosibirsk, Russia

Keywords: chemistry of combustion, solid propellant, mass-spectrometry, modeling

ABSTRACT

The structure of subatmospheric flames of sandwich-type systems consisting of alternating laminae of ammonium perchlorate (AP) or HMX and "base" (polymerized mixture of fine-grained AP and polybutadiene binder) has been studied. The burning surface shape as well as the profiles of concentrations for 17 stable components and of temperature for three crosssections corresponding to the middle of "base" lamina, and to the interface between the laminae have been determined. The hypothesis assuming the existence of three types of flames in sandwiches has been verified experimentally. A concentration gradient of fuel components has been observed at the burning surface of the oxidizer, directed towards the burning surface. Multizone structures and step-by-step mechanisms of reactions in AP and HMX flames have been confirmed. A numerical study for the flame structure of sandwich system based on AP and "base" have been carried out. A simplified set of equations obtained from a complete Navier-Stokes set with the limiting transition $M \rightarrow 0$ have been used in order to construct a solution. Satisfactory agreement between calculated and experimental data on flame structure have been obtained.

INTRODUCTION

An important role in the combustion process for mixed solid fuel (MSF) is played by microflames caused by heterogeneous distribution of the oxidizing agent in the fuel-binder. The dependence of combustion rate on particle fineness and the effect of microflames on the formation of local thermal and diffusion flows point to the necessity of studying the local structure of flames. MSF consist of coarse-grained AP (particle size several hundred micrometers), the space between the particles being filled with the "base" - the mixture composed of a fuel-binder and fine-grained AP (particle size from a few micrometers to a few tens of micrometers). Therefore, oxidizer - "base" sandwiches should be the best models for composite systems. Such sandwiches, however, have been considered only by Price and co workers / 1 /. The other studies performed hitherto dealt with sandwiches consisting of alternating laminae of oxidizer and fuel - binder. There are no published works on combustion of HMX - based sandwiches. The aim of this work was to study chemical and thermal structure of flame for sandwiches on the basis of AP or HMX and the "base" consisting of AP (<50 mkm) and carboxy terminated polibutadiene (CTPB).

EXPERIMENTAL

The sandwiches consisted as a rule of five alternating laminae: three AP (or HMX) laminae and two "base" laminae. An AP-based (system 1) was made of pressed AP plates (density 1.85 g/cm³, thickness 1.3 mm) and the laminae (thickness 1.0 mm) of polymer "base" - the mixture of fine - grained AP (particle size < 50 mkm) and CTPB in a 4:3 ratio. The mixed "base" laminae were prepared by polymerization in Teflon arrays at 100 °C for 24 hours. The sandwich samples were 4.8*6*10 mm. An HMX-based sandwich (system 2) was made of 1 mm thick HMX laminae (mixture of fine-grained AP and CTPB in a 73:27 ratio). The sandwich dimensions were 4.2*6*12 mm.

Thermal structure of the flames was studied using thermocouples (tungsten-rhenium wires 30 and 50 mkm in diameter) embedded in propellant samples. Chemical structure of flame was analyzed by mass-spectrometric probing described elsewhere (2). Quartz cones: 15-20 mkm sampling orifice, 0.45 for system 1 and 0.15 for system 2 external tip diameters, 40-50 grad. interior angular openings. Systems 1 and 2 were examined in helium flow at pressures of 0.03 MPa and 0.053 MPa, burning rates 0.3 mm/s and 0.65 mm/s, respectively. In order to study the structure of burning surface and the shape of oxidizer and "base" laminae, the samples were quenched using rapid depressurization. At low pressures AP-lamina and HMX-lamina protrudes above "base" lamina approximately by 0.5 lamina thickness and has the shape close to a circle segment. At 4 MPa the "base" and AP laminae have similar V-shaped profiles.

SET OF EQUATIONS. METHOD OF SOLUTION

Flow at a MSF combustion surface is defined by Mach numbers of <0.003 and Reynolds numbers of $10-200$. A simplified set of equations obtained from a complete Navier-Stokes set with the limiting transition $M \rightarrow 0$ have been used in order to construct a solution. Thermal and diffusion flows are specified in accordance with (3). In (3). In the present studies in order to construct a solution a splitting method (4) combined with the method of artificial compressibility is used. On the basis of the calculations performed (5) a kinetic mechanism including 58 elementary stages and 35 components is separated.

RESULTS

The following components have been found out in the sandwich flames: H_2 , NH_3 , H_2O , C_2H_2 , HCN , CO , N_2 , NO , HCl , CO_2 , N_2O , NO_2 , $CLOH$, O_2 , C_2H_6 , ClO_2 , Cl_2 , $HClO_4$, whose mole fractions and temperature profiles are shown in figs. 1-2. Analysis of the data obtained testifies to the fact that there are two zones in the flame of sandwich-type system 1 in the cross section corresponding to the middle of AP lamina (fig.1a). The first zone adjoining the burning surface of AP is a narrow (about 0.2 mm) AP flame zone wherein ammonia is oxidized by $HClO_4$ and ClO_2 to yield NO , O_2 , and other substances. In the second, more wide (about 3 mm) zone, O_2 and NO are consumed. Oxygen and nitric oxide are consumed in oxidation reaction of carbon monoxide with CO_2 and N_2 formation; HCN , C_2H_2 and H_2 are oxidized slowly. The experiments have shown that at the distances from sample surface longer than 5 mm CO and N_2 concentrations do not change. It should be noted that the fuel components, i.e. products of "base" destruction, HCN and C_2H_2 , penetrated right up to the oxidizer surface due to diffusion: there is a concentration gradient of the components, directed to the burning surface. These products can react with AP, that may be an additional source of heat release on the burning surface. On the other hand, the probability of such an interaction is confirmed by the work reported by Inami et al. (6), wherein AP decomposition in the presence of gaseous propylene has been studied.

Data on flame structure for system 1 in the crosssection corresponding to the middle of a "base" lamina (fig.1b) also indicate that there are two zones: a narrow (0.3 mm) zone of the oxidation of butadiene (fuel-binder destruction product) by ClO_2 and $HClO_4$ with formation of carbon monoxide and other substances and a wide (2-3mm) zone of consumption of ammonia, carbon monoxide, $HClO$ and accumulation of other substances due to their diffusion from the oxidizer lamina. Inhibition of ammonia oxidation in the presence of butadiene is observed.

Fig.2a shows profiles of mole fractions and temperature in flame of sandwich system 2 in the cross section corresponding to the middle of an HMX lamina. Chemical structure of the flame in this cross section is identical to the chemical structure of pure HMX flame at 0.1 MPa (7). Two zones may be distinguished. The first one is a narrow (of 0.2-0.3 mm width) zone of NO_2 and CH_2O consumption and accumulation of nitric oxide and other substances. The second, more wide (2-3 mm), zone is that of the oxidation of cyanic hydrogen by nitric oxide. As shown by Cohen et al. (8), the reaction of HCN with NO plays the principal role in the high temperature zone of HMX flame. The circularity of laminar system flame (HMX lamina) lies in the fact that cyanic hydrogen is oxidized by nitric oxide incompletely. This may be accounted for by thermal interaction between the laminae. The flame of HMX lamina transfers some heat of "base" flame, the temperature decreases (as compared to adiabatic temperature for HMX), and the rate of the $HCN + NO$ reaction decreases. On the other hand, HMX lamina in the condensed phase receives a portion of the "base" lamina heat and HMX becomes able to burn steadily at 0.053 MPa (at this pressure pure HMX burns unsteadily). The data obtained on HMX flame structure confirm the mechanism adopted by Bizot et al. (9) in the model for HMX combustion and are consistent with data reported by Kubota and co workers (10). The main reaction in the zone adjacent to the HMX burning surface and responsible for the heat transfer to the condensed phase is seemingly the reaction between NO_2 and CH_2O and not the decomposition reaction of HMX vapors, as it was assumed earlier (8, 11).

RESULTS OF CALCULATION

Fig 3 shows results of computer simulation of AP-based sandwich flame (system 1) at 0.03 MPa: profiles of mole fractions H_2 , HCN , C_2H_2 , the shape of combustion surface between the central layer AP ($Z=1.2$) and the central layer "base" ($Z=0$) together with field of velocity (standardized to 1.5 m/sec), the isoline of HCN concentration and temperature. Calculations were carried out for plane-parallel and asymmetrically flows on curvilinear grids with a number of nodes 20×20 , condensed in regions of higher gradients. Blowing mixture from the combustion surface takes a direction on the normal to the surface. At the combustion surface depending on the pressure, the values of temperature, rate, and molar fractions of components A_i are prescribed. At low pressures A_i corresponds to the experiment, and at high pressures to rough extrapolation of data for combustion of AP and a layered system. At the lower and upper boundary of the calculation region conditions are prescribed, and at the outlet conditions are extrapolated. The temperature of the combustion surface in calculations is prescribed by the

relationship $T=673 + 30 \times (1 + \cos(\pi(1 - Z/1.2)))$ and it equals the experimental temperature with $Z=0$ and $Z=1.2$ mm. In both calculations and the experiment a broad mixing layer is observed washing the combustion surface, although there is no total mixing in the region with right-hand boundary $X=3$ mm. The reaction occurs in kinetic region, and the temperature field in sections $X = \text{const}$ (see Fig.3) levels out the concentration fields more intensely. Good agreement of calculations and the experiment is observed. The value for thermal flow over normal to the combustion surface is provided below (W/m^2): 1×10^5 ($Z=1.2$), 2×10^5 ($Z=0.55$), 3×10^5 ($Z=0$). The ratio of this flow to similar flow for a plane combustion surface reaches a maximum value of 2.4 at $Z=1.2$ mm. At high pressures the difference in thermal flows of the combustion for plane -parallel and asymmetries flows does not exceed 3%. The point with the maximum value of thermal flow shifts in the direction of oxidizing agent.

REFERENCES

1. Price E.W., Sambamurthi J.K. et al., Comb. and Flame, 63, 381 (1986).
2. Ermolin N.E., Korobeinichev O.P., Tereschenco A.G., Fomin V.M., Comb., Explos. and Shock Waves, 1, 18, 36 (1982).
3. Ermolin N.E., Korobeinichev O.P., et al., Khim. Fiz., N12, p.1711(1982).
4. Kovenya V.M. and Yanenko N.N., The Spilting Method in Problems of Gas Dynamics (in Russian), Nauka, Novosibirsk (1981).
5. Korobeinichev O.P., Chemov A.A., et al., Fiz. Gorenia Vzryva, 26, 3, 46(1990)
6. Inami S.H., Ragapakse Y.H., Wise H. Comb. and Flame, 17, 189 (1971)
7. Korobeinichev O.P., et al., Comb. Explos. and Schock Waves, 20, 3, 282(1984).
8. Cohen N.S., Lo G.A., Crowley L.H. AIAA-Journal, 23, 2, 276 (1985).
9. Bizot A., Bekstead W.M.. A model for HMX propellant combustion. Paper at the 3-rd Int. Seminar of Flame Structure, Alma-Ata, 1989.
10. Kubota N., Sakamoto S., Propellants, Explosives, Pyrotechnics, 14, 6(1989).
11. Ben-Reuven M., Caveny L.H. AIAA-Journal, 19, 10, 1276 (1981).

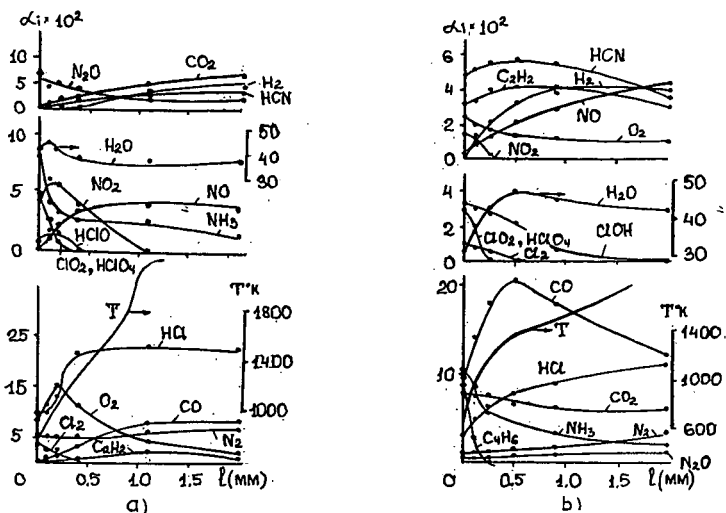


Fig.1. Mole fractions of combustion products and temperature profiles in the AP-based sandwich (system 1) flame obtained by mass-spectrometry probing in the transection corresponding the middle of : a) AP-lamina b) "base" lamina

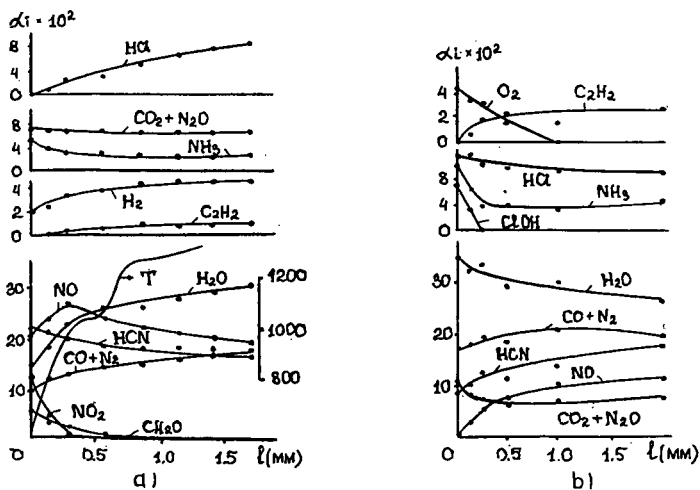


Fig.2. Experimental data of probing HMX-based sandwich flame : a) HMX lamina , b) "base" lamina

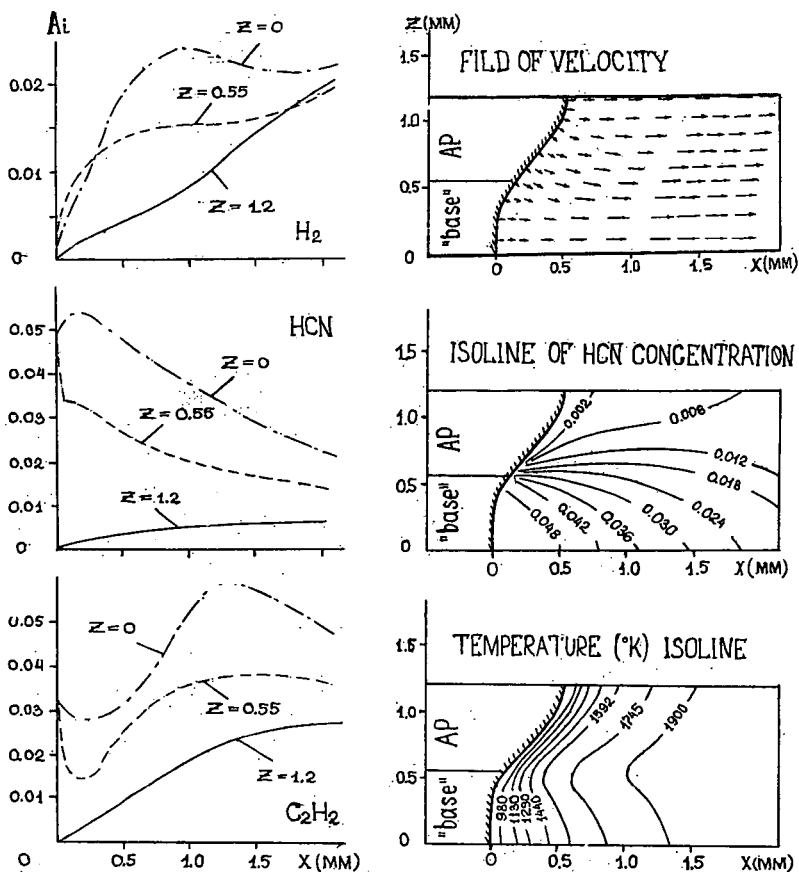


Fig. 3. Results of computer simulation of AP-based sandwich flame (system 1) at $P=0.03$ MPa

MASS-SPECTROMETRIC INVESTIGATION OF THE STRUCTURE OF A STOICHIOMETRIC $H_2/O_2/Ar$ FLAME DOPED WITH TRIMETHYLPHOSPHATE AND N-TRIBUTYLPHOSPHATE

O.P. Korobeinichev, A.A. Chernov, V.M. Shvartsberg
Institute of Chemical Kinetics and Combustion
Siberian Branch Russia Academy of Sciences,
Novosibirsk, 630090 Russia

Key words: chemistry of combustion, waste incineration, mass spectrometry

ABSTRACT

Molecular beam mass-spectrometry was used to study the structure of a stabilized premixed $H_2 / O_2 / Ar$ (25.4% / 12.7% / 61.9%) flame without and with additives (0.034% TMP-trimethylphosphate or TBP-tributylphosphate) at 80 torr (burner temperature: 85°C). The behavior of the TMP, TBP in flames and reactions leading to their destruction in flames have been studied. The promoting effect of the additive on the flame was observed, i.e. in the presence of the additive the combustion zone considerably decreases. Mass-spectrometric analysis of the species sampled from different flame zones, performed under soft ionization (at low ionization energies), was used to identify the intermediate and end products of the reactions destroying TMP in the flame, to measure the concentration profiles of some components in the flame related to these reactions. The data obtained testify that the primary products of the reaction of TMP destruction are either dimethylphosphate or dimethylphosphite or both of them. CH_3OH , CH_2O , CH_3O and the compound, the mass-spectrum of which contains the peak with $m/e=80$ (possibly, CH_3O_2P) were recorded as intermediates. The zone of TBP reacting in the flame is a bit narrower than that of TMP. Butene was registered as intermediate in an $H_2/O_2/Ar$ flame doped with TBP. The distributions of mass peak intensities with $m/e=64$ (HPO_2^+), 63 (PO_2^+), 48 (HPO^+), 47 (PO^+) in flames, characterizing the corresponding phosphorous containing components of the $H_3P_2O_5$ type were measured. The data obtained indicate the following sequence of the transformations of these components in flame:



The possible mechanisms of TMP and TBP transformations in the $H_2/O_2/Ar$ flame are discussed.

INTRODUCTION

The combustion of organophosphorus substances (OPS) is of a great interest in connection with the disposal of toxic and hazardous chemical wastes and other undesirable substances that frequently contain these classes of compounds. One of the most promising techniques for the disposal of wastes is their incineration which provides a high destruction degree of toxic and hazardous substances. However, for better reliability and control over these processes one should know the details of the mechanism of their combustion and especially their chemistry. One of the typical representatives of the class of toxic OPS is the class of alkylphosphates. On the one hand, some of these are industrial wastes (e.g. tri-n-butylphosphate is the product of uranium ore treatment). On the other hand, these can be the models for studying the problems of the incineration of pesticides and the components of a chemical weapon. The chemistry of OPS combustion is practically not understood. The interest in the behavior of phosphorous containing substances in flames is not limited by the problem of their destruction. These substances (e.g. trimethylphosphate, phosphine) can play the role of inhibitors or promoters of the combustion process. These questions were the object of studies in references 1, 2, and 3. The aim of the present paper is to study 1) the behavior of trimethylphosphate (TMP) and n-tributylphosphate (BP) as the simplest representatives of OPS in a well-studied flame of $H_2/O_2/Ar$ stabilized at low pressure on a flat burner and 2) the chemistry of reactions leading to the destruction of TMP in a flame by identifying intermediate and end products (including atoms and radicals) by their mass-spectra, measuring the concentrations and concentration profiles of initial, intermediate and end products. This could be the basis for developing the model of TMP combustion as one of the simplest OPS.

EXPERIMENTAL

The premixed $H_2/O_2/Ar$ (25.4/12.7/61.9) flames of a stoichiometric composition without additives and with TMP (0.034%) or TBP (0.04%) were stabilized at 80 Torr on a flat Spalding-Botha burner⁴ 24 mm in diameter a brass disc with about 250 holes with diameter 0.7 mm each. The total consumption of the gas mixture was 65 cm³/s (NTP). With such a burner, the flames at 80 Torr are sufficiently one-dimensional. A quartz cone, 15 mm high, with an apex angle of 40 degrees, and a 0.17 mm diameter orifice, the width of walls at the top 0.15 mm was used. The probe was coupled with the flange of stainless steel cooled with water. TMP was

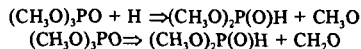
supplied by a peristaltic pump or chromatographic syringe to the evaporator into the flow of preliminary mixed and heated to 85°C combustible mixture. Further the mixture passed to the burner. The temperature of the evaporator and the burner was kept equal to 85°C (in the case of TMP) or 150°C (in the case of TBP) with the help of a thermostat. Flame temperature was measured using a platinum - platinum with 10% rhodium microthermocouple weld of wires with a diameter of 50 microns and covered with a layer 10 microns thick. The thermocouple shoulder was 10 mm. The correction for radiation losses was introduced into the readings of the thermocouple. A molecular beam sampling technique coupled to a quadrupole mass-spectrometer was used for analysis of species and measurement of their concentrations in the flame.

The mass-spectrometric setup with molecular-beam sampling is partially described in reference 5. Synchronous detecting was used to record the modulated component of the molecular beam under ion-counting conditions. The modulation frequency was 12,5 Hz. The mass-spectrometer was supplied by an ion source with a small spread of electrons in energies (± 0.1 eV) which allowed us to work at low ionization energies close to the ionization potentials of atoms, radicals and molecules. The number of accumulations was 80-400. The concentrations of stable species are determined by direct calibration at ambient temperature by a procedure reported by Peeters and Mahnen⁶. The uncertainty in the stable species concentration is estimated as $\pm 10\%$.

RESULTS

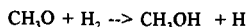
The probe is known to perturb the flame. In this case the lines of equal concentrations near the probe tip shift relative to the unperturbed flame. The value of this shift can be estimated from the formula $Z=0.4 D_p A_p(1/2)$, where D_p is the diameter of probe orifice; A_p is the sampling degree depending on the volumetric rate of sampling and the rate of the flow. For the flame described and the probe used, $Z=0,65$ mm. Although this value is small compared to the width of the combustion zone (2-3 mm), in the represented data this shift was taken into account. In the profiles of measured concentrations the origin of coordinates along the abscissa was put at the distance of 0,65 mm from the burner surface. Figures 1-3 show the data of the study of the structure of the above mentioned flames.

The data in Figure 1 are the experimentally measured profiles of temperature and concentrations of H_2 , O_2 , H_2O , and TMP in the flames with and without TMP. Figure 1 shows also TBP concentration profile in $H_2/O_2/Ar$ flame, doped with TBP. It is seen that small additions of TMP promote combustion process causing an appreciable decrease in the combustion zone width. The zone of TMP reacting is about 1,5 mm and is a bit narrower than that of oxygen and hydrogen in the flame. The same effect of promotion in the $H_2/O_2/Ar$ flame was observed at the addition of TBP. The zone of TBP reacting is a bit narrower than that of TMP. The chemistry of TMP transformations in the flame was studied by measurements of the profiles of peak intensities of masses related to the possible intermediate and end products of TMP transformations at low ionization energies close to the ionization potentials of these products. Several such products have been found. Figure 2 gives the profiles of mass peak intensities with $m/e=32$ (CH_3OH^+), 31 (CH_3O^+), 30 (CH_2O^+) and 140 (TMP^+) and 110 ($C_2H_5O_2P^+$) in the flame. These were measured for different U. The peak with $m/e=110$ is present in the TMP mass-spectrum as a fragmentary ion $C_2H_5O_2P^+$ with the appearance potential $11,9 \pm 0,2$ eV⁸. With $U=11,6$ eV there is practically no contribution to the 110 peak of the fragmentary ion upon TMP ionization. So the $m/e=110$ peak intensity characterizes the concentration profile of the intermediate products resulting from TMP reacting. Such product can be represented either by DMP (dimethylphosphate $(CH_3O)_2P(O)H$) or DMP* (dimethylphosphite $(CH_3O)_2POH$) or their mixture. The possible reactions that can lead to the formation of DMP are the following:



Preferable is the first one. The reaction of DMP isomerization leading to the formation of dimethylphosphite can proceed in parallel. This can, probably, account for the existence of the two maxima on the curve of $(C_2H_5O_2)^+$. CH_3OH^+ and O_2^+ contribute to the peak with $m/e=32$. The contribution of O_2^+ was taken into account by measuring the peak with $m/e=34$ (oxygen isotope).

In the profile of peak intensity with $m/e=32$ in Figure 2 the contribution of O_2^+ ion is subtracted. This profile thus characterizes the concentration profile of CH_3OH . The CH_3OH formation can be explained by the reaction:



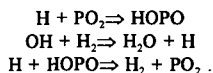
Because the intensity of this peak with $m/e=31$ (CH_3O) was measured with ionization energy

$U=11,6$ eV which is less than the potential of the appearance of this peak ($PA=12,6$ eV) in the mass-spectrum of CH_3OH , the profile of CH_3O^+ intensity in Figure 2 characterizes the concentration profile of CH_3O radical. The profile of the $m/e=30$ peak intensity characterizes the concentration profile of CH_2O , because the intensity of this peak was measured for an ionization energy $U=16,5$ eV, almost equal to the potential of CH_2O^+ ion appearance in the spectrum of CH_3OH ($AP=16,3$ eV). Note also the spatial separation of the concentration profiles of CH_3OH and CH_2O is pointing to the sequence of transformations upon CH_3OH oxidation in the flame.

Figure 3 presents the profiles of mass peak intensities with $m/e=80$ ($CH_3O_2P^+$, HPO_3^+), 64 (HPO_2^+), 63 (PO_2^+), 48 (HPO^+) and 47 (PO^+) with $U=13,1$ eV in the flame. Analyzing the behavior of these peaks in the flame, it is assumed that the contributions to the peak with $m/e=47$ of the PO^+ fragmentary ion, forming from PO_2 , HPO_2 , and HPO ionization, are rather small. Therefore the profiles of the intensities of mass peaks with $m/e=47$ and 64 characterize the concentration profiles of PO and HPO_2 . The maximum in the profile of peak intensity with $m/e=80$ is in the range between two maxima in the peak intensity profile with $m/e=110$ which can be attributed to the formation of CH_3O_2P product due to DMP reaction or the reaction of DMP^* with hydrogen atom. The behavior of the profiles of mass peak intensities with $m/e=64$, 63 , 48 , and 47 points to the following sequence of $H_xP_yO_z$ compound transformations in the flame:



The errors in the measurements of the intensities of mass peaks in Figures 2 and 3 are: $m/e=140 \pm 3\%$; $m/e=110, 30, 32 \pm 10-20\%$; $m/e= 47, 48, 63, 64 \pm 20\%$; and $m/e= 31, 80 \pm 50\%$. The promoting effect of TMP on H_2/O_2 combustion can be explained as in reference 3 by the influence of phosphorous oxides on the reaction of H and OH recombination:



REFERENCES

1. Hastie, J.W.; Bonnell, D.W. *Molecular Chemistry of Inhibited Combustion Systems*, National Bureau of Standards Report No. NBSIR, 1980, 80-2169.
2. Hastie, J.W. *J. Res. N.B.S. Sect. A.*, 1973, 77, 733.
3. Twarowski, A. *Combust. and Flame*, 1993, 94, 91-107.
4. Botha, J.P.; Spalding, D.B. *Proc. R. Soc. Lond. A* 225, 1954, 71-96.
5. Amosov, K.A.; Kuibida, L.V.; Korobeinichev, O.P.; Bol'shova, T.A. *Flame Structure* (Ed. O.P. Korobeinichev) Novosibirsk: Nauka S.B., 1991, 1, 93.
6. Peeters, J.; Mahnen, G. *Fourteenth Symposium (International) on Combustion*, The Combustion Institute: Pittsburgh, 1973, 133-146.
7. Korobeinichev, O.P.; Tereschenko, A.G.; Emel'yanov, I.D.; Rudnitskii, A.L.; Fedorov, S.Yn.; Kuibida, L.V.; Lotov, V.V. *Fiz. Goreniya Vzryva*, 1985, 21, 5, 22-28.
8. Bafus, D.A.; Gallegos, E.J.; Kiser, R.W. *J. Phys. Chem.*, 1966, 70, 8, 2614-2619.

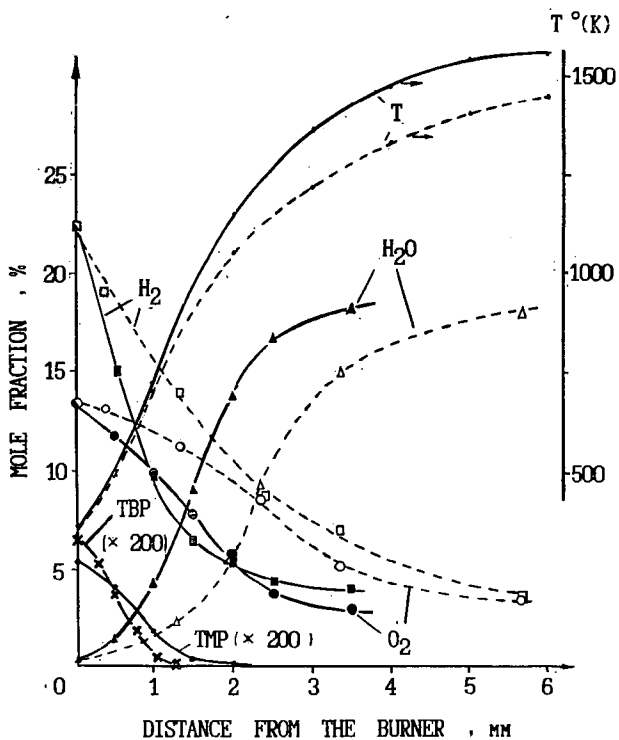


Fig. 1 The profiles of temperature and concentrations of components in H₂/O₂/Ar flame without additions: T, H₂, O₂, H₂O - dotted lines; and with additions of TMP: T, H₂, O₂, H₂O, TMP and with addition of TBP; TBP - solid lines.

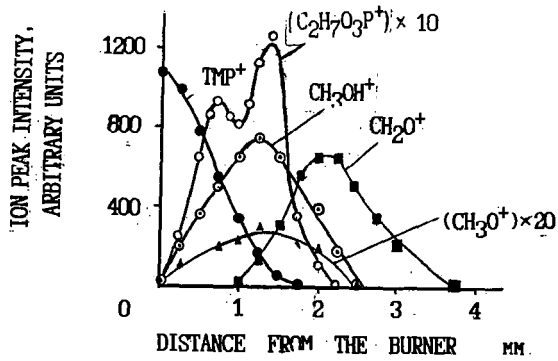


Fig. 2 The profiles of the intensities of mass peaks in the $H_2/O_2/Ar$ flame with TMP additive with: $m/e=32$ (CH_3OH^+), $U=13.1eV$; $m/e=140$ (TMP^+), $U=13.1eV$; $m/e=31$ (CH_3O^+), $U=11.6eV$; $m/e=30$ (CH_2O), $U=16.5eV$; $m/e=110$ ($C_2H_7O_3P^+$), $U=11.6eV$

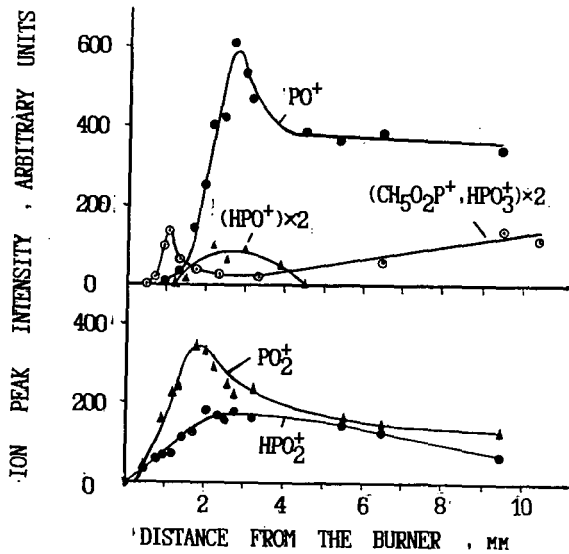


Fig. 3 The profiles of the intensities of mass peaks in the $H_2/O_2/Ar$ flame with TMP additive with: $m/e=47$ (PO^+), 48 (HPO^+), 63 (PO_2^+), 64 (HPO_2^+), 80 (HPO_3^+ , $CH_5O_2P^+$), $U=13.1eV$.